EXPERIMENTAL AND NUMERICAL STUDIES OF THREE-PHASE RELATIVE PERMEABILITY ISOPERMS FOR HEAVY OIL SYSTEMS

A Thesis

Submitted to the Faculty of Graduate Studies and Research

In Partial Fulfillment of the Requirements

For the Degree of

Doctor of Philosophy

In

Petroleum Systems Engineering

University of Regina

By

Manoochehr Akhlaghinia

Regina, Saskatchewan

November, 2013

UNIVERSITY OF REGINA

FACULTY OF GRADUATE STUDIES AND RESEARCH

SUPERVISORY AND EXAMINING COMMITTEE

Manoochehr Akhlaghinia, candidate for the degree of Doctor of Philosophy in Petroleum Systems Engineering**,** has presented a thesis titled, **Experimental and Numerical Studies of Three-Phase Relative Permeability Isoperms for Heavy Oil Systems,** in an oral examination held on October 3, 2013. The following committee members have found the thesis acceptable in form and content, and that the candidate demonstrated satisfactory knowledge of the subject material.

External Examiner:	*Dr. Ian Gates, University of Calgary
Co-Supervisor:	Dr. Farshid Torabi, Petroleum Systems Engineering
Co-Supervisor:	Dr. Christine Chan, Petroleum Systems Engineering
Committee Member:	Dr. Fotini Labropulu, Department of Mathematics and Statistics
Committee Member:	Dr. Fanhua Zeng, Petroleum Systems Engineering
Committee Member:	**Dr. Paitoon Tontiwachwuthikul, Industrial Systems Engineering
Committee Member:	Dr. Daoyong Yang, Petroleum Systems Engineering
Chair of Defense:	Dr. Sandra Zilles, Department of Mathematics & Statistics

*Participated via Tele-conference
**Not present at defense

ABSTRACT

There is a great deal of interest in obtaining reliable three-phase relative permeability data given recent developments in enhanced heavy oil recovery processes associated with multiphase flow in porous media. Experimental measurement of three-phase relative permeability data for heavy oil systems is prohibitively difficult. Such data and research is scarce in the literature since the implementation of steady state experiment is onerous and time consuming. Still results from unsteady state technique do not really coincide with those from steady state experiments. Empirical correlations, such as Stone's models, which are widely used in modern commercial simulators, carry along uncertainties with two-phase relative permeabilities. In addition, their applicability to heavy oil systems has not been proven.

This work proposes a procedure to utilize two- and three-phase unsteady state displacements in order to estimate three-phase relative permeability isoperms. Using residual oil and irreducible water saturations obtained from two-phase heavy oil/water floods, a three-phase flow zone in a ternary diagram was found. Three-phase displacement was conducted in the form of gas injection into a consolidated Berea core saturated with heavy oil and water. A lab-scale three-phase one-dimensional simulator was developed and validated to simulate three-phase displacement experiments. Appropriate three-phase relative permeability data was then selected according to a saturation path drawn across the three-phase flow zone in the ternary diagram. This relative permeability data was continuously fine-tuned until differential pressure, heavy oil production, and water production from the numerical simulator match those from the three-phase displacement experiment. Repeating this procedure for different saturation

paths provides a set of relative permeability data which were used to plot relative permeability isoperms for each phase in ternary diagrams.

The procedure was validated using steady state experiment and, then, used to study the effect of temperature, oil viscosity, and different gas phase on the relative permeability isoperms for heavy oil systems. Results from this study showed that limited three-phase flow zones exist for heavy oil fluid systems due to high values of residual oil saturation. Different curvatures were observed with relative permeability isoperms of all phases. It was observed that, due to significant contrast between viscosities, oil relative permeability values are higher than those for water and carbon dioxide in order of magnitude of three and five, respectively.

It was found that relative permeabilities is no longer a function of saturations as they tend to vary with change in the temperature, oil viscosity, and gas phase. The effect of such parameters on relative permeabilities was shown to be different for each phase. In some cases, opposite and even reversal trends were observed. For instance, oil relative permeability in the presence of carbon dioxide was higher compared to methane, while relative permeability to water phase was higher in presence of methane.

The proposed method takes advantage of the practicability of the unsteady state method to provide three-phase relative permeability isoperms in a fast and reliable way. It minimizes the uncertainties that exist with the unsteady state method, such as inaccurate end-face saturation calculation and erroneous derivatives. Also, extensive study of relative permeabilities in different conditions helps us to improve our understating of three-phase relative permeabilities in simulation of processes such as thermal techniques, Steam Assisted Gravity Drainage (SAGD), Cyclic Steam Stimulation (CSS) etc.

ACKNOWLEDGEMENTS

Foremost, I would like to express my sincere gratitude to my supervisors Dr. Farshid Torabi and Dr. Christine W. Chan for the continuous support of my PhD study and research, for their patience, motivation, enthusiasm, and immense knowledge. Their guidance helped me throughout my research and the writing of this thesis. I could not have imagined having better advisors for my PhD study.

In addition to my supervisors, I would like to thank Dr. Ian D. Gates, Dr. Paitoon (P.T.) Tontiwachwuthikul, Dr. Fotini Labropulu, Dr. Daoyong (Tony) Yang, and Dr. Fanhua (Bill) Zeng, for their encouragement, insightful comments, and useful questions.

I would like to thank the Petroleum Technology Research Centre (PTRC), Faculty of Graduate Studies and Research (FGSR), and Natural Sciences and Engineering Research Council of Canada (NSERC) for funding support.

I further thank Dr. Fanhua (Bill) Zeng, and my friends Alireza Qazvini Firouz and Ryan R. Wilton who helped me whenever I needed their support.

DEDICATION

To Lovely Razieh & My Family

TABLE OF CONTENTS

LIST OF TABLES

LIST OF FIGURES

LIST OF APPENDICES

NOMENCLATURE

A	area	ft^2
B_g	gas formation volume factor	bbl/scf
B_o	oil formation volume factor	bbl/STB
B_w	water formation volume factor	bbl/STB
k	absolute permeability	Darcy
k_r	relative permeability	Fraction
k_{rgo}	two-phase relative permeability to gas in oil/gas system	Fraction
k_{ro}	three-phase relative permeability to oil	Fraction
k_{rog}	two-phase relative permeability to oil in oil/gas system	Fraction
k_{row}	two-phase relative permeability to oil in oil/water system	Fraction
k_{rwo}	two-phase relative permeability to water in oil/water system	Fraction
P	pressure	Psia
q_{gsc}	gas flow rate	scf/D
q_{osc}	oil flow rate	STB/D
q_{wsc}	water flow rate	STB/D
S	saturation	fraction
S_g	gas saturation	fraction
S_{om}	three-phase residual oil saturation	fraction
S_{or}	residual oil saturation	fraction
S_{org}	two-phase residual oil saturation in oil/gas system	fraction
S_{orw}	two-phase residual oil saturation in oil/water system	fraction

S_w	water saturation	fraction
S_{wc}	connate water saturation	fraction
S_{wi}	irreducible water saturation	fraction
T	absolute temperature	ºR
t	time	day
x	length	ft
Z	compressibility factor	dimensionless
α_c	volume conversion factor	dimensionless
β_c	transmissibility conversion factor	dimensionless
β_g	defined by Equation (2.15)	
β_w	defined by Equation (2.15)	
μ	viscosity	cP
φ	porosity	fraction

Subscripts

g	gas
max	maximum
nor	normalized saturation
o	oil
og	oil/gas system
s	normalized relative permeability according to Equations (2.29) to (2.32)
w	water
wg	water/gas system

wo water/oil system

σ probability function defined by Equations (2.21) and (2.22)

Abbreviations

PV pore volume

FVF formation volume factor

CHAPTER 1

INTRODUCTION

1.1 Heavy Oil Reservoirs

By definition, heavy oils are considered to have an API (American Petroleum Institute) gravity that is less than 20 (Meyer and Dietzman, 1979). Although this definition is widely used in the petroleum industry (Parker et al., 1986), many researchers and engineers may use viscosity to describe the flow characteristics of crude oil (Gibson, 1982). This might be because some low API gravity crude oils have been reported to show considerably low viscosities at reservoir temperatures when compared to high API gravity crude oils (Briggs et al., 1988). Although there are several categories of heavy oils, all crude oils with viscosities of more than 100 cP must be stimulated in order to be recovered, and therefore, are considered heavy oils (Briggs et al., 1988).

According to the International Energy Agency reports, heavy oil reservoirs, which represent almost 50 percent of the world's recoverable oil resources, will play a vital role in quenching the growing demand of world economies for energy (Marin et al., 2008; IEA, 2010). Among those countries with heavy oil resources, Canada (Alberta and Saskatchewan) and Venezuela (Orinoco Belt) are at the forefront of heavy oil production, with 45% and 25%, respectively, of all oil productions coming from heavy oil resources (Dusseault, 2001; Ghannam et al., 2012).

1.2 Enhanced Heavy Oil Recovery

Enhanced oil recovery refers to the stages of oil recovery that are beyond primary production and waterflooding. In the case of heavy oil and bitumen, with minor or no primary production and/or waterflooding, enhanced oil recovery is the first step. A summary of known enhanced oil recovery techniques developed for light and heavy oils are given below (Farouq Ali and Thomas, 1994):

- Non-Thermal Techniques
    - Chemical Flooding
        - Polymer Flooding
        - Surfactant Flooding
        - Alkaline Flooding
    - Miscible Displacements
        - Enriched Gas Drive
        - Vaporizing Gas Drive
        - Alcohol Flooding
        - Carbon Dioxide Flooding
        - Nitrogen Flooding
    - Gas Drives
        - Inert Gas
        - Flue Gas
        - Immiscible Carbon Dioxide
        - (Vapor Extraction) VAPEX
- Thermal Techniques
    - Steam Injection
        - Cyclic Steam Stimulation (CSS)
        - Steam Flooding
        - Huff and Puff
        - Steam Assisted Gravity Drainage (SAGD)

    - Hot Water Flooding
    - In-Situ Combustion
    - Electrothermal Heating
- Other Techniques
    - Mining
    - Cold Heavy Oil Production from Sands (CHOPS)
    - Microbial Techniques

The level of interest in different enhanced oil recovery techniques strongly depends on the oil price which, in turn, depends on the world economy and political situation. In fact, the number of field projects for enhanced oil recovery techniques is not necessarily related to its success or effectiveness (Farouq Ali and Thomas, 1994).

1.2.1 Thermal techniques

Thermal techniques are more widely applied in sandstone formations when compared to gas injection methods (Alvarado and Manrique, 2010). Cyclic steam injection (or Huff & Puff), steam flooding, and most recently, Steam Assisted Gravity Drainage (SAGD) have been the most widely used recovery methods for heavy and extra-heavy oil in sandstone reservoirs during the last decades. For instance, Canada, Former Soviet Union, United States, Venezuela, Brazil, and China to a lesser extent, have utilized these techniques (De Haan and Van Lookeren, 1969; Hanzlik, 2003; Ramlal, 2004; Jelgersma, 2007; Lacerda et al., 2008; Ernandez, 2009).

Steam injection and SAGD represent two important thermal enhanced oil recovery techniques to increase oil production in the oil sands. SAGD has received attention in Canada and Venezuela, owing vast heavy and extra-heavy oil reserves due to

applicability in unconsolidated reservoirs with high vertical permeability (Manrique and Pereira, 2007).

In-situ combustion is considered the second most important recovery method for heavy crude oils. Despite the large number of inconclusive or failed pilots, perhaps due to lack of understanding of the process and applications in reservoirs, there are several ongoing in-situ combustion projects in heavy oil reservoirs in Canada (Moritis, 2008), Romania (Machedon et al., 1994; Panait-Paticaf et al., 2006), India (Roychaudhury et al., 1997; Sharma et al., 2003; Chattopadhyay et al., 2004; Doraiah et al., 2007) and the United States (Long and Nuar, 1982).

Other approaches to thermal enhanced oil recovery methods, such as Toe-to-Heel Air Injection (THAI) (Xia et al., 2002; Greaves et al., 2005) and Electrothermal heating (Islam et al., 1991; Sierra et al., 2001; Hascakir et al., 2008; Rodriguez et al., 2008; Das, 2008), have been proposed, yet have had little or no impact on heavy oil production.

1.2.2 Non-thermal techniques

Chemical methods, the most important non-thermal enhanced oil recovery techniques, were widely applied in the 1980s. However, since the 1990's, oil production from chemical methods have been negligible around the world, except for China and the Netherlands to a lesser extent (Moritis, 2008).

Polymer flooding, the most important chemical enhanced oil recovery, is mostly used in China, with almost 20 ongoing projects. In addition to polymers, the injection of alkali, surfactant, alkali-polymer (AP), surfactant-polymer (SP), and Alkali-Surfactant-Polymer (ASP) have been conducted in a limited number of pilot projects (Moritis,

2008). Although chemical recovery methods were seen as promising approaches since 1980, the high concentrations and cost of chemicals, combined with low oil prices during 1990s, limited their use. However, the development of technology and surfactant chemistry have led to a renewed interest in chemical floods in recent years, especially in enhanced oil production in mature and waterflooded fields (Bou-Mikael, 2000).

Gas flooding is considered a non-thermal technique suitable for recovery from light, condensate, and volatile oil reservoirs. Although ongoing field implementation of nitrogen injection is very limited, it is believed to increase oil recovery under miscible conditions favouring the vaporization of light fractions of light oils and condensates (Moritis, 2008). Except North Alaska, where large natural gas resources are available without transportation expenses, hydrocarbon gas injection projects in onshore sandstone reservoirs have not made a significant impact on oil recovery in Canada and the United States. Pressure maintenance projects with gas and Water Alternate Gas (WAG) processes have been shown to be more promising as compared to gas injections (Moritis, 2008).

1.3 Three-Phase Relative Permeability

The dependency of international economies on energy from heavy oil resources has led the petroleum industry to develop several enhanced oil recoveries techniques. Numerical reservoir simulators have become a major tool in production optimization and performance prediction of all enhanced oil recovery processes (Ambastha and Kumar, 1999; Esmail, 1985). Relative permeability data is essential for any kind of reservoir development that describes the mechanism of a multiphase flow through reservoir. There are several studies in the literature that have addressed the significant role of three-phase

relative permeability data in numerical simulations of different enhanced oil recovery techniques, such as Water Alternate Gas injection (WAG) (Land, 1968; Christensen et al., 2001; Element et al, 2003; Spiteri and Juanes, 2006; Shahverdi et al., 2011), Cyclic Steam Stimulation (CSS) (Dietrich, 1981; Lake, 1989; Dria et al., 1993), gas injections (Muqeem et al., 1993; kalaydjian et al., 1996; Shojaei et al., 2012), in-situ combustion (Schneider and Owens, 1970), Surfactant flooding (Foulser et al., 1992), Steam Assisted Gravity Drainage (SAGD) process (Chalier et al., 1995), Gas Assisted Gravity Drainage (GAGD) process (Blunt et al., 1995), and CO_2 geological sequestrations in depleted reservoirs (Koide et al., 1992).

In the past decades, numerous attempts have been made to reduce uncertainty in the input data of the numerical simulators (Capen, 1976; Hastings et al., 2001; Caldwell and Heather, 2001). Inaccurate relative permeability data is said to be a major source of uncertainty in performance predictions involving numerical simulators (Demond et al., 1996; Boukadi et al., 2005). Due to the scarcity of three-phase relative permeability data, it is often tuned or obtained by history matching. However, the manipulation of three-phase relative permeability data can cause flow parameters to be compromised (Li and Horne, 2008).

1.4 Motivation and Objectives

Three-phase relative permeability data obtained from steady state experiments is rare (especially for heavy oil systems) due to the laborious nature of the procedure. As stated in the next chapter, despite several decades of study, there is no general unsteady state technique that provides three-phase relative permeability data consistent with that from a steady state technique. With several proven uncertainties, modern commercial

reservoir simulators widely use three-phase relative permeabilities from the empirical correlations based on two-phase relative permeability data.

This work focuses on the estimation of three-phase relative permeability data for heavy oil systems, knowing that few available data, measurement techniques, and correlations are based on synthetic or conventional light oils. The main objectives of this study are as following:

- Performing two and three-phase displacement experiments with water, gas (carbon dioxide and methane), and heavy oil.
- Investigating the feasibility of applying the Johnson-Bossler-Naumann (JBN) technique in heavy oil systems.
- Developing and validating a three-phase, fully implicit, and one-dimensional numerical simulator to simulate three-phase displacement experiments, since available reservoir simulators can be supplied only with empirical correlations.
- Proposing a procedure to utilize two- and three-phase unsteady state displacement experiments combined with developed numerical simulator in order to estimate all relative permeability isoperms.
- Verifying estimated relative permeability isoperms with steady state experiments and, also, through conducting sensitivity analysis.
- Investigating the effect of key parameters, such as heavy oil viscosity, temperature, and different gas phase (carbon dioxide and methane) on three-phase relative permeability data.

1.5 Outline of the Thesis

This thesis is organized into seven chapters. Chapter 1 briefly introduces the importance of production of heavy oil reservoirs in the world energy market. This chapter also points out the crucial role of accurate three-phase relative permeability data in the performance prediction of enhanced oil recovery techniques. In Chapter 2, a comprehensive literature review of scientific research into the relative permeability concept and measurement techniques is given. Advantages and disadvantages of techniques developed for three-phase relative permeability data are discussed. Chapter 3 summarizes the material, experimental setups, and experimental procedures used in this study. Chapter 4 investigates the applicability of the Johnson-Bossler-Neumann (Johnson et al. 1959) technique when measuring two-phase relative permeabilities in heavy oil systems. Chapter 5 describes and tests a procedure for estimating three-phase relative permeability isoperms using two- and three-phase displacement experiment (combined with a suitable lab-scale simulator). The proposed procedure is then used in Chapter 6 to investigate the effect of important parameters such as temperature, oil viscosity, and different gas phase on three-phase relative permeabilities. Conclusions based on the findings of this study, along with some recommendations for future work, are presented in Chapter 7.

CHAPTER 2

LITERATURE REVIEW

2.1 Background

A porous medium is commonly represented as a solid, such as a rock, sand pack, membrane or filter, containing void spaces or pores, either connected or disconnected, and distributed within that solid regularly or randomly. These pores may contain a variety of fluids, such as air, gas, water, brine, oil, etc. In addition, these pores, which represent a portion of the bulk volume, form a complex network capable of carrying fluids through them. Petroleum engineering, chemical engineering, hydrology, and soil mechanics, among others, are some of the numerous disciplines in which porous media play an important role or where the technology requires them as a tool (Heinemann, 2005).

According to the American Petroleum Institute (API) Code 27, absolute permeability is defined with the help of Darcy's law, Equation (2.1), as a property of porous media and is "a measure of the capacity of the medium to transmit fluids" (Amyx et al., 1988).

$$v_s = -\frac{k}{\mu}\left(\frac{dP}{ds}\frac{\rho g}{1.0133}\frac{dz}{ds} \times 10^{-6}\right) \tag{2.1}$$

where

s = distance in the direction of flow, cm

v_s = volume flux across a unit area of the porous medium in unit time along flow path s, cm/sec

z = vertical coordinate, cm

ρ = density of the fluid, gm/cm^3

g = acceleration of gravity, 980.665 cm/sec^2

dP/ds = pressure gradient along s at the point to which v_s refers, atm/cm

μ = viscosity of the fluid, cP

k = absolute permeability of the medium, darcies

This term is applicable if a single fluid flows through the porous media. Because, in petroleum reservoirs, multiphase flow is encountered, the basic definition of permeability stated by API Code 27 needs to be modified. Accordingly, effective permeability is used to describe simultaneous flow of more than one fluid (e.g., oil, water, gas). In the definition of effective permeability, all fluids present in the porous media are absolutely immiscible. With this assumption, along with several others given by Darcy, Equation (2.1) can be written for each fluid individually (Amyx et al., 1988):

$$v_{s,o} = -\frac{k_o}{\mu_o}\left(\frac{dP_o}{ds}\frac{\rho_o g}{1.0133}\frac{dz}{ds} \times 10^{-6}\right) \tag{2.2}$$

$$v_{s,w} = -\frac{k_w}{\mu_w}\left(\frac{dP_w}{ds}\frac{\rho_w g}{1.0133}\frac{dz}{ds} \times 10^{-6}\right) \tag{2.3}$$

$$v_{s,g} = -\frac{k_g}{\mu_g}\left(\frac{dP_g}{ds}\frac{\rho_g g}{1.0133}\frac{dz}{ds} \times 10^{-6}\right) \tag{2.4}$$

where subscripts o, w, and g refer to oil, water, and gas, respectively.

Since effective permeabilities (k_o, k_w, k_g) are functions of fluid saturations, each fluid saturation should be specified so as to define the condition at which a given permeability exists. This means that, unlike absolute permeability, different values of

effective permeability exist for different fluid conditions. In petroleum engineering, relative permeability is the ratio of the effective permeability of the fluid at a given value of saturation to the effective permeability of that fluid at 100 percent saturation. With this definition of relative permeability definition, it can also be defined as a ratio of the effective permeability of a fluid at a given saturation to the absolute permeability. For a system of oil, water, and gas, relative permeability is defined by the following equations (Amyx et al., 1988):

$$k_{ro} = \frac{k_o}{k} \tag{2.5}$$

$$k_{rw} = \frac{k_w}{k} \tag{2.6}$$

$$k_{rg} = \frac{k_g}{k} \tag{2.7}$$

Relative permeability depends mostly on the microscopic characteristics of the porous medium, pore scale dynamics or capillary number, saturation, saturation history, and wettability. It is commonly expressed as a function of local fluid saturation (Marle, 1981; Blunt and King, 1991; Heaviside et al., 1991).

Three-phase relative permeability is one of the primary flow parameters required to model multi-phase flow through porous media. It is important for designing and controlling processes, such as the production of oil or gas from underground reservoirs and all types of enhanced oil recovery techniques (Land, 1968; Schneider and Owens, 1970; Dietrich, 1981; Lake, 1989; Foulser et al., 1992; Koide et al., 1992; Dria et al., 1993; Muqeem et al., 1993; Chalier et al., 1995; Blunt et al., 1995; Kalaydjian et al., 1996; Christensen et al., 2001; Element et al, 2003; Spiteri and Juanes, 2006; Shahverdi et al., 2011). In light of the increasing demand for multi-phase relative permeability data

for predicting the performance of various multi-phase flow recovery processes, a simple and reliable method to obtain such data is extremely desirable (Sarem, 1996; Saraf and Fatt, 1967; Silpngarmlers and Ertekin, 2002).

2.2 Three-Phase Relative Permeability Measurements

Extensive documentation of the various experimental methods used to obtain three-phase relative permeability data has been presented by Manjnath and Honarpour (1984), Parmeswar and Maerefat (1986), Honarpour et al. (1986), Honarpour and Mahmood (1988), Pejic and Maini (2003), and Jounes (2003). Available techniques of obtaining three-phase relative permeability data can be classified into three major categories:

- Steady state experiments
- Unsteady state experiments
- Empirical models

Each of the techniques or methodologies given above used by different researchers is explained in the following sections.

2.2.1 Steady state experiments

The steady state technique is considered to be the most reliable method for measuring three-phase relative permeability data. In this technique, all fluids (e.g., oil, water, gas) are simultaneously forced into the porous media under a constant rate or pressure constraints. After establishing an equilibrium condition between injected and produced fluids, saturations of each fluid can be easily obtained using material balance.

Consequently, relative permeability of each phase at a determined saturation point can be directly calculated through the application of Darcy's law and by using flow rates and differential pressure across the porous media. Different saturations can be achieved by repeating the above procedure with different injection flow rates (Dandekar, 2006). Although the steady state technique is superior to other techniques, such as the unsteady state method or the use of correlations in reliability and providing a wide range of saturation values, it is inherently time consuming. For example, other researchers have suggested that it may take several days to attain an equilibrium condition at each saturation level (Blunt, 2000).

2.2.1.1 Leverett and Lewis (1941)

For the first time in 1941, Leverett and Lewis used nitrogen, kerosene, and brine to study steady-state three-phase flow in unconsolidated sands. It was found that the relative permeability to the wetting phase (water) is a unique function of the wetting phase saturation, as shown in Figure (2.1). They speculated that the wetting phase occupies relatively smaller pores of the core. Therefore, at a specific wetting-phase saturation, the same portion of the pores is occupied by the wetting phase irrespective of the saturation of the other two phases (Leverett and Lewis, 1941). Unlike the relative permeability of water in the wetting phase, the relative permeability of gas and oil were found to be dependent on the saturation of other phases in the rock. Figure (2.2) shows the relative permeability for oil (a) and gas (b) in a ternary diagram.

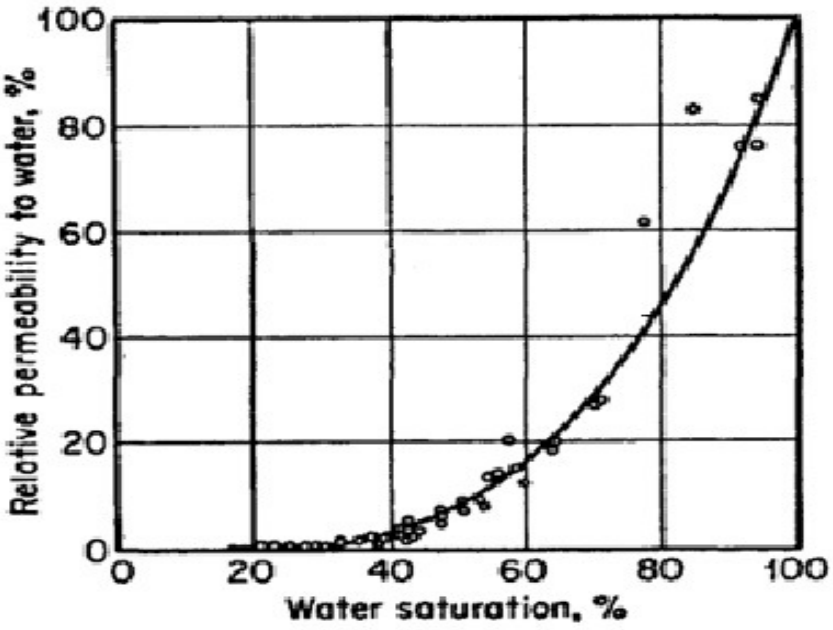

Figure 2.1: Relative permeability to water as a function of water saturation (Leverett and Lewis, 1941).

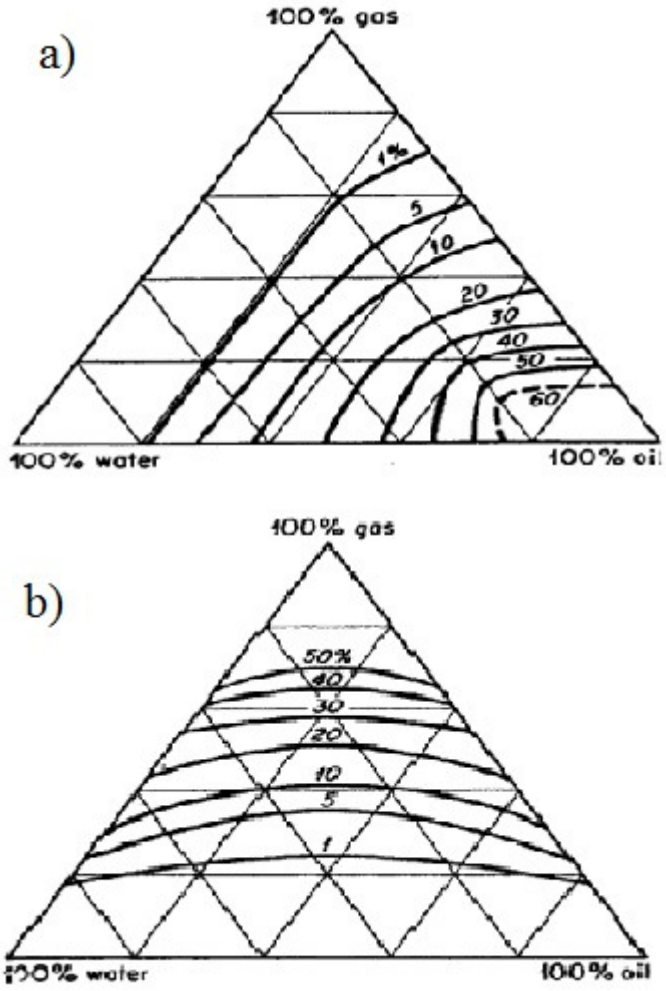

Figure 2.2: Ternary diagram of oil (a) and gas (b) relative permeability isoperms (Leverett and Lewis, 1941).

In order to understand the oil phase behavior, Leverett reasoned that the oil phase has a greater tendency than the gas phase to wet the solid. In addition, the interfacial tension between water and oil is less than that between water and gas. Large pore spaces are occupied by the gas phase and average pore spaces are then occupied by the oil phase. Therefore, at lower water saturations, the oil occupies more of the smaller pores. Gas relative permeability at constant gas saturations as a function of other phase saturations is shown in Figure (2.2-b). Leverett indicated that the particular behavior of the gas phase is not definitive and other investigators speculate that gas relative permeability should be a function of gas saturation itself (Leverett and Lewis, 1941).

As mentioned earlier, Leverett and Lewis were the first group of researchers to introduce the concept of a three-phase flow zone. They suggested that the saturation region where the simultaneous flow of all three phases occurs is quite small. This small saturation region is shown in the dashed area of Figure (2.3). This means that in most cases, two-phase relative permeability curves can be used instead of three-phase relative permeability triangular diagrams (Leverett and Lewis, 1941).

2.2.1.2 Caudle et al. (1951)

Steady state experiments were performed in consolidated sandstone with Penn State setup. Since isoperms for all three phases showed curvatures, Figure (2.4), Caudle et al. concluded that the relative permeability to each phase depends on the saturation of all three phases. It was also found that if oil relative permeability increases and water relative permeability is kept at irreducible water saturation, then all relative permeabilities decrease (Caudle et al., 1951).

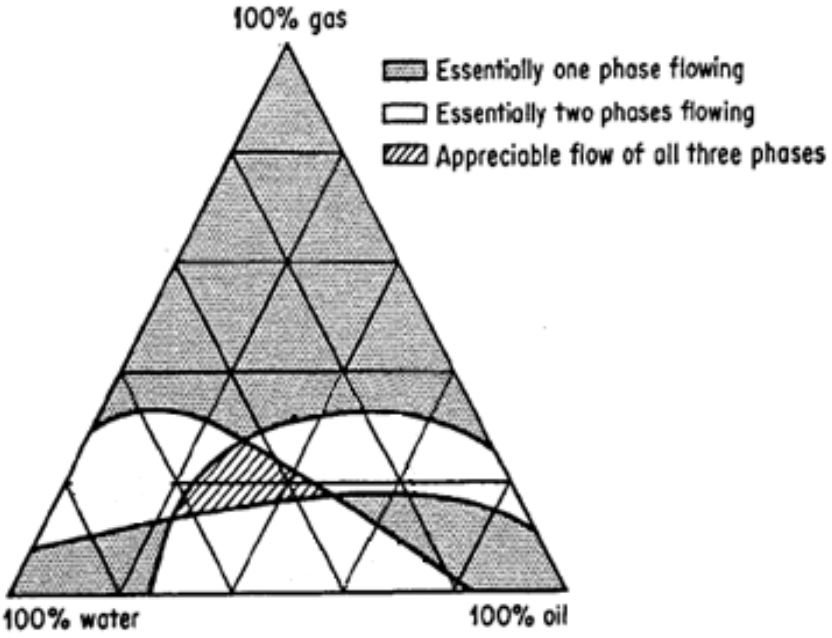

Figure 2.3: Two-phase and three-phase flow regions (Leverett and Lewis, 1941).

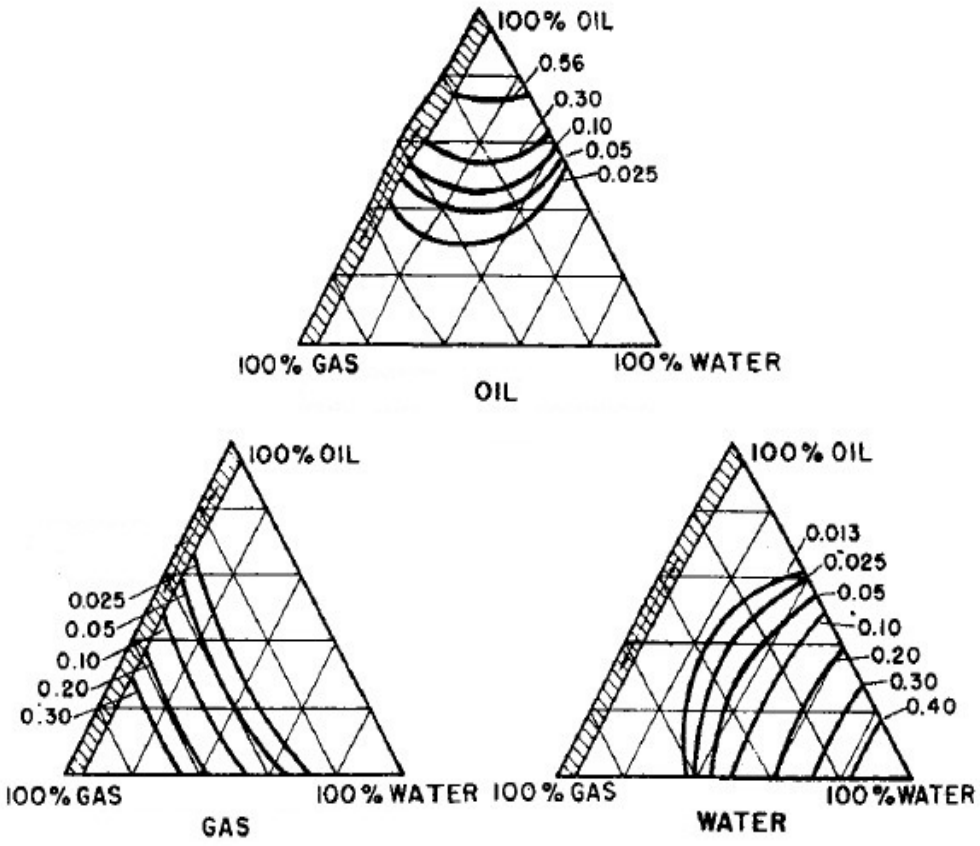

Figure 2.4: Three-phase relative permeability isoperms (Caudle et al., 1951).

2.2.1.3 Corey et al. (1956)

Corey et al. (1956) performed three-phase relative permeability measurements in nine consolidated Berea sandstone cores. Modified Hassler's capillary setup was utilized to measure brine (wetting phase), oil, and gas relative permeability values. Capillary pressure was controlled only over gas and water. This means that no control was applied over the pressure difference between the oil and brine phases. In the case of gas relative permeability curves, it was found that the presence or absence of the brine in the core has no impact on the gas relative permeability. Therefore, gas isoperms in the triangular diagrams were plotted with a straight line as shown in Figure (2.5). In addition, it was suggested that gas relative permeability is a function of total liquid saturation, as seen in Figure (2.6).

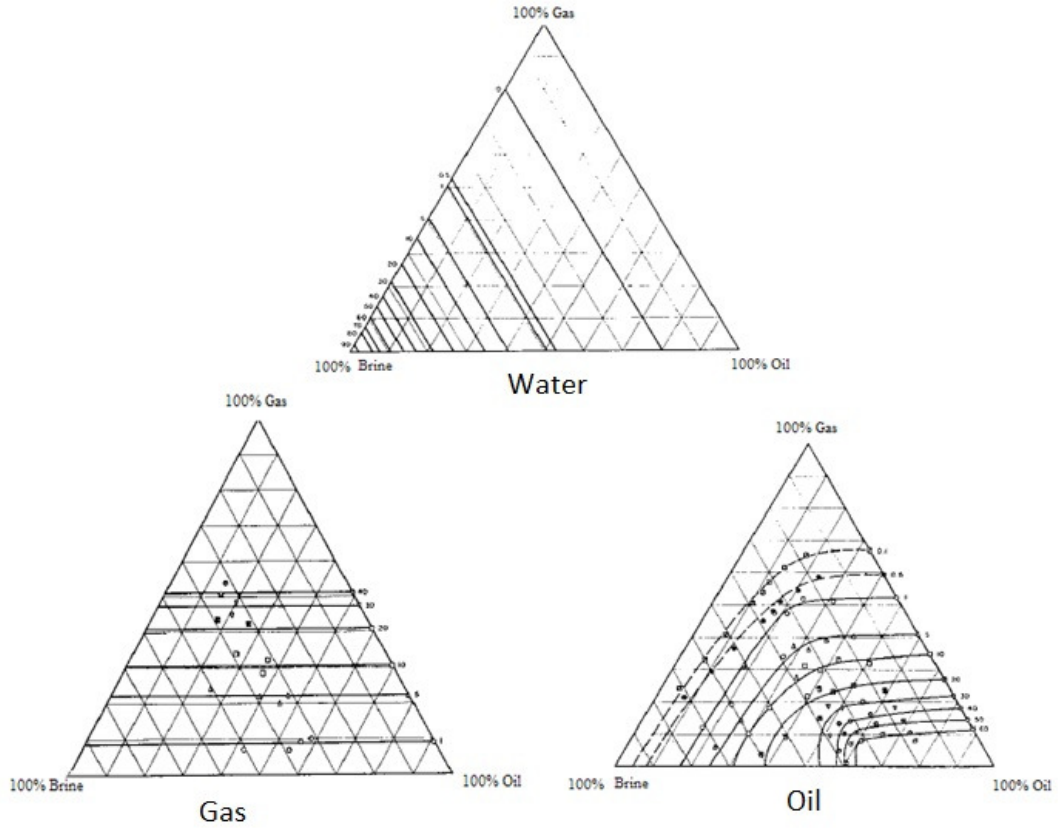

Figure 2.5: Three-phase relative permeability data (Corey et al., 1956).

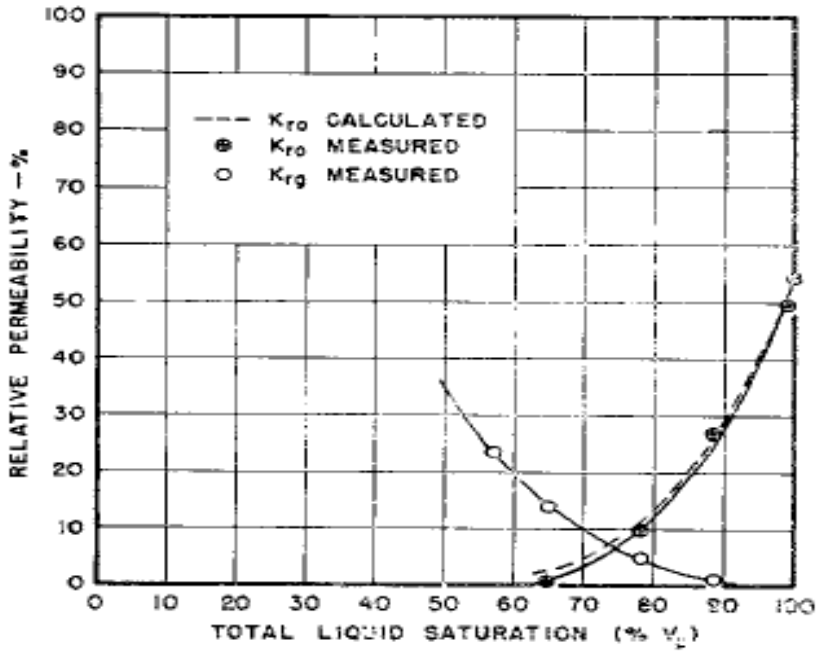

Figure 2.6: Gas and oil relative permeability versus total liquid saturation (Corey et al., 1956).

Burdine's tortuosity concept (1953) was applied to the equations developed by Wyllie and Spangler (1952) to obtain the oil relative permeability equations shown in Equations 2.8 and 2.9 for oil-wet and water-wet systems.

For oil wet systems:

$$k_{ro} = \left[\frac{S_o - S_{or}}{1 - S_{or}}\right]^2 \frac{\int_0^{S_o} dS_o / {P_c}^2}{\int_0^1 dS_o / {P_c}^2} \tag{2.8}$$

Water wet system:

$$k_{ro} = \left[\frac{S_L - S_W}{1 - S_{Lr}}\right]^2 \frac{\int_{S_W}^{S_L} dS_L / {P_c}^2}{\int_0^1 dS_L / {P_c}^2} \tag{2.9}$$

where:

P_C = capillary pressure

S_W = water saturation

S_L = total liquid saturation

S_{Lr} = irreducible water saturation

S_o = oil saturation

S_{or} = residual oil saturation

C = constant value

As can be seen in Figure (2.5), the oil isoperms show a curvature towards the gas and brine sides of the triangular diagram. An increase in oil permeability at a given level of oil saturation takes place when the water saturation is increased at the expense of gas saturation. Water relative permeability curves are similar to those found earlier by

Leverett and Lewis (1941) and the wetting phase relative permeability is only dependent on wetting phase saturation, Figure (2.6).

2.2.1.4 Reid (1956)

Reid (1956) used Leverett and Lewis' (1941) method to obtain relative permeability isoperms, shown in Figure (2.7). Care was taken to eliminate end effects by measuring the saturation and pressure gradient away from the core end, but hysteresis was neglected. Water and oil saturations were measured respectively with resistivity and gamma ray absorption techniques. Isoperms were not extrapolated for the area of the ternary diagram in which three-phase steady state flow does not occur. Although Reid (1956) used the same method of Leverett and Lewis (1941), isoperms for all phases have sensible curvatures indicating the dependency of isoperms on all phase saturation.

2.2.1.5 Snell (1962, 1963)

Snell (1962a, 1962b, 1963) also used Leverett and Lewis' (1941) procedure to investigate three-phase flow in an unconsolidated water wet sand pack. Snell took advantage of neutron counting and radio frequency to measure gas and water saturations. Saturations of the oil and gas phases were uniform over a certain length whenever the wetting phase saturation was uniform over the same length. Curvatures were found in each phase's isoperms, illustrated in Figure (2.8).

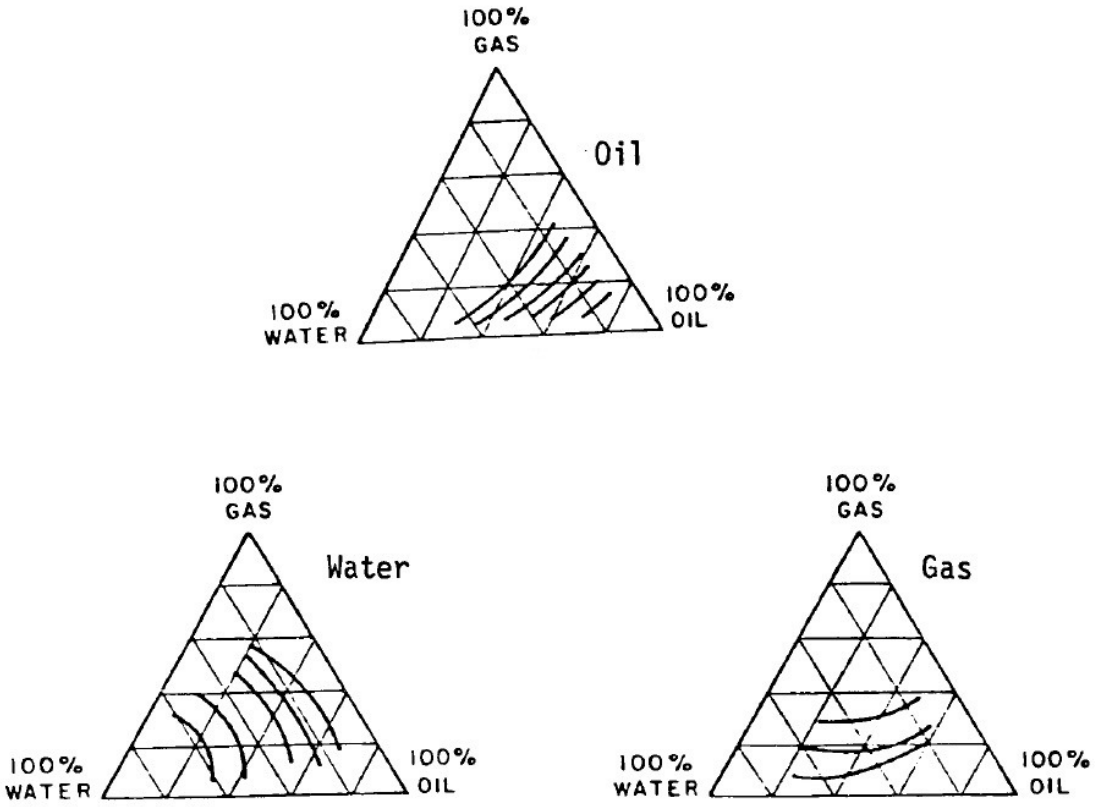

Figure 2.7: Three-phase relative permeability data (Reid, 1956).

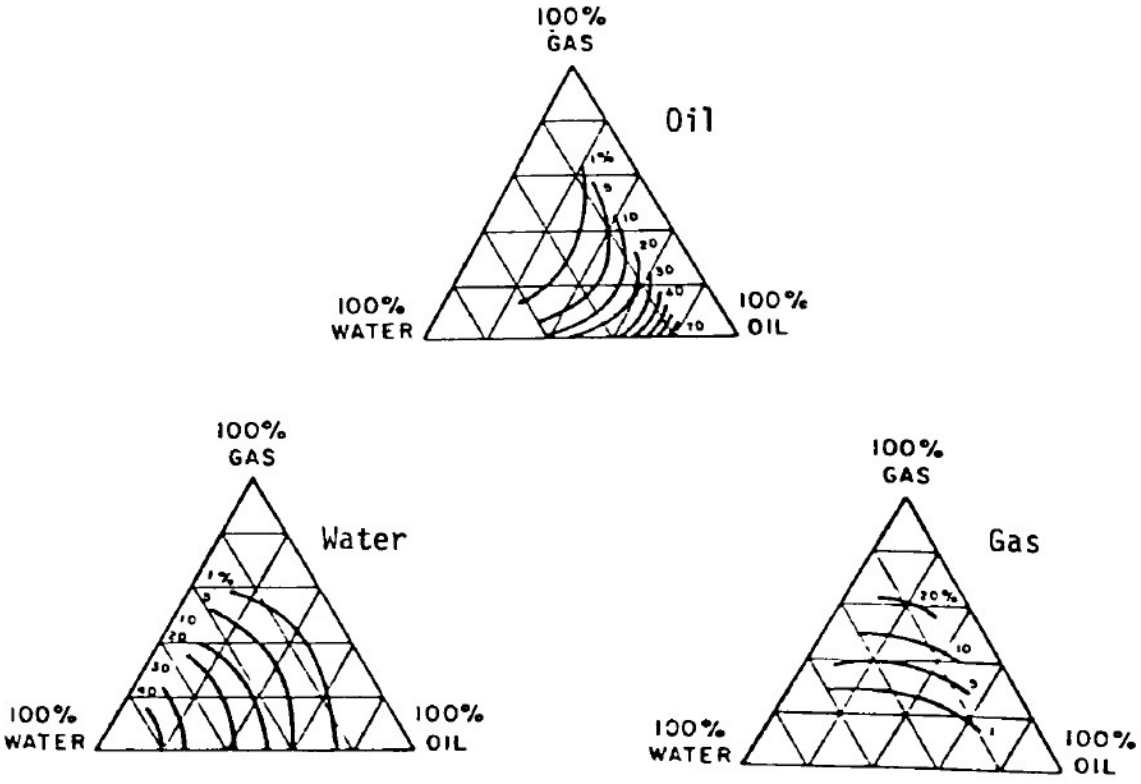

Figure 2.8: Three-phase relative permeability data (Snell, 1962).

2.2.1.6 Saraf and Fatt (1967)

The application of the Nuclear Magnetic Resonance (NMR) technique for measuring three-phase relative permeability and estimating fluid saturations was first introduced by Saraf and Fatt (1967). Experiments were conducted in Boise sandstone for a range of saturations in which all three phases could flow. In the case of three-phase relative permeability, all results were similar to those of the Corey et al. (1956) experiments, as shown in Figure (2.9). It was found that three-phase water permeability depends only on water saturation, while three-phase oil permeability depends on both oil and water saturations, and that of the gas phase depends on the liquid saturation.

2.2.1.7 Oak (1988, 1990, 1991)

Oak conducted a comprehensive steady-state measurement of two and three-phase relative permeabilities in water-wet Berea sandstones using a data set of 1800 tests (Oak and Ehrlich, 1988; Oak, 1990; Oak et al., 1990; Oak, 1991). Water, oil, and gas were injected into the core sample at fixed rates and an X-ray was used for saturation measurement. Oak stated that experimental data did not support Stone's model, as one can infer from Figure (2.10). It was concluded that oil three-phase relative permeability was subject to the displacement of trapped oil by gas. Oak also showed that there was a certain level of oil saturation needed to initiate three-phase flow from water–oil two-phase flows. In the case of water (wetting phase) relative permeability, a similarity was found between two- and three-phase relative permeabilities at the same water saturations. Gas (non-wetting phase) relative permeability behavior was found to be similar to the water phase behavior.

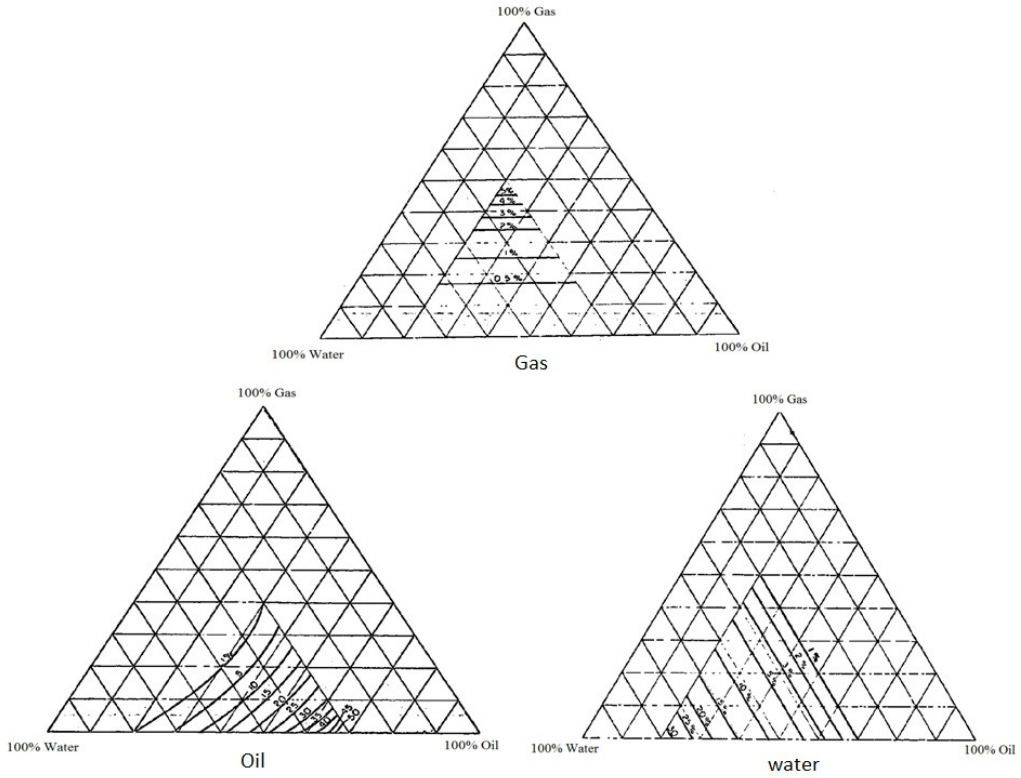

Figure 2.9: Three-phase relative permeability data (Saraf and Fatt, 1967).

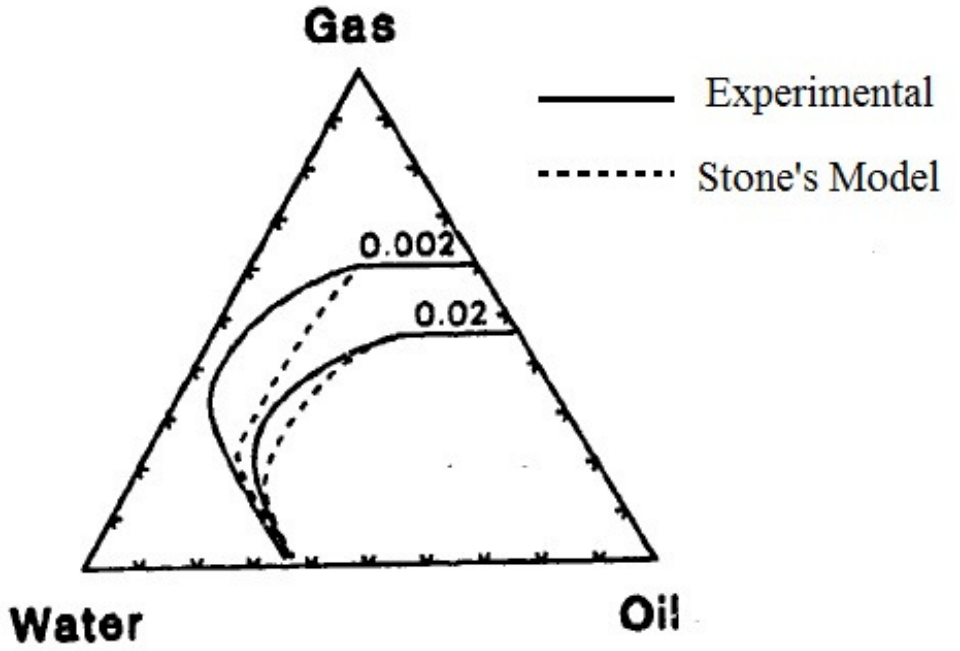

Figure 2.10: Evaluation of Stone's model using experimental data (Oak, 1990).

2.2.1.8 Poulsen et al. (2000)

Poulsen et al. (2000) performed two and three-phase relative permeability experiments using steady-state methods to investigate the effect of capillary pressure. Relative permeability showed a considerable shift when capillary pressure was included. It was stated that neglecting capillary effect leads to an underestimate of oil relative permeability.

Other studies, such as those of Schneider and Owens (1970), Cromwell et al. (1984), and Hove (1987), utilized advanced tools of X-Ray absorption and X-Rays computerized tomography (CT) in determining fluid saturations of the core samples during steady state three-phase relative permeability measurement.

2.2.2 Unsteady state experiments

The unsteady state method has been proposed based on the Buckley and Leverett theory (1942) as a fast and convenient alternative to the steady state experiments. In this method, fluid is injected at a constant flow rate or pressure into the porous medium with the other two fluid saturations present. Fractional flow and pressure drop are measured against pore volume injected or time. The relative permeability of each phase is then determined using the method introduced by Welge (1952), Johnson Bossler and Naumann (1959), and Jones and Roszelle (1978). This technique is quick since the saturation equilibrium no longer needs to be attained. Unlike the steady state technique, in which each test gives only one point in a relative permeability curve, the unsteady state method provides an entire curve of relative permeability against saturation. Although there are

several advantages to the unsteady state technique, the main limitation is that relative permeability data cannot be determined where shock fronts exist. In addition, data analysis of this method is more analytically complicated as compared to the steady-state method, which results in more uncertainties in the data (Christiansen et al., 1997).

2.2.2.1 Sarem (1966)

Sarem (1966) modified a gas-oil unsteady state relative permeability device to investigate oil, water, and gas flow in a Berea and a reservoir core. Cores were saturated with water and oil and then subjected to gas drives. Production rates, pressure drop, and temperature were recorded as required parameters during the experiments. Assuming fractional flow and relative permeability as a function of saturation, and neglecting capillary and gravity effects, Buckley-Leverett's theory was extended to a three-phase flow system. Calculations resulted in equations for water, oil, and gas relative permeability from laboratory measureable quantities. They are given as:

$$k_{ro} = f_{o2} \frac{d(\frac{1}{Q})}{d(\frac{\Delta PkA}{L\mu_o q_T Q})} \tag{2.10}$$

$$k_{rw} = f_{w2} \frac{d(\frac{1}{Q})}{d(\frac{\Delta PkA}{L\mu_w q_T Q})} \tag{2.11}$$

$$k_{rg} = k_{ro} \frac{\mu_g f_g}{\mu_o f_o} \tag{2.12}$$

where:

f_{o2} = oil fractional flow at outlet

f_{w2} = water fractional flow at outlet

Q = cumulative injection volume, PV

ΔP = differential pressure, atm

k = absolute permeability, darcies

A = cross sectional area, cm^2

f = fractional flow

L = length, cm

μ = viscosity, cP

q_T = volumetric flow rate, cc/sec

Generated isoperms are parallel to the sides of the saturation ternary diagram. Sarem also commented that the initial saturation conditions affect oil and water relative permeability, but provide limited impact on gas relative permeability.

2.2.2.2 Donaldson and Dean (1966)

Donaldson and Dean (1966) used an extension of Welge's two-phase theory (1952) to obtain three-phase relative permeability data from displacement experiments conducted in Berea sandstone and Arbuckle limestone. They found out that because the terminal saturations govern the flow of fluid in the core, the isoperms are therefore functions of terminal saturations rather than average saturations. Hysteresis was ignored, but high differential pressure was applied to minimize end effects. Different relative permeability curves were obtained for sandstone and limestone due to the presence of vugs and channels in the limestone core. This is seen in Figure (2.11).

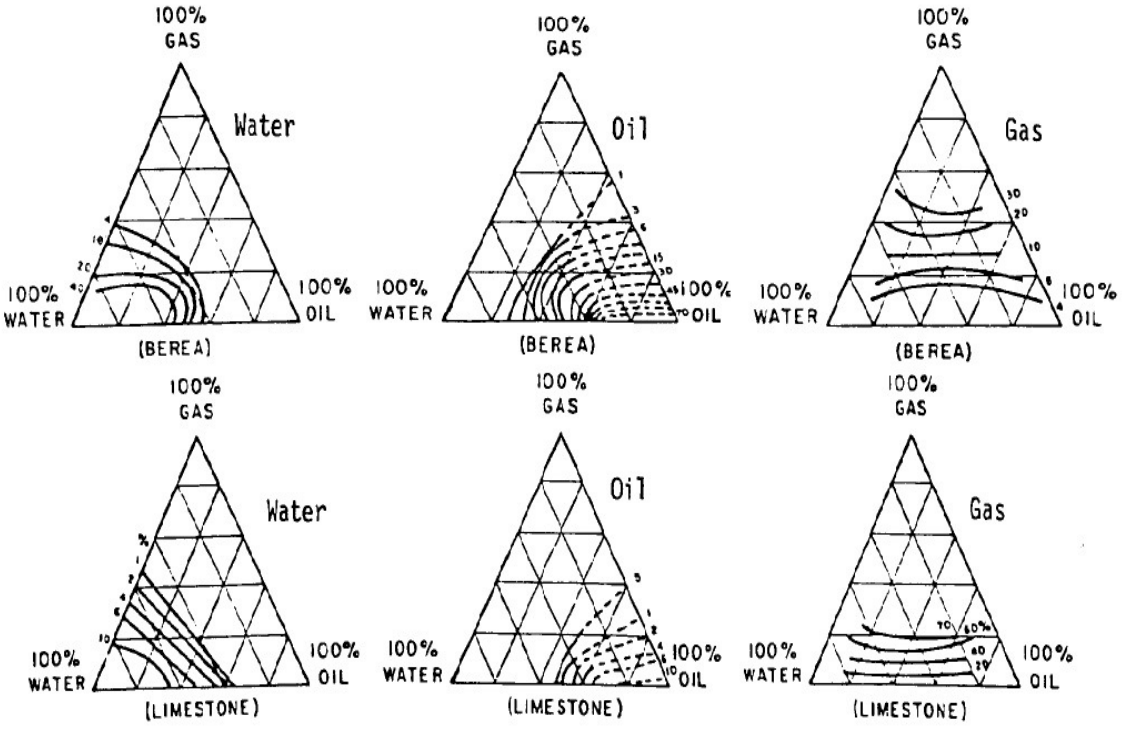

Figure 2.11: Unsteady state three-phase isoperms for sandstone and limestone (Donaldson and Dean, 1966).

2.2.2.3 Schneider and Owens (1970)

Schneider and Owens (1970) investigated steady and unsteady state relative permeability measurement in carbonate and sandstone core samples. During the imbibition process in water wet systems, oil relative permeability was found to be insensitive to the presence of the gas phase when gas saturation is increasing. Oil relative permeability was shown to be depending on its own saturation. The non-wetting relative permeability-saturation relationship in three-phase depends on the saturation history of both non-wetting phases and on the saturation ratio of the second non-wetting phase and the wetting phase.

2.2.2.4 Van Spronsen (1982)

In 1982, Van Spronsen extended the centrifuge apparatus to measure three-phase oil and water relative permeabilities on Weeks and Berea sandstones. Effects of capillary pressure gradients, mobility effects, non-constant centrifugal acceleration, desaturation, build-up of centrifuge speed, and time lag in production measurement were analytically investigated. The results of oil relative permeability were similar to those of earlier studies. However, in the case of water relative permeability, it was reported that the curvature tends towards the oil/gas sides of the triangular diagram, as depicted in Figure (2.12). This suggests that the water three-phase relative permeability is not a function of its own saturation. The Van Spronsen report lacks gas relative permeability isoperms found in earlier studies.

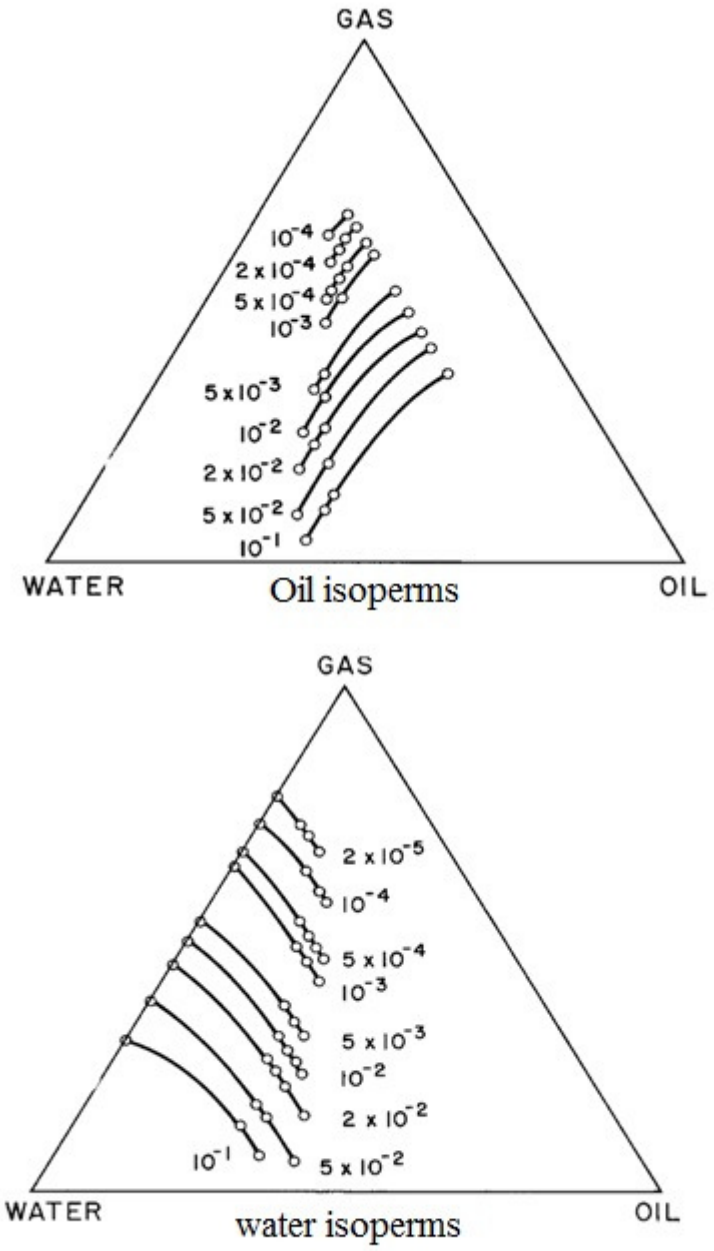

Figure 2.12: Three-phase isoperms for oil (top) and water (bottom) from centrifuge experiment (Van Spronsen, 1982).

2.2.2.5 Grader and O'Meara (1988)

In 1988, Grader and O'Meara extended the Welge-Johnson-Bossler-Naumann (Welge-JBN) theory to mitigate difficulties in dynamic displacement relative permeability measurements, such as capillary end effects and viscous fingering. Water, benzyl alcohol, and decane were used instead of conventional oil, water, and gas systems. In order to monitor saturation changes, material balance analysis was applied. For all three phases, relative permeability isoperms showed a sensible curvature. This implies that the relative permeabilities of each phase are dependent on the other phase saturations.

2.2.2.6 Siddiqui et al. (1995)

Siddiqui et al. (1995) applied X-ray computerized tomography to verify the Buckley-Leverett three-phase theory. They examined the Buckley-Leverett theory extension in regards to three immiscible fluids. Three-phase relative permeability measurements were completed on pre-sieved, spherical glass beads as porous media. Distilled water, benzyl alcohol, and decane were used as the three immiscible liquids. It was concluded that the measurement of three-phase relative permeabilities using the extended Buckley-Leverett theory was theoretically and experimentally sound and reliable.

2.2.3 Three-phase relative permeability models

Although unsteady state techniques of measuring three-phase relative permeability data are very fast and convenient when compared to those of the steady state

method, the reliability of the results are still under question due to the limitations in providing relative permeability data where shock fronts and error prone derivative calculations exist (Donaldson and Kayser, 1981; Boukadi et al., 2005). In the last few decades, several relative permeability models have been developed as an alternative to the steady state technique (Deitrich and Bondar, 1976; Manjnath and Honarpour, 1984; Honarpour et al., 1986; Baker, 1988; Delshad and Pope, 1989; Oak, 1990; Juanes, 2003; Oliveira and Demond, 2003; Masihi et al., 2011). These empirical models often utilize two-phase relative permeability data as inputs to predict three-phase relative permeability data. A brief overview of the major proposed three-phase relative permeability models are given below:

2.2.3.1 Stone I and II (1970)

Stone (1970) used the channel flow theory to develop his first model. Stone assumed porous media as a flow channel in which only one fluid can flow through the channels. Relative permeability to wetting and non-wetting phases (water and gas) are functions of their own saturations and are the same in a two-phase system as in a three-phase system. The relative permeability of intermediate phase (oil) depends on which intermediate wetting phase intermediate channels it occupied and, in turn, should therefore be represented as function of wetting and non-wetting phase saturations. This model is given as:

$$k_{ro} = S_{onor}\beta_w\beta_g \tag{2.13}$$

where:

$$S_{onor} = \frac{S_o - S_{or}}{1 - S_{wi} - S_{or}} \quad (2.14)$$

$$\beta_w = \frac{k_{row}}{1 - S_{wnor}} \quad (2.15)$$

$$\beta_g = \frac{k_{rog}}{1 - S_{gnor}} \quad (2.16)$$

$$S_{wnor} = \frac{S_w - S_{wc}}{1 - S_{wc} - S_{om}} \quad (2.17)$$

$$S_{gnor} = \frac{S_g}{1 - S_{wc} - S_{om}} \quad (2.18)$$

S_{om} can be used as an adjustable parameter to minimize the deviations between the experimental and calculated values of the oil relative permeability.

In his second model, Stone (1973) used all four two-phase relative permeability relationships from the oil-gas and oil-water systems to predict three-phase oil relative permeability by introducing σ_w and σ_g as probabilities of contributions to flow in the two-phase systems. His second model is given as:

$$k_{ro} = (k_{row} + k_{rwo})\left(k_{rog} + k_{rgo}\right) - (k_{rwo} + k_{rgo}) \quad (2.19)$$

$$k_{ro} + k_{rgo} + k_{rw} = \sigma_w \sigma_g \quad (2.20)$$

$$\sigma_w = k_{row} + k_{rwo} \quad (2.21)$$

$$\sigma_g = k_{rog} + k_{rgo} \quad (2.22)$$

2.2.3.2 Hirasaki (1976)

Hirasaki (Dietrich and Bondor, 1976) proposed a model based on a reduction in the oil relative permeability due to the presence of a third phase: $k_{row,max}$ that is a two-phase oil relative permeability measured at connate water saturation. Their model is:

$$k_{ro} = k_{row} + k_{rog} - k_{row,max} + (S_w + S_o)\frac{(k_{row,max} - k_{row})(k_{row,max} - k_{rog})}{k_{row,max}} \quad (2.23)$$

2.2.3.3 Aziz and Settari (1979)

Aziz and Settari (1979) suggested modifying both Stone I and Stone II models so that they reduce to the two-phase data only if the end-point relative permeabilities are equal to one. The modified Stone I and Stone II are given as the following:

Modified Stone I:

$$k_{ro} = k_{row,max} S_{onor} \beta_w \beta_g \tag{2.24}$$

$$\beta_w = \frac{k_{row}}{k_{row,max}(1-S_{wnor})} \tag{2.25}$$

$$\beta_g = \frac{k_{rog}}{k_{row,max}(1-S_{gnor})} \tag{2.26}$$

Modified Stone II:

$$k_{ro} = k_{row,max}\left[\left(\frac{k_{row}}{k_{row,max}} + k_{rwo}\right)\left(\frac{k_{rog}}{k_{row,max}} + k_{rgo}\right) - (k_{rwo} + k_{rgo})\right] \tag{2.27}$$

2.2.3.4 Aleman and Slattery (1988)

Aleman and Slattery (1988) developed a model for oil relative permeability with modified formula for the normalization of two-phase functions given as:

$$k_{ro} = k_{row,max} S_{onor} \frac{k_{rogs}(1-k_{rgos})(k_{rows}-k_{rwos}) - k_{rwos}(1-k_{rows})(k_{rgos}-k_{rgos})}{(1-k_{rgos})(k_{rows}-k_{rwos}) - (1-k_{rows})(k_{rgos}-k_{rogs})} \tag{2.28}$$

$$k_{rows} = \frac{k_{row}/k_{row,max}}{S_{onor}} \tag{2.29}$$

$$k_{rogs} = \frac{k_{rog}/k_{rog,max}}{S_{onor}} \tag{2.30}$$

$$k_{rwos} = \frac{k_{row}/k_{rwo,max}}{S_{wnor}} \tag{2.31}$$

$$k_{rgos} = \frac{{}^{k_{rgo}}/_{k_{rgo,max}}}{S_{gnor}} \quad (2.32)$$

2.2.3.5 Baker (1988)

Baker (1988) used saturation-weighted interpolation between oil-water and oil-gas two-phase data to obtain the three-phase relative permeability to oil. Baker assumed that end points of the two-phase data are the same as in the three-phase system. Baker's model is given as:

$$k_{ro} = \frac{(S_w - S_{wc})k_{row} + (S_g - S_{gro})k_{rog}}{(S_w - S_{wc}) + (S_g - S_{gro})} \quad (2.33)$$

Where S_{gro} is residual gas saturation in the oil/gas two-phase system.

2.2.3.6 Pope and Delshad (1989)

Pope and Delshad (1989) proposed a three-phase model in which the two-phase relative permeability does not appear explicitly, namely:

$$k_{ro} = \frac{1}{2} k_{row,max}\left[{S_{onor}}^{eog}(1 - S_{wnor})^{eow-eog} + {S_{onor}}^{eow}(1 - S_{gnor})^{eog-eow}\right] \quad (2.34)$$

The exponents *eow* and *eog* are determined by fitting two-phase data.

$$k_{row} = k_{row,max}{S_{ownor}}^{eow} \quad (2.35)$$

$$k_{rog} = k_{rog,max}{S_{ognor}}^{eog} \quad (2.36)$$

$$S_{ownor} = \frac{S_{ow} - S_{orw}}{1 - S_{wc} - S_{orw}} \quad (2.37)$$

$$S_{ognor} = \frac{S_{og} - S_{org}}{1 - S_{wrog} - S_{org} - S_{gro}} \quad (2.38)$$

Where S_{wrog} is the residual water saturation at which the oil/gas two-phase experiment has been conducted.

2.2.3.7 Kokal and Maini (1989)

Kokal and Maini (1989) modified the Stone I model to address two limitations. First, the measurements of two-phase oil–gas relative permeability are not always done at connate water saturation and, second, the measured values of $k_{row,max}$ and $k_{rog,max}$ are not equal. Their revised model is given as:

$$k_{ro} = S_{onor} \frac{k_{row}}{k_{row,max}(1-S_{wnor})} \frac{k_{rog}}{k_{rog,max}(1-S_{gnor})} \frac{k_{rog,max}S_{gnor}+k_{row,max}S_{wnor}}{1-S_{onor}} \quad (2.39)$$

2.2.3.8 Husted and Hansen (1995)

Husted and Hansen (1995) incorporated all six residual values from three two-phase experiments in their model, given below as:

$$k_{ro}(S_{omnx}) = \frac{S_w}{S_w+S_g} k_{row}(S_{omnx}) + \frac{S_g}{S_w+S_g} k_{rog}(S_{omnx}) \quad (2.40)$$

Oil saturation is normalized between the values S_{omn} and $S_{omnx.}$

$$S_{omnx} = \frac{S_o-S_{omn}}{S_{omx}-S_{omn}} \quad (2.41)$$

$$S_{omn} = \frac{S_wS_{orw}+S_gS_{org}+S_{org}S_{orw}(S_o-1)}{S_g(1-S_{orw})+S_w(1-S_{org})} \quad (2.42)$$

$$S_{omx} = \frac{S_wS_{grw}+S_gS_{wrg}+S_{gor}S_{wro}(S_o-1)}{S_g(1-S_{wro})+S_w(1-S_{gro})} \quad (2.43)$$

Other available models can be found elsewhere (Naar and Wygal, 1961; Fayers and Matthews, 1984; Moulu et al., 1997, Balbinski et al., 1997; Blunt, 1999).

2.3 Parameter Estimation

The history matching or parameter estimation technique is a sequence by which input description parameters are altered to reach an acceptable agreement between model results and observations (e.g., differential pressure and production data) (Coats, 1987).

There are several publications in the literature that applied history matching to estimated two-phase relative permeability from two-phase displacement or centrifuge experiments.

Archer and Wong (1973) first discussed history matching for measuring two-phase relative permeability data. Relative permeability data was manually adjusted to obtain a match to the production behavior of displacement experiments. Similar approaches examined by Sigmund and McCaffery (1979), Batycky et al. (1981), Qadeer et al. (1988), Jennings et al. (1988), and Fassihi (1989) indicated that the history-matching approach was more accurate than the Johnson-Bossler-Naumann (JBN) technique. Kerig and Watson (1986; 1987), and Watson et al. (1988) suggested representing two-phase relative permeabilities via spline functions to obtain a higher quality of fit. In order to shorten the time of history matching, Hyman et al. (1991; 1992) and Ohen et al. (1991) used relative permeability expressions suggested by Brooks and Corey (1966) to define a procedure for the extrapolation of the behavior of the experiment. Other interesting advances in two-phase relative permeability estimation with parameter estimation can be found in MacMillan (1987), Lai and Brandt (1988), Civan and Donaldson (1989), and Udegbunam (1991).

In contrary to two-phase systems, few studies in the literature have addressed parameter estimation techniques in three phase systems. Virnovsky et al. (1996) described a one-dimensional three-phase simulator to interpret steady state flow conditions and, hence, estimate three-phase relative permeability data. The simulator was validated with generic data. Hicks and Gardner (1996) estimated three-phase relative permeability of a water/benzyl alcohol/ decane system with parameter estimation. A numerical simulator was developed based on wave theory (or coherence theory) to model horizontal one

dimensional three-phase fluid displacements. Nordtvedt et al. (1997) proposed B-spline functions as a flexible representation of three-phase relative permeability for history matching purposes. Chavent et al. (1999) used synthetic data to investigate the feasibility of estimating three-phase relative permeability data. Quasi-Newton optimization was found to be a strong tool in obtaining satisfactory relative permeability data. Lichiardopol (2009) used EnKF to estimate three-phase relative permeability data from synthetic production data from before and after the moment of water breakthrough. It was shown that accuracy depends on the initial estimates of three-phase relative permeability data. Li (2011) also obtained satisfactory results with synthetic field data using an Ensemble-based history matching technique. Shahverdi et al. (2011) used a Generic Algorithm and quadratic B-Spline representation to obtain three-phase relative permeability of a light oil system.

2.4 Chapter Summary and Statement of Problem

Reliable three-phase relative permeability data is essential in the numerical simulation of different enhanced oil recovery techniques, such as Water Alternate Gas injection (WAG), Cyclic Steam Stimulation (CSS), gas injections, in-situ combustion, Surfactant flooding, Steam Assisted Gravity Drainage (SAGD) process, Gas Assisted Gravity Drainage (GAGD) process, and CO_2 geological sequestrations in depleted reservoirs.

Three-phase relative permeability data based on steady state experiments, as most reliable data, are scarce due to the tedious and time-consuming nature of the procedure. Although the unsteady state technique is faster and more convenient than the steady state

technique, the validity of the three-phase relative permeability based on the unsteady technique is questionable, and, requires further investigation. Probabilistic models based on two-phase relative permeability offer another alternative to the steady state technique. Although several models have been developed, predicted three-phase relative permeability data is still not consistent with that from steady state experiments. The application of probabilistic models in modern numerical simulators is also in question given that predicted three-phase relative permeability data are routinely manipulated to improve simulation outputs.

Parameter estimation has been shown to be a strong tool in estimating two-phase relative permeability data as it produces more acceptable results than the Johnson-Bossler-Neumann (JBN) technique. Compared to two-phase studies, few studies have applied parameter estimation techniques for three-phase systems. Most of the available studies use synthetic data to investigate the feasibility of this technique in estimating three-phase relative permeability data.

Three-phase relative permeability data for heavy oil systems has not been investigated. All studies considered in this chapter use kerosene, alcohols, condensates, and very light oil as the oil phase in their research. For several decades, this kind of data has been fed into commercial numerical simulators to predict production performance of enhanced heavy oil recovery projects without any consideration of the effect on heavy oil viscosity.

The purpose of this research is to experimentally and numerically investigate three-phase relative permeability data in heavy oil systems. A procedure is proposed to obtain all relative permeability isoperms for heavy oil systems. A series of two- and three-

phase dynamic displacement experiments were conducted in different temperature, oil viscosity, and gas phase conditions. A fully implicit one-dimensional three-phase numerical simulator was developed to interpret the experiments. Following the verification of the results using steady state experiments, the effects of oil viscosity, temperature, and different gas phase on the shape of isoperms was investigated.

CHAPTER 3

EXPERIMETAL SETUPS AND MATERIAL

3.1 Introduction

A high-pressure experimental apparatus and data acquisition system was designed to conduct the following tests:

- Two-phase heavy oil/water displacement experiment
- Two-phase heavy oil/gas displacement experiments
- Three-phase displacement experiments
- Three-phase steady state experiment

As this study aims to investigate the effect of temperature on relative permeabilities data, all experiments were conducted at constant temperature. It was designed to mimic the conditions found in most Canadian reservoirs. Berea sandstone was selected as porous media, while brine, heavy oil, carbon dioxide, and methane were used as fluids.

3.2 Experimental Setup

Three different experimental setups were used to perform multi-phase (two- and three-phase) steady and unsteady state experiments. Schematic diagrams of each of these experiments are presented in Figures (3.1), (3.2), and (3.3), respectively. Images of experimental setup and major components are presented in Appendix A.

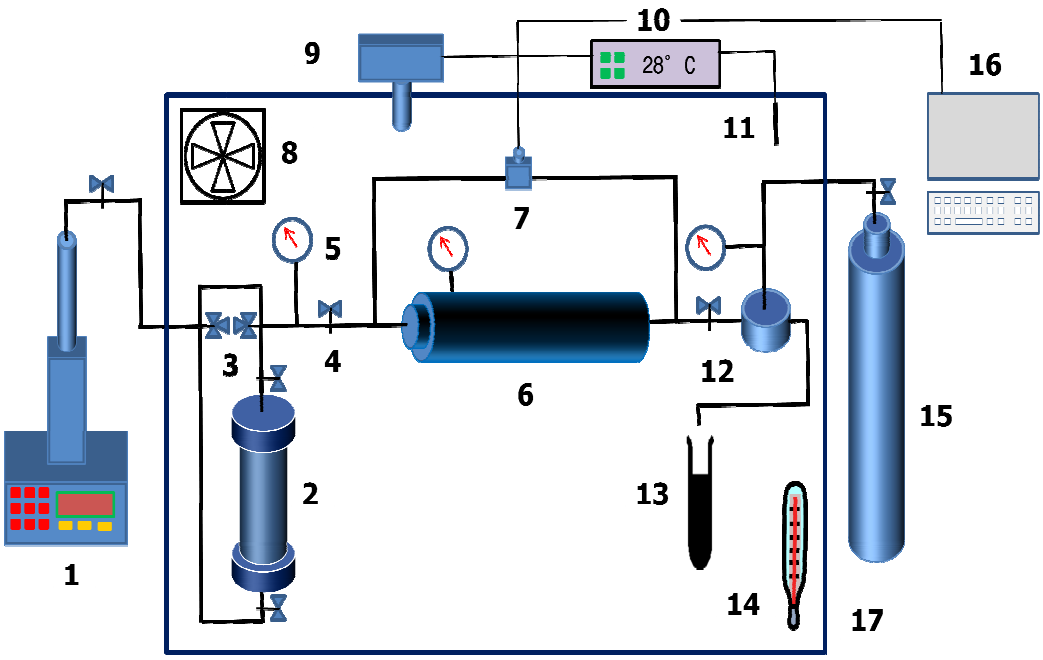

Figure 3.1: Schematic diagram of experimental setup for heavy oil / water displacement experiments.

1. Syringe pump
2. Transfer cylinder
3. Three-way valve
4. Two-way valve
5. Pressure gauge
6. Core holder
7. Pressure transducer
8. Fan
9. Heat gun
10. Temperature controller
11. Temperature probe
12. Back pressure regulator
13. Test tube
14. Thermometer
15. Nitrogen Cylinder
16. Computer
17. Air bath

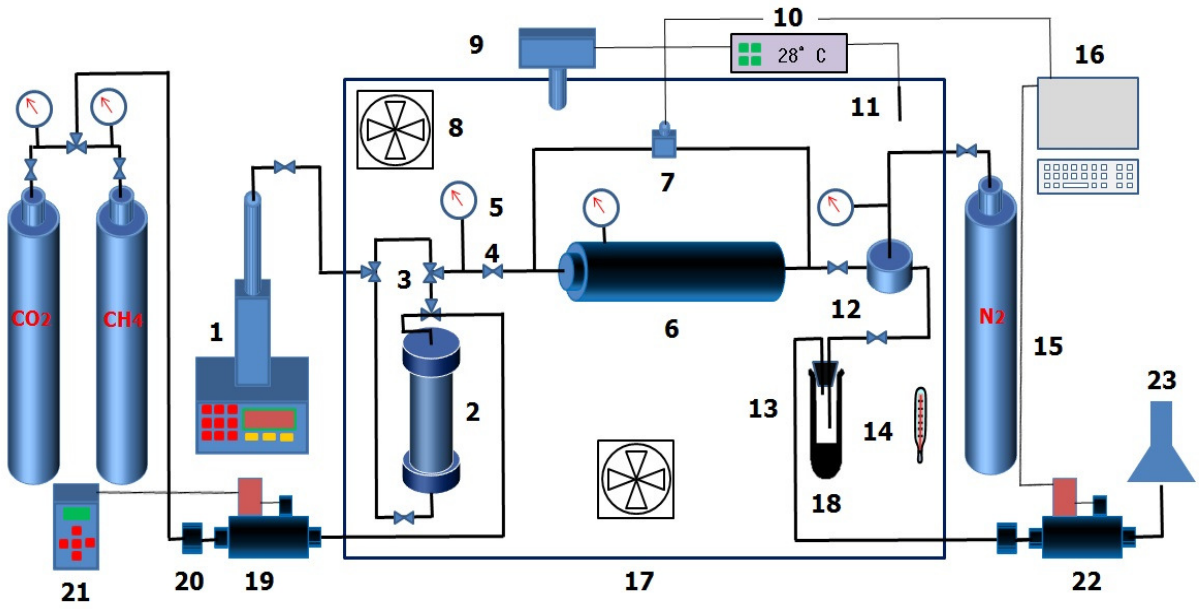

Figure 3.2: Schematic diagram of the setup for two-phase (heavy oil / gas) and three-phase displacement experiments.

1. Syringe pump	2. Transfer cylinder	3. Three-way valve
4. Two-way valve	5. Pressure gauge	6. Core holder
7. Pressure transducer	8. Fan	9. Heat source
10. Temperature controller	11.Temperature probe	12. Back pressure regulator
13. Test tube	14. Thermometer	15. Nitrogen Cylinder
16. Computer	17. Air bath	18. Separation Tube
19. Gas Flow Controller	20. Gas Filter	21. Control Module
22. Gas Flow Meter	23. Ventilation hood	

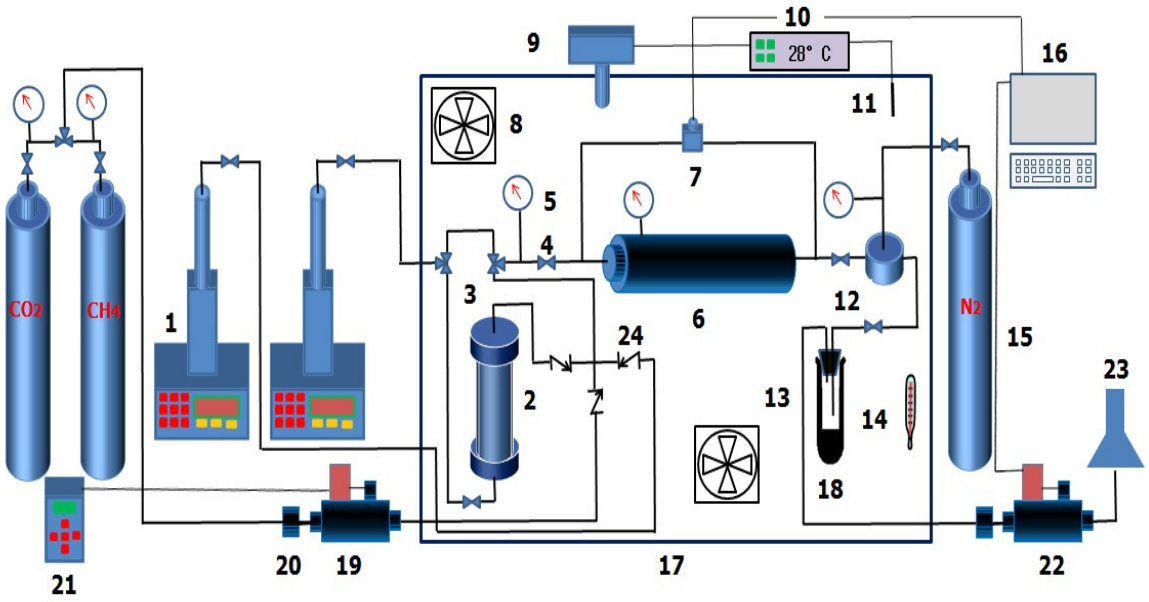

Figure 3.3: Schematic diagram of the setup for three-phase steady state experiments.

1. Syringe pump	2. Transfer cylinder	3. Three-way valve
4. Two-way valve	5. Pressure gauge	6. Core holder
7. Pressure transducer	8. Fan	9. Heat source
10. Temperature controller	11.Temperature probe	12. Back pressure regulator
13. Test tube	14. Thermometer	15. Nitrogen Cylinder
16. Computer	17. Air bath	18. Separation Tube
19. Gas Flow Controller	20. Gas Filter	21. Control Module
22. Gas Flow Meter	23. Ventilation hood	24. Check Valve

The main elements of the setups are a syringe pump, gas flow controller, gas flow meter, core holder, transfer cylinder for injecting oil, temperature controlling system, back pressure regulator, and pressure transducer system.

3.2.1 Core holder

All experiments were conducted using a high pressure, 1-inch triaxial-type TEMCO holder (TEMCO-TCHR5000). This is a typical hydrostatic core holder, as depicted in Figure (A-2), with two steel end plugs on two sides and a rubber sleeve inside to hold core samples. This core holder was designed for gas and liquid permeability testing and waterflooding experiments. The radial pressure applied by injecting water into the annulus space of the core holder shows a simulation of reservoir overburden pressure. On top of the core holder, there was a port for a high pressure gauge to monitor confining pressure.

3.2.2 Fluid injection system

The fluid injection system consisted of a pump, a transfer cylinder, tubing flow lines, and Swagelok-type autoclave valves. The pump is an ISCO 500D (D Series with flow accuracy of 0.5% of setpoint) syringe pump, shown in Figure (A-3). It had a digital controller front panel. Flow rate, flow pressure and operating mode could be controlled by user input. In this research, the pumps were operated in constant flow rate mode. Brine injection was performed directly from the syringe pump, except in the case of heavy oil injection, where a transfer cylinder was used.

3.2.3 Pressure transducer system

The Validyne UPC2100 (Total system error 0.02%) data acquisition system was responsible to receive and record signals from a pressure transducer. Pressures from the inlet and outlet of the core holder were introduced to both sides of a diaphragm inside the pressure transducer. The pressure transducer sends an electronic signal proportional to the pressure of the computer. With a calibration, recorded signals can be converted back to the pressure values.

3.2.4 Fluid collection system

A low flow rate EQUILIBAR Back Pressure Regulator (BPR) (precision within 0.5%) was mounted on the fluid discharge line to control the flow. The BPR operated via a balanced pressure system. In this system, nitrogen, at the desired set point pressure, was injected into the dome of the regulator. This pressure restricts the fluid flow from the process. Once the fluid flow pressure exceeds the preset dome pressure, the metal diaphragm inside the BPR will flex so as to allow fluids to flow and to maintain the system pressure. Effluent fractions were collected in the graduated centrifuged tubes and were centrifuged for fractional and recovery analysis.

3.2.5 Temperature controlling system

A MAKITA heating gun (Model HG1100) was used as the heating source. It is depicted in Figure (A-4). In order to keep temperature constant, a temperature controller (COLE PARMER 89000-00 with accuracy within 0.4°C) measures the temperature inside the airbath via a probe in order to periodically turn off/on the heat gun. Two fans have

been used to circulate air inside the airbath. This system has been successfully tested for temperatures up to 60°C.

3.2.6 Gas injection system

Gas injection was conducted using a custom-made precise HIGH-TECH BRONKHORST (accuracy within 0.5%) gas flow controller. This controller is visualized in Figure (A-5). It was fed with a constant pressure of 700 psi from a carbon dioxide cylinder so as to accurately inject gas at constant rates. This gas flow controller is capable of injecting any gas at constant flow rate up to 100 mln/min (normal milliliter per minute) and can function up to a maximum pressure of 4000 psi.

3.2.7 Separation system

A resin-sealed separator, shown in Figure (A-6), was used to separate liquid effluent from the produced gas. Produced oil and water fractions that were collected in the graduated tubes were then centrifuged for fractional flow analysis. Gas effluent was passed through a COLE PARMER (accuracy within 1-2%) gas flow meter, shown in Figure (A-7), to record the gas flow rate out of the core holder.

3.3 Core Properties

All experiments were performed in Berea consolidated sandstone. The basic rock properties are listed in Table (3.1). Absolute permeability of the brine was measured at 28°C after plotting differential pressures versus flow rates and applying Darcy's law, as visualized in Figure (3.4). It should be noted that absolute permeability and porosity presented in Table (3.1) are average values after several measurements (error less than 3%).

Table 3.1: Basic properties of Berea core sample.

Length (cm)	29.7
Diameter (cm)	2.54
Dry weight (g)	292.5
Saturated weight (g)	321.8
Bulk volume (cm^3)	150.49
Pore volume (cm^3)	29.01
Porosity (%)	19.27
Absolute Permeability (Darcy)	1.56

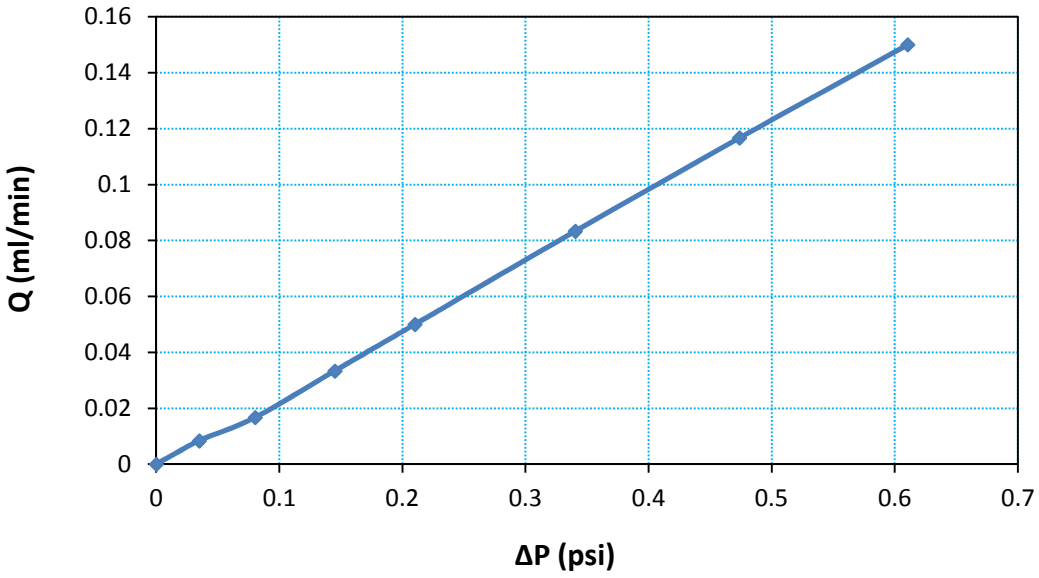

Figure 3.4: Linear relationship between flow rate and differential pressure in absolute permeability measurement.

Porosity was measured using the vacuum saturation method described as follows:

- Dry weight of the core was measured accurately with a precision balance.
- Core was placed into the core holder; 750 psi pressure was applied as overburden pressure.
- Carbon dioxide was injected for 1 hour to remove moist left in the core.
- Core was vacuumed for 2 hours.
- Brine was exposed to the vacuumed core for 2 hours.
- Saturated core was removed and weighted.
- Difference between the dry and saturated core was evaluated as the weight of the brine occupy the pore volume.
- Pore volume was then calculated using the density of the brine (1.0101 g/cm^3).

3.4 Fluid Properties

3.4.1 Heavy oil / water properties

Two-phase relative permeability measurements were conducted for heavy oil-water and heavy oil-gas systems. In order to prevent any chemical alteration in the core, a 1wt% NaCl in de-ionized water solution was used in all experiments as aqueous phase. Using a BROOKFIELD digital viscometer (accuracy within 1% of the range), the viscosity of the original heavy oil (API = 11) was measured to be 4338 cP at 28°C. The heavy oil was filtered and the viscosity was altered through the addition of kerosene as a diluant. Two heavy oil samples were obtained by this method (3.5wt% and 5.5wt% kerosene). The viscosity of the diluted oils and brine are plotted as function of temperature is presented in Figure (3.5).

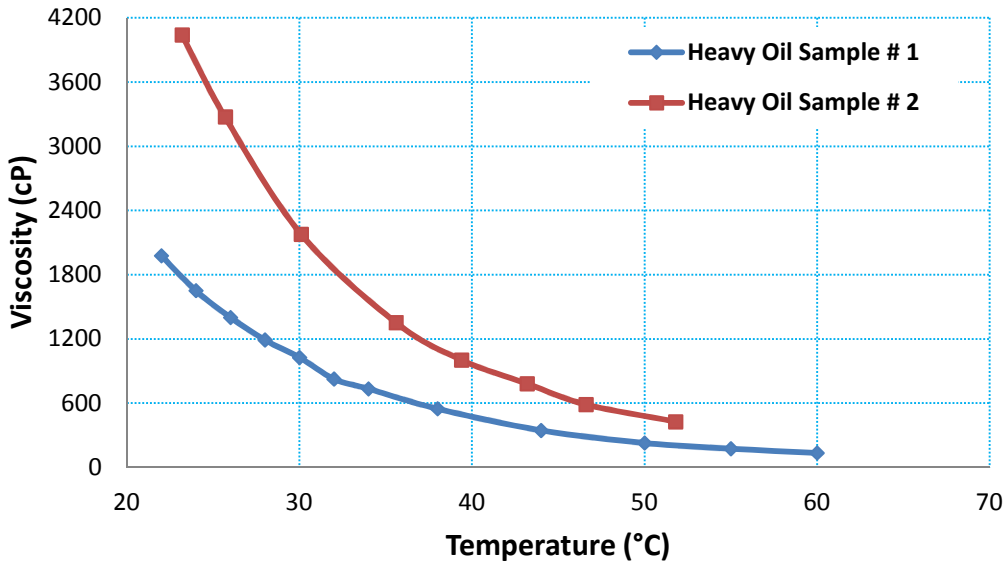

(a)

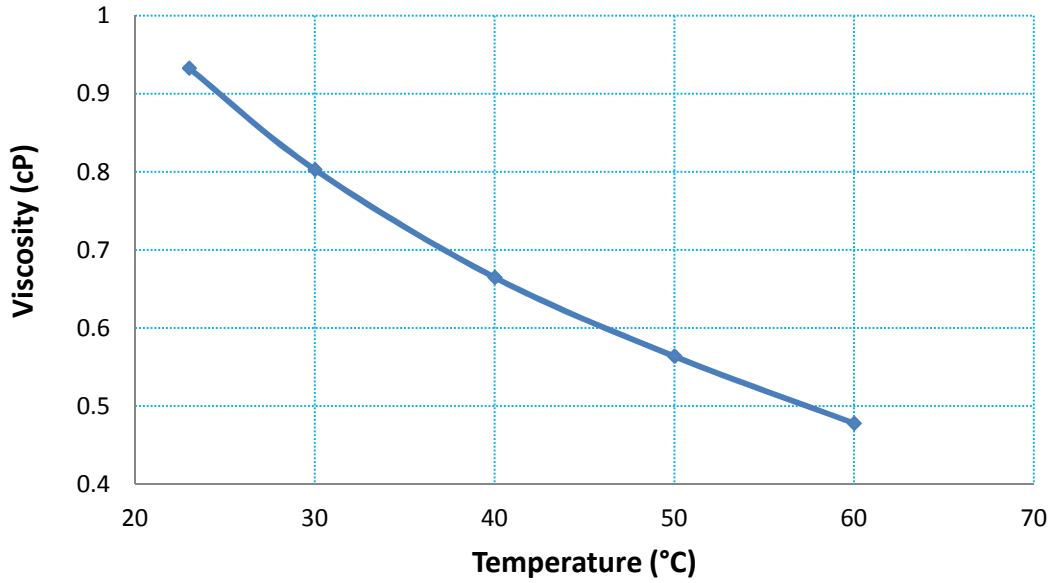

(b)

Figure 3.5: Viscosity versus temperature for a) heavy oil samples used in the experiments and b) for 1wt% NaCl water.

3.4.2 Gas properties

Carbon dioxide and methane were purchased from Praxair Canada with stated purities of 99.99% and 99.97% respectively. WINPROP module of the CMG reservoir simulator was used to obtain the gas properties. Figure (3.6) shows the viscosity and compressibility factor versus pressure at three different temperatures (28°C, 40°C, and 52°C) of carbon dioxide and methane, respectively. These two figures will also be used later to numerically simulate the three-phase displacement experiments.

3.5 Experimental Procedures

3.5.1 Core cleaning

Before each experiment, the core was carefully cleaned in order to completely remove all residual liquids from previous tests. After each test, the core was cleaned by flushing with 10 PVs of kerosene, followed by 10 PVs of toluene. The core was hot air dried by exposing it to a heating fan for 36 hours at a temperature of 60ºC. Before starting each test, porosity and permeability were measured to ensure that the miscible cleaning process did not alter the properties of the core. The core was then flushed with 20 pore volumes of brine at a very low rate of 0.05 ml/min to restore any wettability alteration by miscible cleaning.

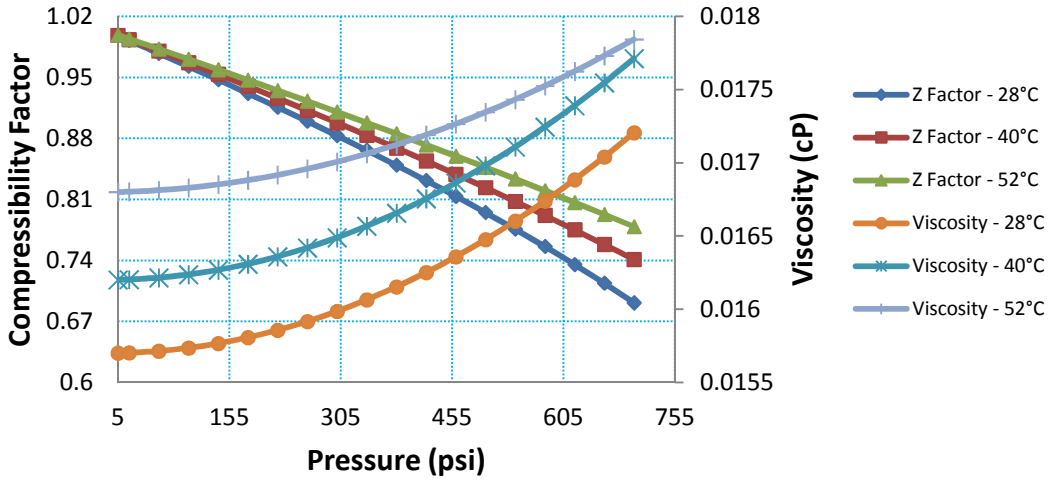

(a)

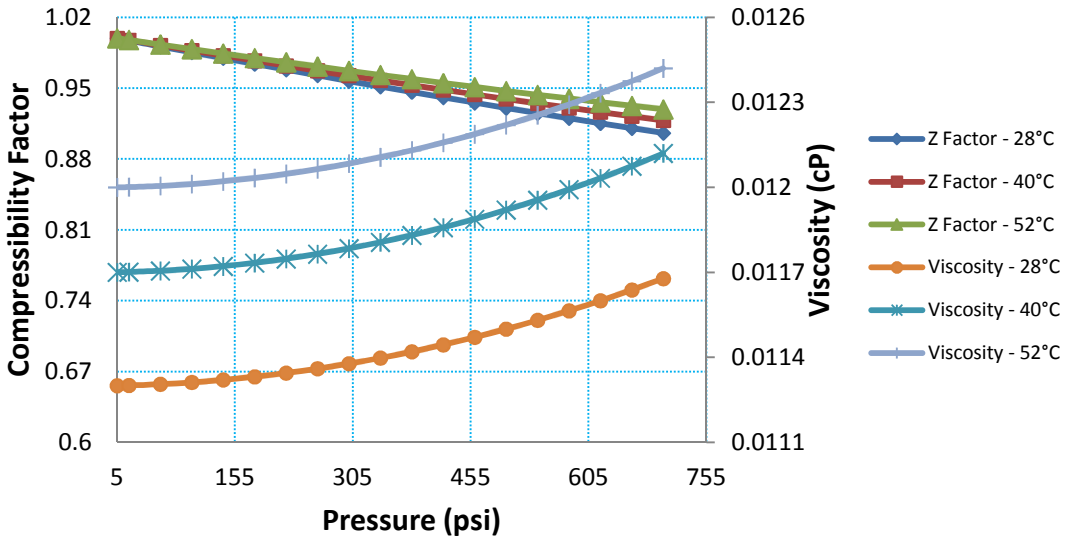

(b)

Figure 3.6: Viscosity and compressibility factor versus pressure at different temperature for a) carbon dioxide and b) methane (from CMG-WINPROP).

3.5.2 Two-phase heavy oil / water displacement experiment

The following procedure was carried out for each of the heavy oil / water displacement experiments using the setup previously shown in Figure (3.1):

- The clean, dried core was first weighed and then placed into the core holder.
- After applying 750 psi overburden pressure, carbon dioxide gas was injected at a high rate for one hour to remove any remaining toluene, from the cleaning process, in the core.
- The desired temperature was set on the temperature controller and the transfer cylinder was filled with heavy oil and allowed to equilibrate for 24 hours.
- The pressure transducer was calibrated by an ISCO syringe pump at constant pressure mode.
- The core was vacuumed for two hours and saturated with brine to measure porosity and to establish the initial conditions of 100% brine saturation.
- Back pressure was maintained by an EQUILIBAR Precision back pressure regulator (BPR) set to 150 psi.
- The core was aged using 20 PVs of brine at a low rate of 0.05 ml/min to restore any wettability alteration by miscible cleaning.
- Absolute permeability was measured by brine injection at several different flow rates.
- Assuring there was no change in the porosity and absolute permeability, oil was injected at a constant rate of 0.1 ml/min via a transfer cylinder.

This rate is equivalent to 1 ft/day of a common flow rate in field scale waterflooding projects.

- Oil injection was continued until irreducible water saturation was established.
- During oil injection, effluent fractions were collected in the graduated tubes while recording time.
- Oil injection was then stopped and the core assembly was given 12 hours in order to allow the pressure gradient along the core to reach equilibrium.
- In the next phase of the experiment, brine was injected at a constant rate of 0.1 ml/min until residual oil saturation is achieved.
- Graduated test tubes were centrifuged for fractional and recovery analysis.

3.5.3 Two-phase heavy oil / gas displacement experiment

The procedure for two-phase heavy oil / gas displacement experiment is almost the same as that of a heavy oil / water system, as previously shown in Figure (3.2). A precise BRONKHORST gas flow controller, given in Figure (A-5), was used to accurately inject gas (11 mln/min) into the core. A resin-sealed separator, seen in Figure (A-6), was used to separate liquid effluent from the produced gas. Gas effluent was passed through a COLE PARMER gas flow meter, seen in Figure (A-7), to record the gas flow rate out of the core holder.

3.5.4 Three-phase displacement experiment

The idea behind a three-phase displacement experiment is to permit simultaneous flow of three phases in the porous media over a wide range of saturations. This can be

achieved by injecting one phase (gas) into the core saturated with other phases (heavy oil and water). The following procedure was used to perform a three-phase displacement experiment:

- The clean, dried core was first weighed and then placed into the core holder.
- After applying an overburden pressure of 750 psi, carbon dioxide gas was injected at a high rate for one hour to remove any remaining toluene, from the cleaning process, in the core.
- The desired temperature was set on the temperature controller and the transfer cylinder was filled with heavy oil and allowed 24 hours to equilibrate.
- The pressure transducer was calibrated using an ISCO syringe pump at constant pressure mode.
- The core was vacuumed for two hours, and saturated with brine to measure porosity and to establish the initial conditions of 100% brine saturation.
- Back pressure was maintained by an EQUILIBAR Precision back pressure regulator (BPR) set to 150 psi.
- The core was aged using 20 PVs of brine at a low rate of 0.05 ml/min to restore any wettability alteration that may have occurred by miscible cleaning.
- Absolute permeability was measured by brine injection at several different flow rates.

- Assuring there was no change in the porosity and absolute permeability, oil was injected at a constant rate of 0.1 ml/min via a transfer cylinder. This rate is equivalent to 1 ft/day of a common flow rate in field scale waterflooding projects.
- Effluent fractions were collected in the graduated tubes.
- Oil injection was continued until establishing the desired heavy oil and water saturation through the core. It should be mentioned that, although, in other studies (Sarem, 1966) the oil phase injection was stopped immediately after breakthrough, it was decided to stop oil injection a few milliliters before breakthrough to allow more water phase remains in the core.
- Oil injection was then stopped and the core assembly was given 12 hours to allow the pressure gradient along the core to reach equilibrium.
- In the next phase of the experiment, carbon dioxide was injected via a HIGH-TECH BRONKHORST gas flow controller at a constant rate of 5 mln/min.
- A COLE PARMER gas flow meter records gas effluent while liquid fractions were collected in graduated test tubes.
- Graduated test tubes were centrifuged for fractional and recovery analysis.

3.6 Chapter Summary

As this study aims to extensively investigate two- and three-phase relative permeability data, three different experimental setups were designed to conduct a series

of two-phase, three-phase, unsteady state, and steady state experiments. All experiments were carried out at constant temperature in order to study the effect of temperature on relative permeabilities. Porous media and fluids were selected that match those of typical Canadian reservoirs. Regardless of the number of technically failed experiments, 22 successful experiments were performed in this study. Tables (3.2) and (3.3) showcase the results of each of the tests conducted in this work.

Table 3.2: Summary of three- phase experiments.

State	Temperature	Oil Sample	Gas Phase
Unsteady State	28°C	Sample 1	CO_2
Unsteady State	40°C	Sample 1	CO_2
Unsteady State	52°C	Sample 1	CO_2
Unsteady State	28°C	Sample 2	CO_2
Unsteady State	28°C	Sample 1	CH_4
Unsteady State	40°C	Sample 1	CH_4
Unsteady State	52°C	Sample 1	CH_4
Unsteady State	28°C	Sample 2	CH_4
Steady State	28°C	Sample 1	CO_2
Steady State (different flow rate)	28°C	Sample 1	CO_2

Table 3.3: Summary of two- phase displacement experiments.

Fluids	Temperature	Oil Sample
Heavy Oil / Water	28°C	Sample 1
Heavy Oil / Water	40°C	Sample 1
Heavy Oil / Water	52°C	Sample 1
Heavy Oil / Water	28°C	Sample 2
Heavy Oil / CO_2	28°C	Sample 1
Heavy Oil / CO_2	40°C	Sample 1
Heavy Oil / CO_2	52°C	Sample 1
Heavy Oil / CO_2	28°C	Sample 2
Heavy Oil / CH_4	28°C	Sample 1
Heavy Oil / CH_4	40°C	Sample 1
Heavy Oil / CH_4	52°C	Sample 1
Heavy Oil / CH_4	28°C	Sample 2

CHAPTER 4

TWO-PHASE RELATIVE PERMEABILITY WITH JBN TECHNIQUE

4.1 Introduction

This chapter investigates application of the Johnson-Bossler-Naumann (JBN) (Johnson, 1959) technique in order to calculate two-phase relative permeabilities using two-phase displacement experiments. As described in the previous chapter, a series of two-phase coreflood tests were conducted at different temperatures (28ºC, 40ºC, 52ºC) and, as well, at different oil viscosities and gas phases (carbon dioxide and methane). The effects of such parameters on relative permeability curves of heavy oil / water, heavy oil / carbon dioxide, and heavy oil / methane systems were studied.

4.2 JBN Technique

Although unsteady state relative permeability measurements can be made faster than steady state measurements, there are more calculations involved in the unsteady-state technique. The theory was first developed by Buckley and Leverett (1942) and, later, extended by Weldge (1952) for general use in calculating two-phase relative permeability under unsteady-state conditions (Amyx et al., 1988). A summary of the JBN technique for waterflooding process is given below:

Combining Darcy's law with capillary pressure in differential form gives the following equation:

$$f_{w2} = \frac{1+\frac{k_o}{q_t \mu_o}\left(\frac{\partial P_c}{\partial x} - g.\Delta\rho.sin\theta\right)}{1+\frac{k_o \mu_w}{k_w \mu_o}} \tag{4.1}$$

where:

f_{w2} = fractional water in the outlet stream

q_t = superficial velocity of total fluid leaving the core

θ = angle between direction *x* and horizontal

$\Delta\rho$ = density difference between displacing and displaced fluids

In the case of horizontal flow and negligible capillary pressure,

$$S_{w,av} - S_w = f_{o2}.Q_w \tag{4.2}$$

where the subscript 2 denotes the outlet end of the core and;

$S_{w,av}$ = average water saturation

Q_w = cumulative water injected in pore volumes

f_{o2} can be obtained from the slope of a plot of Q_w as a function of $S_{w,av}$.

In addition, from the definition of fractional flow, the relative permeability ratio $\frac{k_{rw}}{k_{ro}}$ can be obtained as:

$$f_{o2} = \frac{1}{1+\frac{\mu_o k_{rw}}{\mu_w k_{ro}}} \tag{4.3}$$

This method was extended as the JBN method to obtain individual phase relative permeability from unsteady-state test data.

$$k_{ro} = \frac{f_{o2}}{\frac{d\left(\frac{1}{Q_w I_r}\right)}{d\left(\frac{1}{Q_w}\right)}} \tag{4.4}$$

$$k_{rw} = \frac{f_{w2}}{f_{o2}} \frac{\mu_w}{\mu_o} k_{ro} \tag{4.5}$$

$$I_r = \frac{(\frac{q_{wt}}{\Delta P})}{(\frac{q_{wt}}{\Delta P})_{at\ start\ of\ injection}} \tag{4.6}$$

Where I_r is called relative injectivity.

As an example, feed data for the JBN technique and, also, calculated saturations and relative permeabilities are presented in Table (4.1) for heavy oil / water at 28ºC.

Table 4.1: Relative permeability data calculated by JBN technique at 28ºC for heavy oil (sample#1)/ water.

Injected Water (PV)	Produced Oil (PV)	Differential Pressure (Psi)	Water Saturation (Fraction)	Water Relative Permeability	Oil Relative Permeability
0.502	0.318	43.887			
0.834	0.405	18.771	0.354	0.00162	0.12232
0.937	0.425	16.032	0.374	0.00174	0.11720
1.041	0.432	14.346	0.381	0.00183	0.11206
1.263	0.440	13.685	0.386	0.00194	0.09970
1.456	0.456	14.290	0.403	0.00120	0.08990
1.664	0.464	13.041	0.409	0.00211	0.08397
1.871	0.474	12.660	0.418	0.00218	0.07821
2.079	0.476	12.346	0.420	0.00225	0.07337
2.286	0.477	11.881	0.421	0.00233	0.06949
5.493	0.512	10.506	0.449	0.00294	0.04002

4.3 Two-Phase Relative Permeabilities Based on JBN Technique

Table (3.3) presents the results of eight successful two-phase displacements experiment performed at three different temperature (28ºC, 40ºC, 52ºC), using two heavy oil samples (different viscosity), in the presence of carbon dioxide and methane. With differential pressure and fractional effluent data, the JBN technique was applied to calculate heavy oil, water, and gas relative permeabilities. Average saturations were calculated using the material balance method. Attempts was made to ensure that dead volumes in the system are as low as possible so as minimize errors in the material balance calculation. Sample data and, also, detailed procedure of applying JBN technique can be found in the papers published out of this section (Akhlaghinia et al. 2013-a; Akhlaghinia et al. 2013-b).

4.3.1 Heavy oil / water systems

The procedure described previously in Sec 3.4.2 was repeated four times at different temperatures 28ºC, 40ºC, 52ºC, as well as two samples of heavy oils of different oil viscosity. Figure (4.1) shows the heavy oil and water relative permeability data at different temperature/oil samples taken by brine injection into sandstone core saturated with heavy oil at irreducible water saturation.

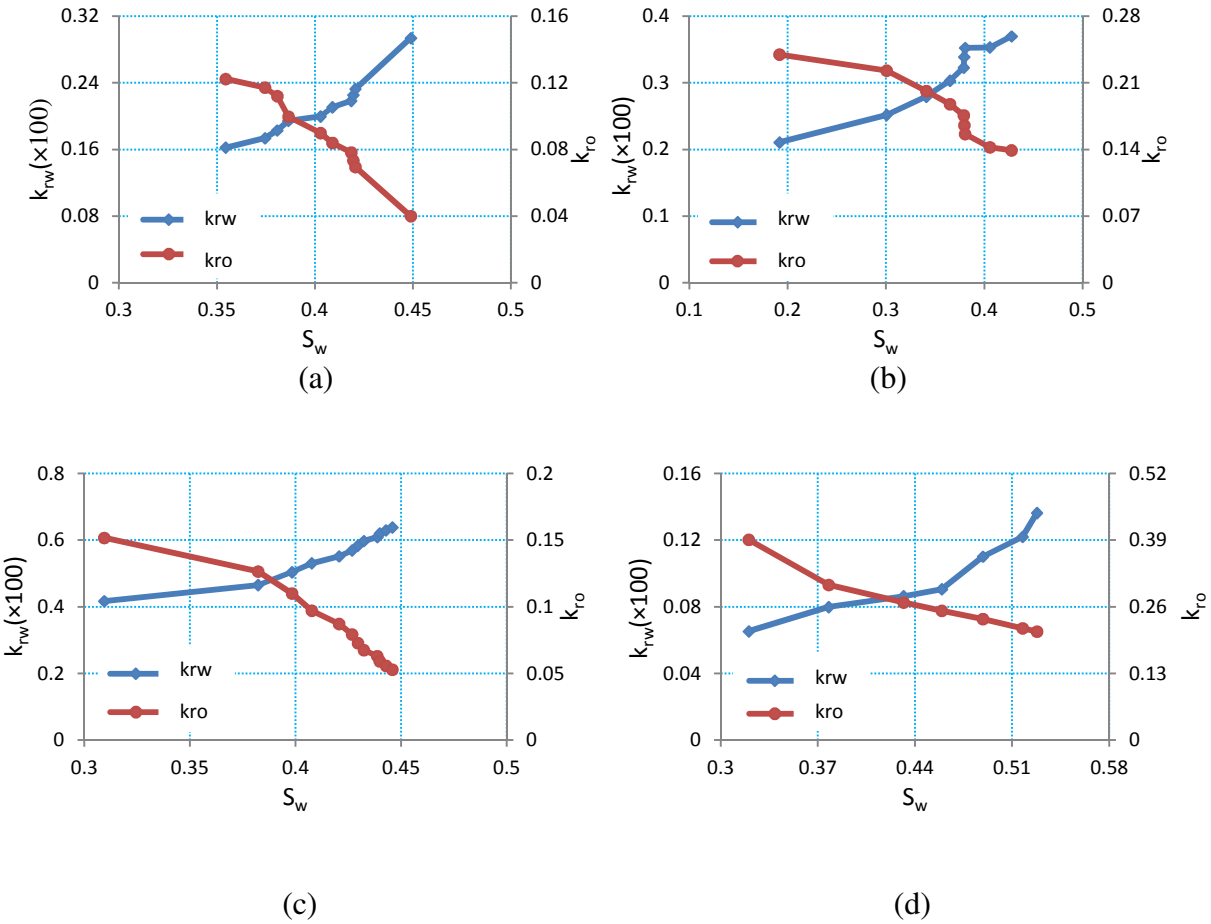

Figure 4.1: Heavy oil / water relative permeabilities; a: (T=28°C, Oil#1), b: (T=40°C, Oil#1), c: (T=52°C, Oil#1), d: (T=28°C, Oil#2).

Figure (4.2) reveals that temperature has different effects on the water and oil relative permeability curves. In the case of water relative permeability, the curves shifted upward by about 66% when temperature ranged between 28ºC to 40ºC. Almost the same increase is observed for relative permeability curves at 40ºC and 52ºC. With the same difference between these curves, it can be concluded that temperature linearly increases the water relative permeability curves. In the case of oil relative permeability curves, although a 69% increase in relative permeabilities is found between 28ºC to 40ºC, the relative permeability values decrease by about 32% when temperature ranged between 40ºC to 52°C. It can be concluded that oil relative permeability shifts up until an optimum temperature before the trend reverses as temperature increases further.

Two heavy oil / water experiments were performed at 28ºC using two different oil viscosities, with the results given in Figures (4.3-a) and (4.3-b). Heavy oil and water relative permeabilities were compared in both cases. In contrast to the effect of temperature on heavy oil / water relative permeabilities, the effect of oil viscosity, as expected, is found to be such that water relative permeability is inversely proportional to the oil viscosity for heavy oil / water systems. As one can determine from Figure (4.3-a), water is more mobile in presence of lighter oil (1174 cP) since relative permeability values are higher than those in the presence of heavier oil (2658 cP). In contrary, oil relative permeability is proportional to oil viscosity. This means that oil relative permeability increases as oil viscosity increases, as shown in Figure (4.3-b).

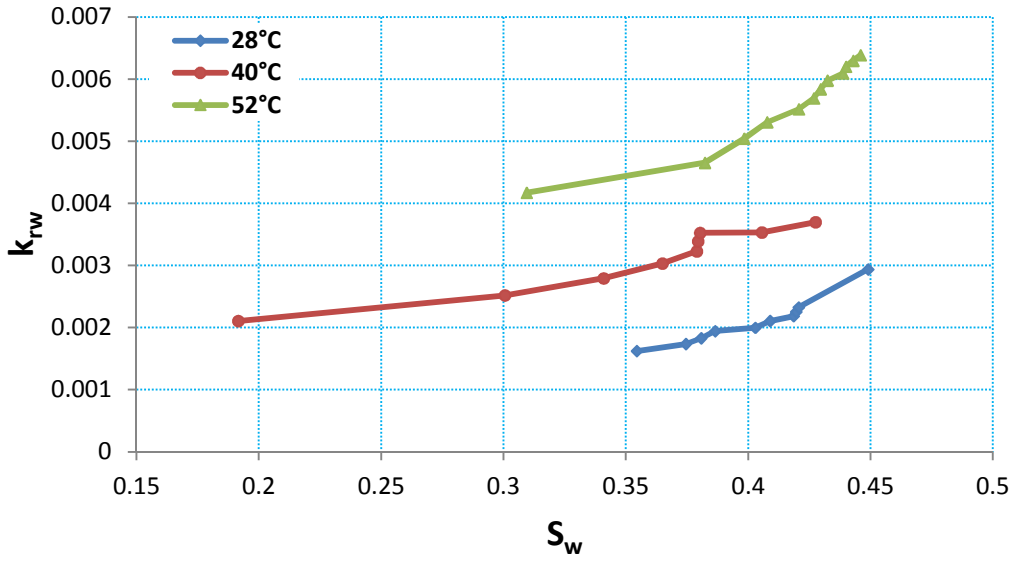

(a)

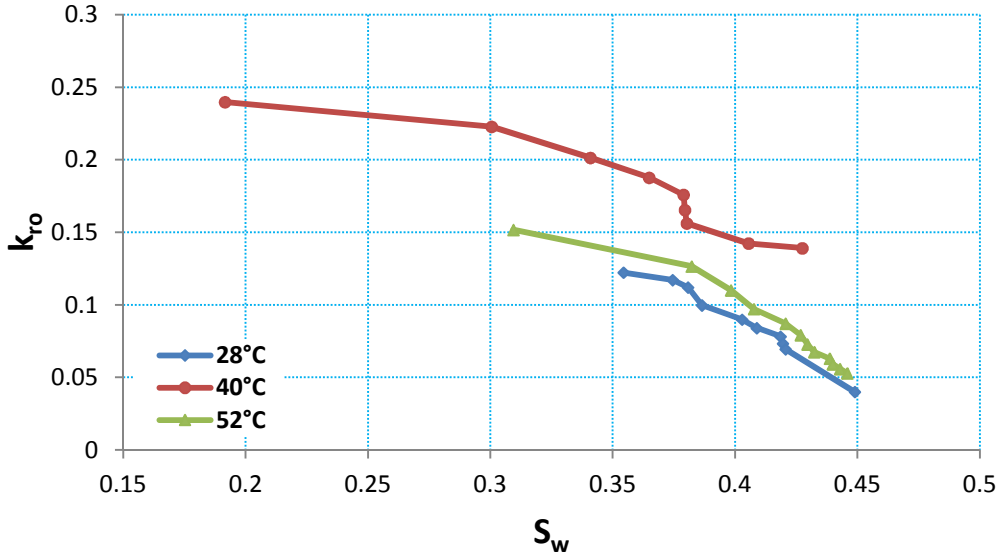

(b)

Figure 4.2: Effect of temperature on water (a) and heavy oil (b) relative permeabilities.

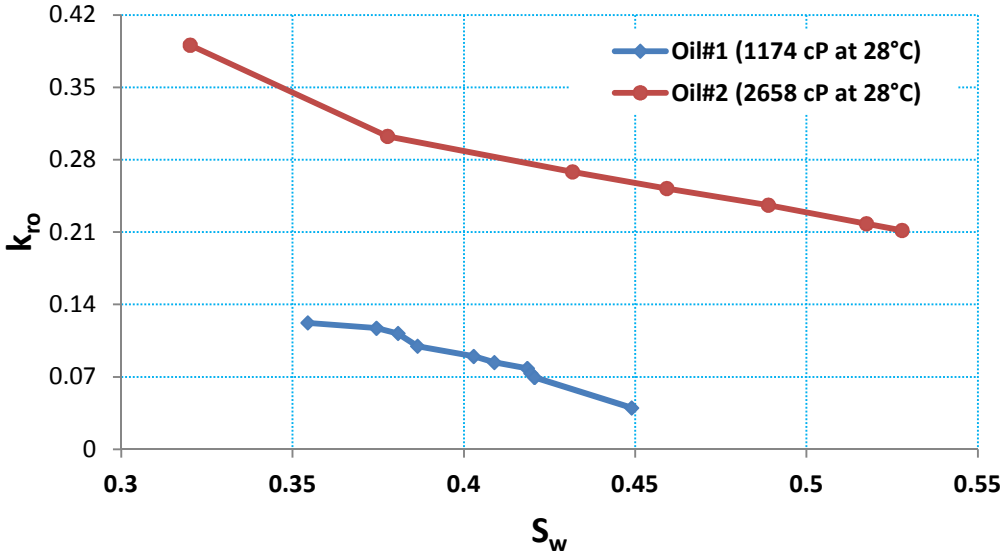

(a)

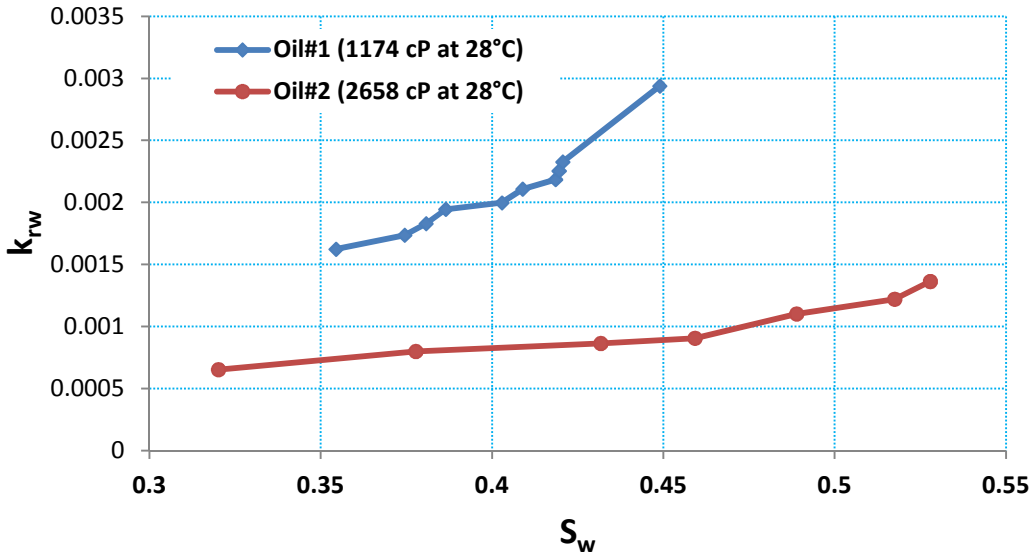

(b)

Figure 4.3: Effect of oil viscosity on water (a) and heavy oil (b) relative permeabilities.

4.3.2 Heavy oil / gas systems

The procedure mentioned above for heavy oil / water system was also repeated for heavy oil / carbon dioxide, with the results given in Figure (4.4), and heavy oil / methane, with the results given in Figure (4.5). The experimental procedure was previously described in Sec 3.4.3. The solubility of carbon dioxide and methane in heavy oil was considered negligible due to the high viscosity of the oil. Also, since gas injections were performed in short span of time (less than three hours), no sensible solution of gas in the heavy oil could occur during the experiments allows using the JBN technique to calculate relative permeabilities. Quantitative measurement of different gas solubility in heavy oil at different temperature/pressure conditions can be found elsewhere (Tharanivasan et al., 2006; Etminan, 2009; Marufuzzaman, 2010).

Heavy oil viscosity was routinely measured to ensure that no alteration in heavy oil viscosity occurs due to the probable vaporization of kerosene during the experiments. No viscosity change was observed even for the oil produced, indicating that no considerable mass transfer occurred in the cases of gas injections. Low differential pressure (up to 5 psi) across the core after breakthrough allowed assuming that both gas volume and rate do not change considerably in the core. In the case of derivative calculations, the tangent line passing through each point was taken to be the derivative in order to avoid the difficulties that had been experienced while fitting the data using conventional curve fitting techniques,

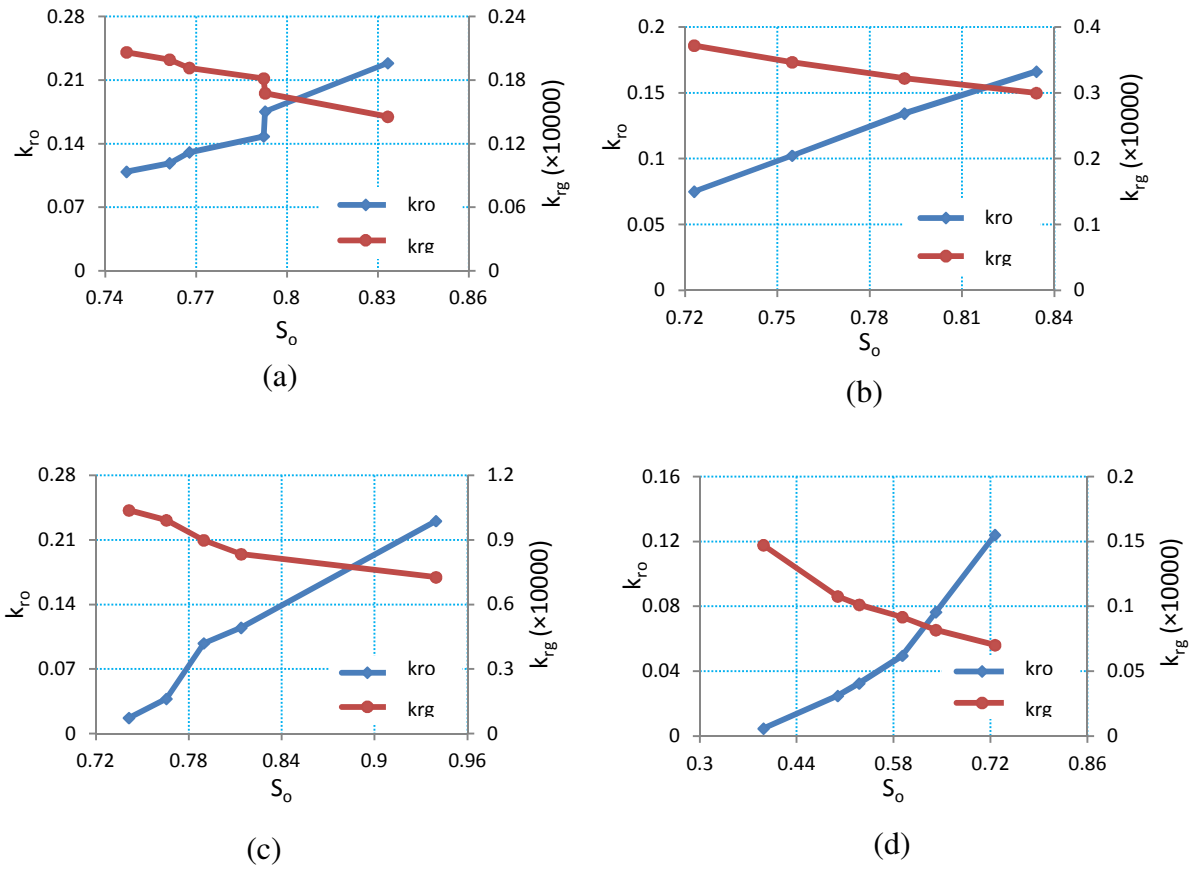

Figure 4.4: Heavy oil / CO_2 relative permeabilities; a: (T=28°C, Oil#1), b: (T=40°C, Oil#1), c: (T=52°C, Oil#1), d: (T=28°C, Oil#2).

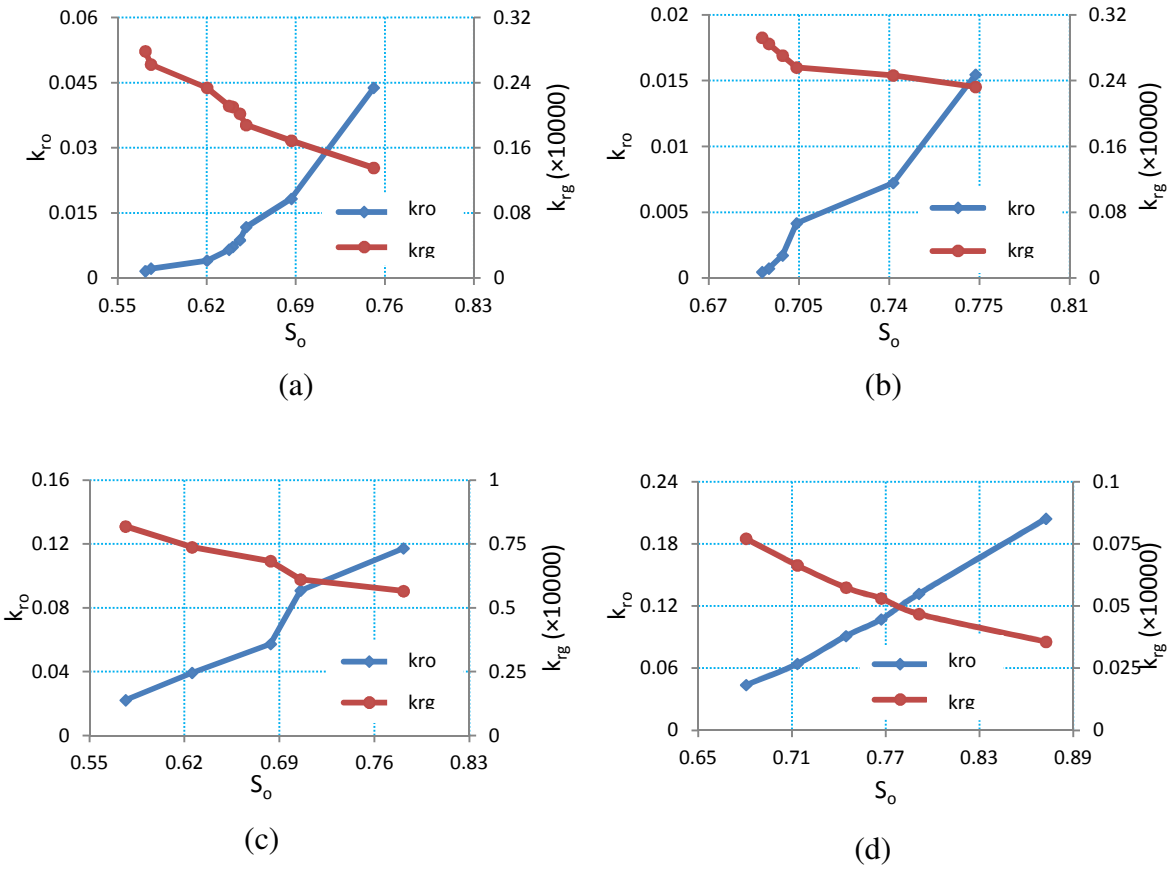

Figure 4.5: Heavy oil / CH_4 relative permeabilities; a: (T=28°C, Oil#1), b: (T=40°C, Oil#1), c: (T=52°C, Oil#1), d: (T=28°C, Oil#2).

Figure (4.6) presents the results of applying the JBN technique to heavy oil / methane and heavy oil / carbon dioxide systems. The effect of increase in temperature on both methane and carbon dioxide relative permeabilities are the same as those for water. Figures (4.6-b) and (4.6-d) indicate that as temperature increases from 28ºC to 52ºC, methane and carbon dioxide relative permeabilities increase. Unexpectedly, heavy oil relative permeability in presence of methane tends to decrease from 28ºC to 40ºC and then, as temperature further increases, it dramatically increases. This phenomenon is seen in Figure (4.6-a). This graph indicates a reversal trend of the heavy oil relative permeability by the temperature. In the case of oil relative permeability in presence of carbon dioxide, it is seen to fall as temperature climbs. This is observed in Figure (4.6-c).

The effect of oil viscosity on relative permeabilities of heavy oil / methane and heavy oil / carbon dioxide was also investigated in this study. Figure (4.7) shows that the effect of oil viscosity of heavy oil and gas (carbon dioxide and methane) relative permeabilities is exactly the same as that previously observed for heavy oil / water system. Methane, as one can see from Figure (4.7-b), and carbon dioxide, as Figure (4.7-d) shows, relative permeabilities are inversely proportional to the oil viscosity of heavy oil / gas systems. Oil relative permeability is proportional to oil viscosity such that it increases as oil viscosity increases. This is seen in Figures (4.7-a) and (4.7-b).

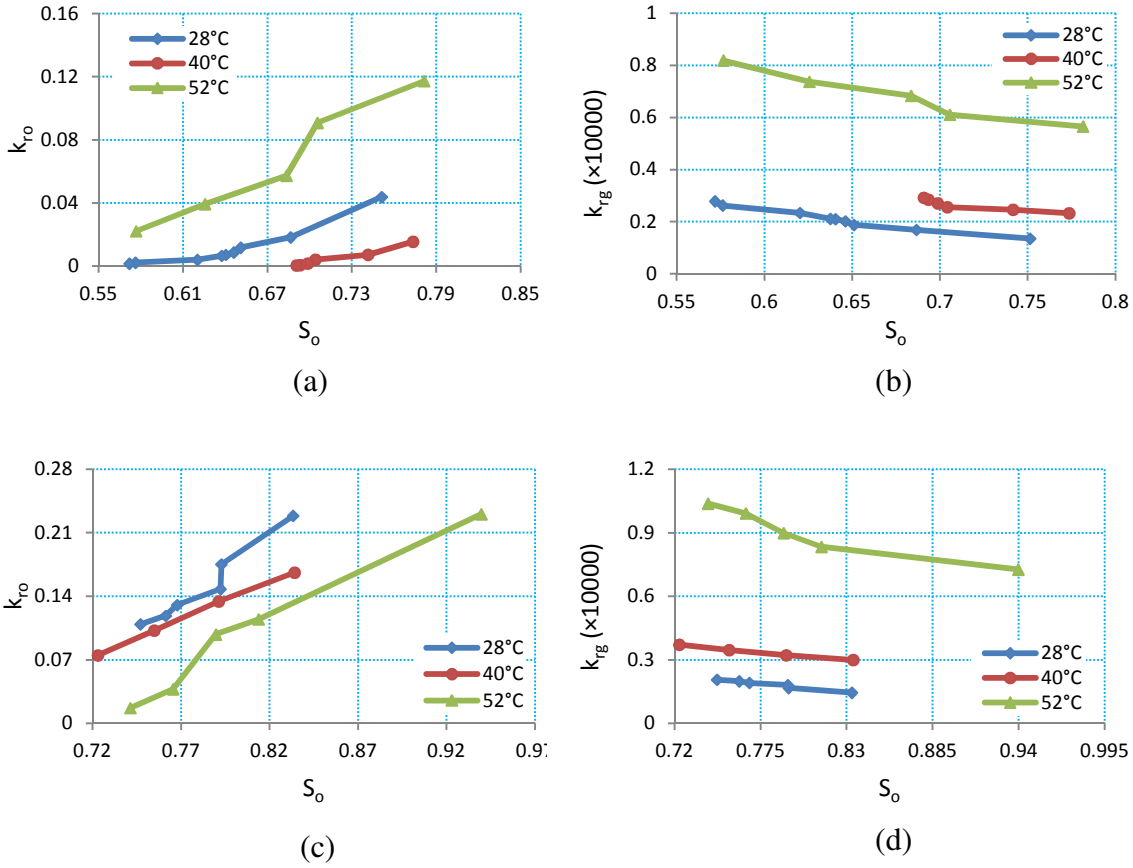

Figure 4.6: Effect of temperature on heavy oil / gas relative permeabilities; a and b (CH_4), c and d (CO_2).

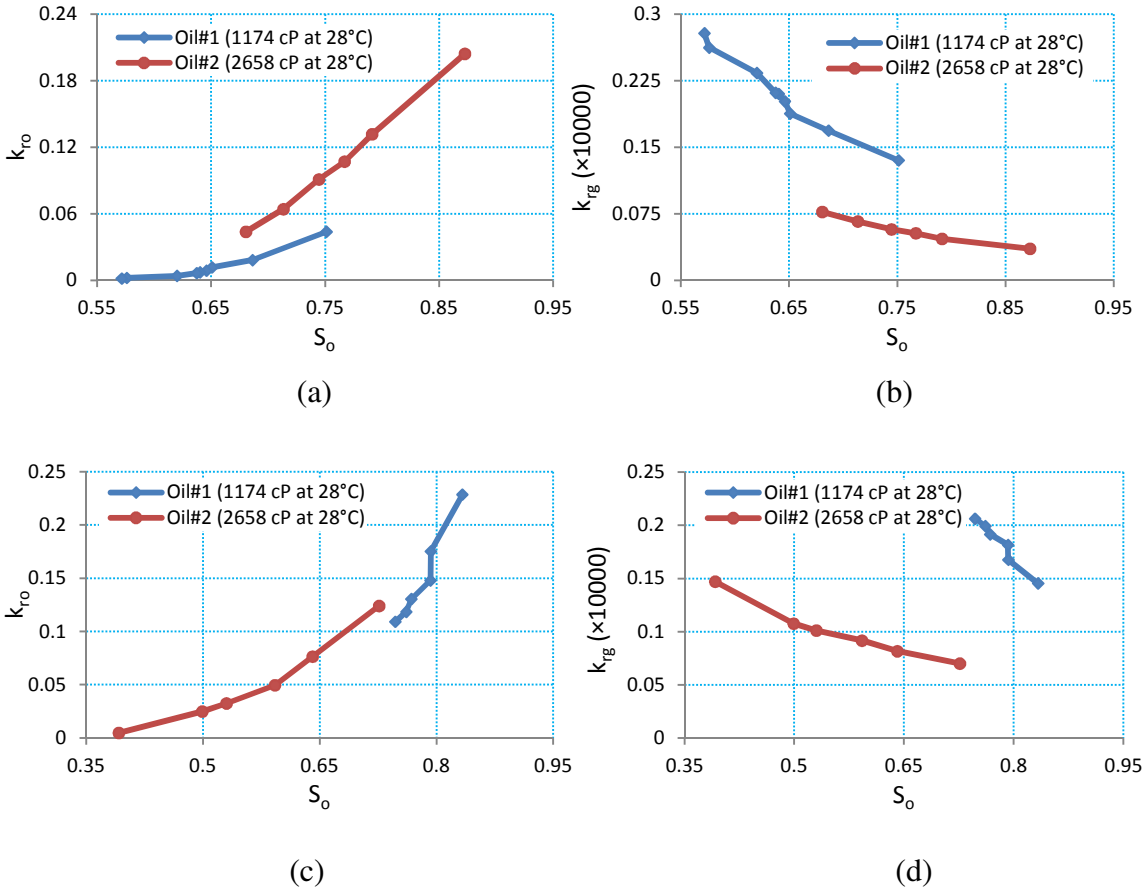

Figure 4.7: Effect of oil viscosity on heavy oil / gas relative permeabilities; a and b (CH_4), c and d (CO_2).

4.4 Chapter Summary

Two-phase unsteady state experiments were performed in order to measure heavy oil-water, heavy oil carbon dioxide, and heavy oil-methane relative permeabilities. Using fractional effluents measured with precision meters and differential pressure data records, the JBN technique was applied to calculate two-phase relative permeability in a consolidated sandstone core. A series of coreflood tests were conducted at three different temperatures (28ºC, 40ºC, and 52ºC) and using two oil samples of different viscosities. Analysis of the data obtained for heavy oil-water system show a linear increase of about 65% and 50% in water relative permeabilities when temperature ranged 28ºC to 40ºC and 40ºC to 52ºC, respectively. However, while the oil relative permeability curve shows an increase of about 70% when temperature increases from 28ºC to 40ºC, it dramatically falls by about 30%, when temperature rises from 40ºC to 52ºC. Both methane and carbon dioxide relative permeabilities increase non-linearly at higher temperatures. Oil relative permeability in presence of carbon dioxide decreases when temperature increases. In contrast, in presence of methane, oil relative permeability experiences a reduction of 80% from 28ºC to 40ºC, followed by a considerable increase of fifteenfold from 40ºC to 52ºC. The effect of oil viscosity for all three systems was observed to be the same. Methane, carbon dioxide, and water relative permeabilities are inversely proportional to the oil viscosity. On the other hand, oil relative permeability tends to increase as its viscosity increases. A summary of the results obtained in this chapter is presented in Tables (4.2) and (4.3). Also, detailed discussion on the applicability of JBN technique for heavy oil systems can be found in the papers published out of this chapter (Akhlaghinia et al. 2013-a; Akhlaghinia et al. 2013-b).

Table 4.2: Summary of effect of increase in temperature on the relative permeability of two-phase systems.

	k_{rw}	k_{rg}	k_{ro}
Heavy Oil-Water	Increase	-----	Increase/Decrease
Heavy Oil-Carbon Dioxide	-----	Increase	Decrease
Heavy Oil-Methane	-----	Increase	Decrease/Increase

Table 4.3: Summary of effect of increase in oil viscosity on the relative permeability of two-phase systems.

	k_{rw}	k_{rg}	k_{ro}
Heavy Oil-Water	Decrease	-----	Increase
Heavy Oil-Carbon Dioxide	-----	Decrease	Increase
Heavy Oil-Methane	-----	Decrease	Increase

CHAPTER 5

THREE-PHASE RELATIVE PERMEABILITY ISOPERMS

5.1 Introduction

With a three-phase displacement experiment, it is possible to have simultaneous flow of three phases in the porous media over a wide range of saturations. This condition cannot be achieved in the steady state experiment since saturation is homogenous and constant in the porous medium while all phases flow at steady rates through that medium. In this chapter, a technique is brought forward to generate relative permeability isoperms (for three-phase systems) using a three-phase displacement experiment that involves injecting gas into Berea consolidated core saturated with heavy oil and water. After validating this technique, the effects of parameters such as temperature, oil viscosity, and gas phase on the relative permeability isoperms are investigated. The highlights of this chapter include:

- Proposing a technique to generate three-phase relative permeability isoperms based on two- and three-phase displacement experiments combined with a suitable lab-scale simulator.
- Validation of the generated three-phase relative permeability isoperms by comparing the findings with results obtained from the steady state experiment and, also, through conducting a sensitivity analysis.

- Investigating of the effect of temperature, oil viscosity, and different gas phase on the three-phase relative permeability isoperms.

5.2 Procedure

An algorithm was constructed to utilize two- and three-phase unsteady state displacements in order to estimate the relative permeability isoperms of a fluid system of heavy oil / water / gas. The four main elements of this algorithm are:

- Two-phase displacement experiment as needed to determine the boundaries of the relative permeability isoperms.
- Three-phase displacement experiment.
- Three-phase simulator able to handle three-phase relative permeabilities in explicit form.
- A tool to plot isoperms/contours using generated relative permeability data.

Using residual oil saturation (S_{or}) and irreducible water saturation (S_{wi}) obtained from two-phase heavy oil / water floods, a three-phase flow zone in a ternary diagram was assigned. Three-phase displacement was conducted in the form of gas injection into a consolidated Berea core saturated with heavy oil and water. A three-phase lab scale simulator was developed to simulate a three-phase displacement experiment. Appropriate three-phase relative permeability data was selected that corresponds to a saturation path drawn across the three-phase flow zone in the ternary diagram (e. g., saturation path 1, 2, and 3 in Figure (5.1)). This relative permeability data was continuously fine-tuned until differential pressure, heavy oil production, and water production from the numerical simulator match those of the three-phase displacement experiment. Repeating this

procedure for different saturation paths leads to a set of relative permeability data that can be used to plot isoperms/contours in a ternary diagram. Figure (5.1) presents a typical three-phase flow zone of the heavy oil / water / gas system. This entire procedure is visualized in a flowchart in Figure (5.2).

5.3 Determination of Three-Phase Flow Zone

Leverett and Lewis (1941) introduced the concept of the three-phase flow zone in a ternary diagram. They proposed that, while ignoring the irreducible gas saturation S_{gi}, the saturation region is one in which simultaneous flow of all three phases is limited by irreducible water saturation S_{wi}, and residual oil saturation S_{or}. Figure (5.3) presents a typical three-phase flow zone of the heavy oil / water / gas.

Irreducible water saturation S_{wi}, and residual oil saturation S_{or} used in this chapter were found using the heavy oil / water displacement experiments described in Sec 4.3.1 at three different temperatures and two different oil viscosities. Figure (5.4) and Figure (5.5) indicate how oil and water saturation changed until irreducible water saturation and residual oil saturation were achieved. Note that the average saturation calculated by material balance was used in this study.

Results show that increasing temperature tends to make Berea core more water wet, since irreducible water saturation increases at higher temperatures. In contrast, residual oil saturation decreases as temperature increases. In addition, it can be observed that oil flooding with more viscous oil results in lower irreducible water saturation, because the process is more piston-like. A summary of test the conditions and, as well as the established irreducible water saturation (S_{wi}) and residual oil saturation (S_{or}) are presented in Table (5.1).

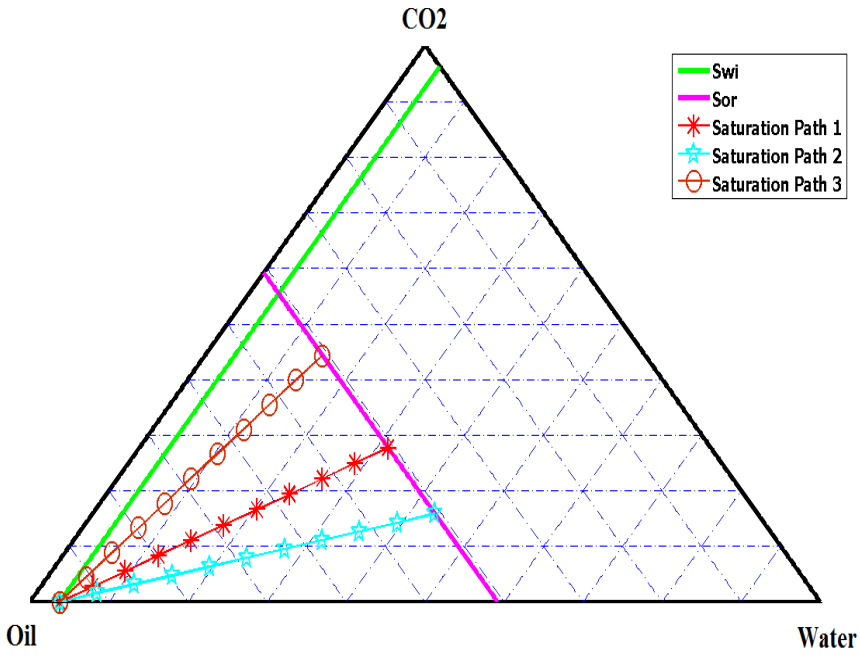

Figure 5.1: Saturation path selection through the three-phase zone (original in color).

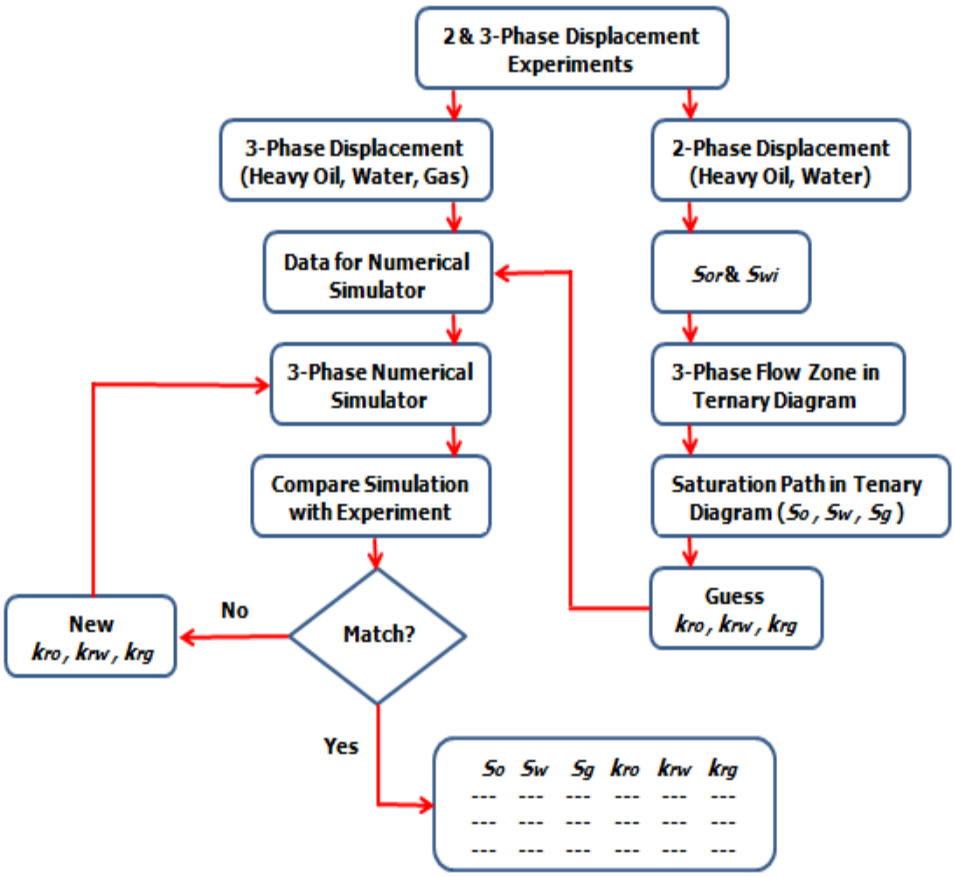

Figure 5.2: Procedure used to estimate three-phase relative permeability data from unsteady state displacement experiments.

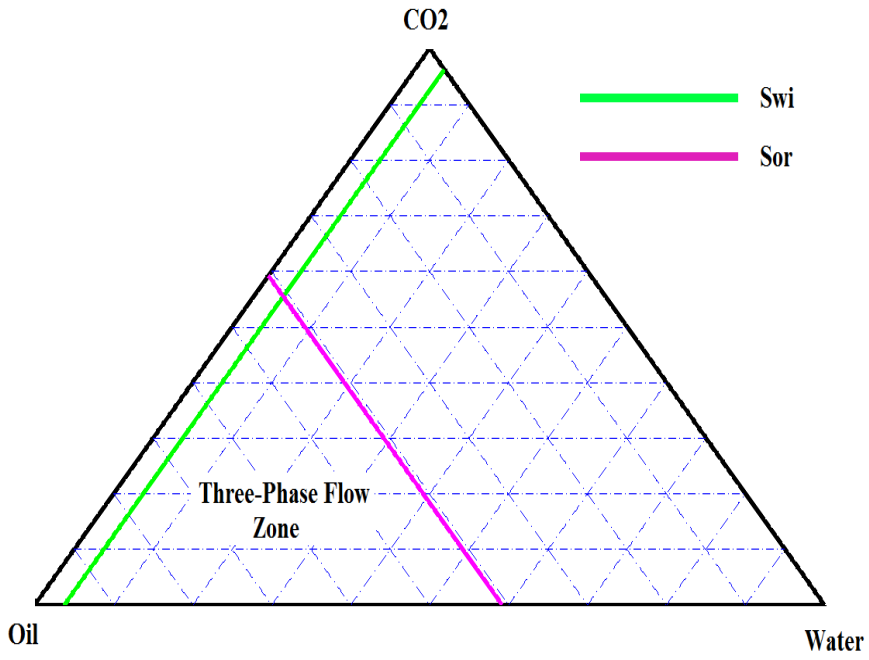

Figure 5.3: Typical three-phase flow zone for heavy oil/water/gas system (original in color).

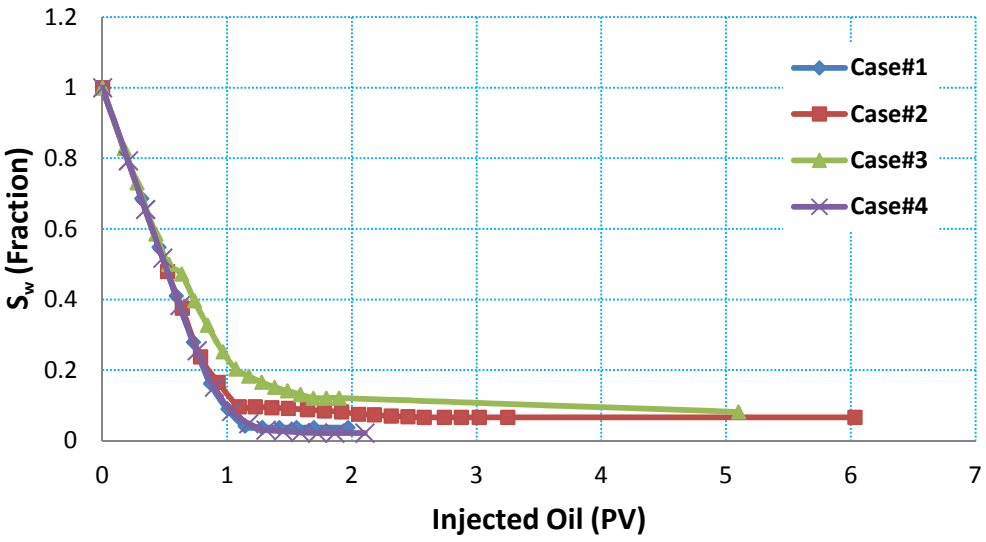

Figure 5.4: Average water saturation change during oil injection.

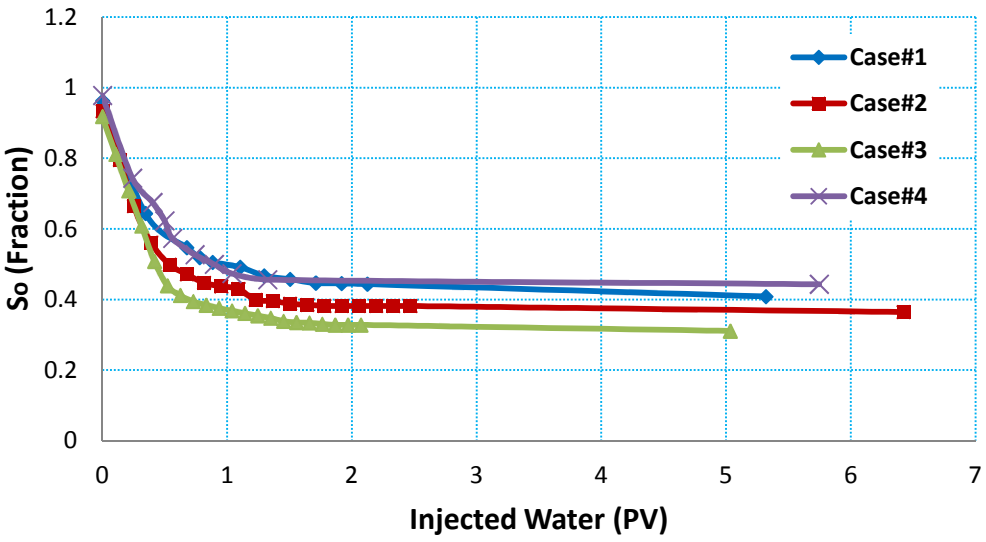

Figure 5.5: Average oil saturation change during water injection.

Table 5.1: Summary of condition for four two-phase tests conducted.

	T (°C)	Oil Sample	Oil Viscosity (cP)	Water Viscosity (cP)	Injection Rate (ml/min)	BPR (psi)	Overburden Pressure (psi)	S_{wi} (Fraction)	S_{or} (Fraction)
Case#1	28	1	1174	0.84	0.1	150	750	0.0375	0.4085
Case#2	40	1	496	0.665	0.1	150	750	0.0665	0.3643
Case#3	52	1	208	0.56	0.1	150	750	0.0816	0.3107
Case#4	28	2	2658	0.84	0.1	150	750	0.0217	0.4433

5.4 Three-Phase Displacement Experiments

As mentioned earlier, a three-phase displacement experiment allows simultaneous flow of three phases in a porous medium over a wide range of saturations. On the contrary, each steady state experiment provides a single relative permeability data point in a ternary diagram. In this study, three-phase displacement experiments were conducted involving gas (carbon dioxide, methane) injection into a consolidated Berea core at fixed heavy oil and water saturations. Preparations for this test are the same as those described for two-phase displacement. It is desirable to achieve two-phase saturation in the core before gas injection. In the unsteady state experiments conducted by Sarem (1966), oil injection into the core 100% saturated with brine was stopped immediately after breakthrough. In this study, oil injection is halted few milliliters before breakthrough as to guarantee that more water phase remains in the core. After establishing two-phase saturation in the core (e.g. $S_w = 0.30$, $S_o = 0.70$), the core assembly was given 12 hours to enable the pressure gradient along the core to reach equilibrium. In the next phase, gas was injected via a BRONKHORST gas flow controller at constant rate of 5 mln/min. A COLE PARMER gas flow meter recorded gas effluent, while liquid fractions were collected in the graduated test tubes (details of the experimental procedure previously described in Sec 3.4.4). In total, 8 successful three-phase displacement experiments at different temperatures, oil viscosities, and gas phase were conducted in this study. Oil and water saturations established before gas injection are presented in Table (5.2). As a base case, Figure (5.6) presents pressure drop, water production, and oil production observed during the carbon dioxide injection process (initially saturated with 30% water and 70% heavy oil). Similar plots for the rest of tests are found in Appendix B.

Table 5.2: Oil and water saturations before gas injections.

	Gas	Temperature (°C)	Oil Sample	Oil Viscosity (cP)	Water Viscosity (cP)	S_w (Fraction)	S_o (Fraction)
Test#1	CO_2	28	1	1174	0.84	0.30	0.70
Test#2	CO_2	40	1	496	0.665	0.28	0.72
Test#3	CO_2	52	1	208	0.56	0.28	0.72
Test#4	CO_2	28	2	2658	0.84	0.29	0.71
Test#5	CH_4	28	1	1174	0.84	0.29	0.71
Test#6	CH_4	40	1	496	0.665	0.29	0.71
Test#7	CH_4	52	1	208	0.56	0.30	0.70
Test#8	CH_4	28	2	2658	0.84	0.29	0.71

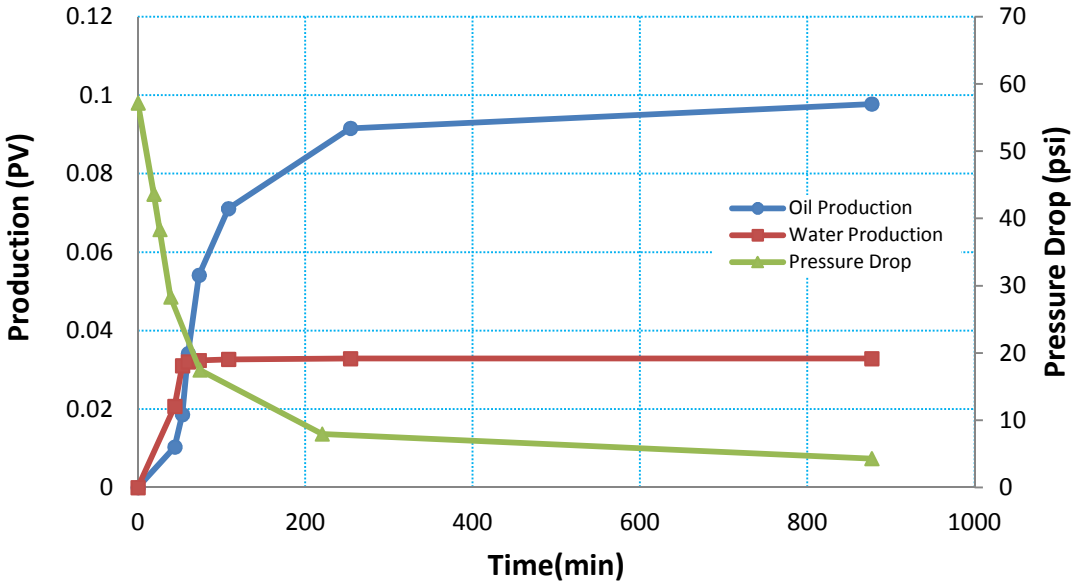

Figure 5.6: Results from three-phase displacement for base case (carbon dioxide injection at 28°C).

5.5 Numerical Simulation

The algorithm employed in this study for the estimation of the three-phase relative permeability isoperms requires a numerical simulation of the three-phase displacement experiments. Unlike commercial numerical simulators, such as CMG and ECLIPSE, which use probabilistic models based on two-phase relative permeability data, the numerical simulator developed in this study can use explicit three-phase permeability data.

A one-dimensional three-phase numerical simulator was developed that used a continuity equation for the immiscible flow of each phase through porous media, one that includes the Darcy equation as a momentum term. These equations were solved by an implicit technique as to eliminate any uncertainty in the numerical modeling. Details of the procedure are given in Appendix C. The MATLAB code of the simulator is found in Appendix D.

Before using the lab scale simulator to simulate a three-phase displacement experiment, its integrity needed to be validated. To do so, a generic, one-dimensional, and three-phase model was utilized to compare this simulator with CMG-IMEX simulator. Details of the generated model, including initial condition, dimension, rock/fluid properties, and injector/producer constraints, are presented in Table (5.3). Figure (5.7) shows oil / water and liquid / gas relative permeability curves used in both the developed simulator and CMG-IMEX to simulate carbon dioxide injection at a constant rate into a model saturated with 63.29% oil, 30.2% water, and 6.51% carbon dioxide. Figure (5.8) shows acceptable agreement between results (injection pressure, oil production, and water production) from developed simulator and CMG-IMEX.

Table 5.3: Details of the model used to validate developed simulator with CMG-IMEX.

Total Bulk Reservoir Volume		cc	962.29
Total Pore Volume		cc	187.29
Total Hydrocarbon Pore Volume		cc	131.10
Original Oil in Place, OOIP		cc	118.53
Original Gas in Place, OGIP		cc	3236.59
Original Water in Place, OWIP		cc	56.56
Porosity		%	19.46
Initial Oil Saturation		%	63.29
Initial Gas Saturation		%	6.51
Initial Water Saturation		%	30.2
Absolute Permeability		md	1560
Temperature		°F	186
Water Viscosity		cP	0.45
Oil Viscosity		cP	0.8
Grids		No.	50×1×1
I Dimension		ft	50×0.0573228
J Dimension		ft	1×0.108888
K Dimension		ft	1×0.108888
Injector Constraint	CO2 Injection Rate (MAX)	ft3/day	0.00847552
	Bottom Hole Pressure (MAX)	psi	4000
Producer Constraint	Bottom Hole Pressure (MIN)	psi	515

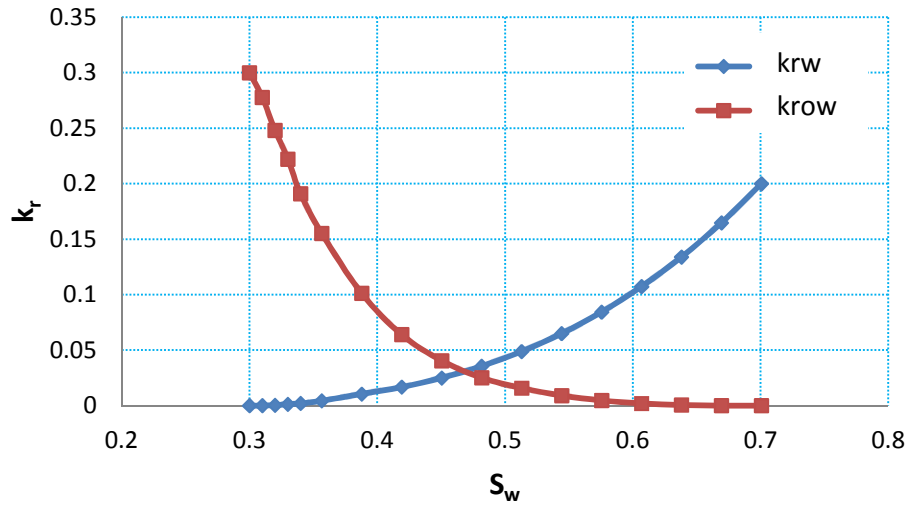

(a)

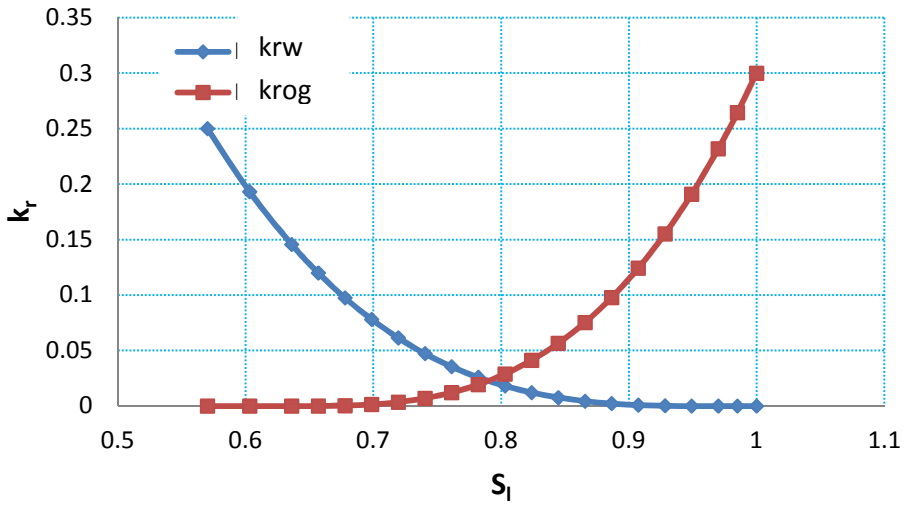

(b)

Figure 5.7: Relative permeability data used to validate developed simulator with CMG-IMEX; a: oil/water relative permeability, b: liquid/gas relative permeability.

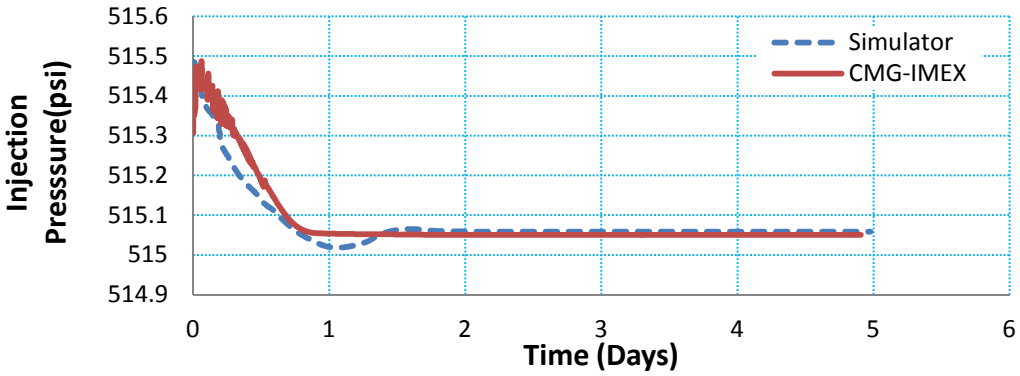

(a)

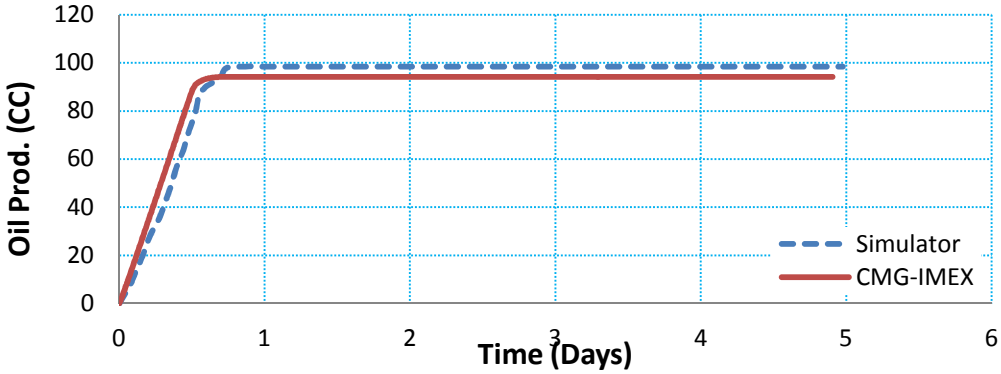

(b)

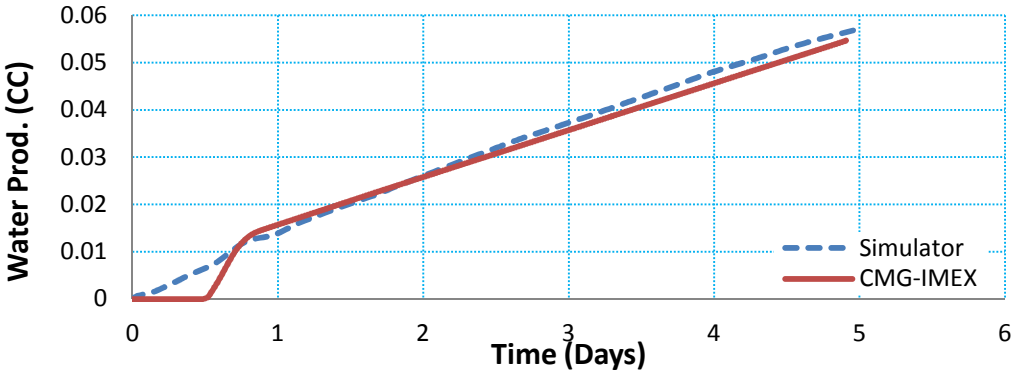

(c)

Figure 5.8: Comparing results from generated simulator with CMG-IMEX using a generic model.

5.6 Three-Phase Relative Permeability Isoperms (Base Case)

After validation of the lab scale simulator, it was used to simulate three-phase displacement experiments. As a base case, results from Test#1 (see Table (5.2)) are presented in this section. Results for the rest of the tests will be presented in the next and focus on the effects of temperature, oil viscosity, and gas phase on the relative permeability isoperms. As shown in the flowchart of Figure (5.2), pressure drop, oil production, and water production observed from the three-phase displacement experiment are matched to those predicted by the developed simulator. This procedure was performed using three sets of relative permeability data (corresponding to three saturation paths across a three-phase flow zone) to obtain data points in the three-phase flow zone for plotting isoperms/contours. Figures (5.9), (5.10), and (5.11) showcase the results of three saturation paths shown in Figure (5.1).

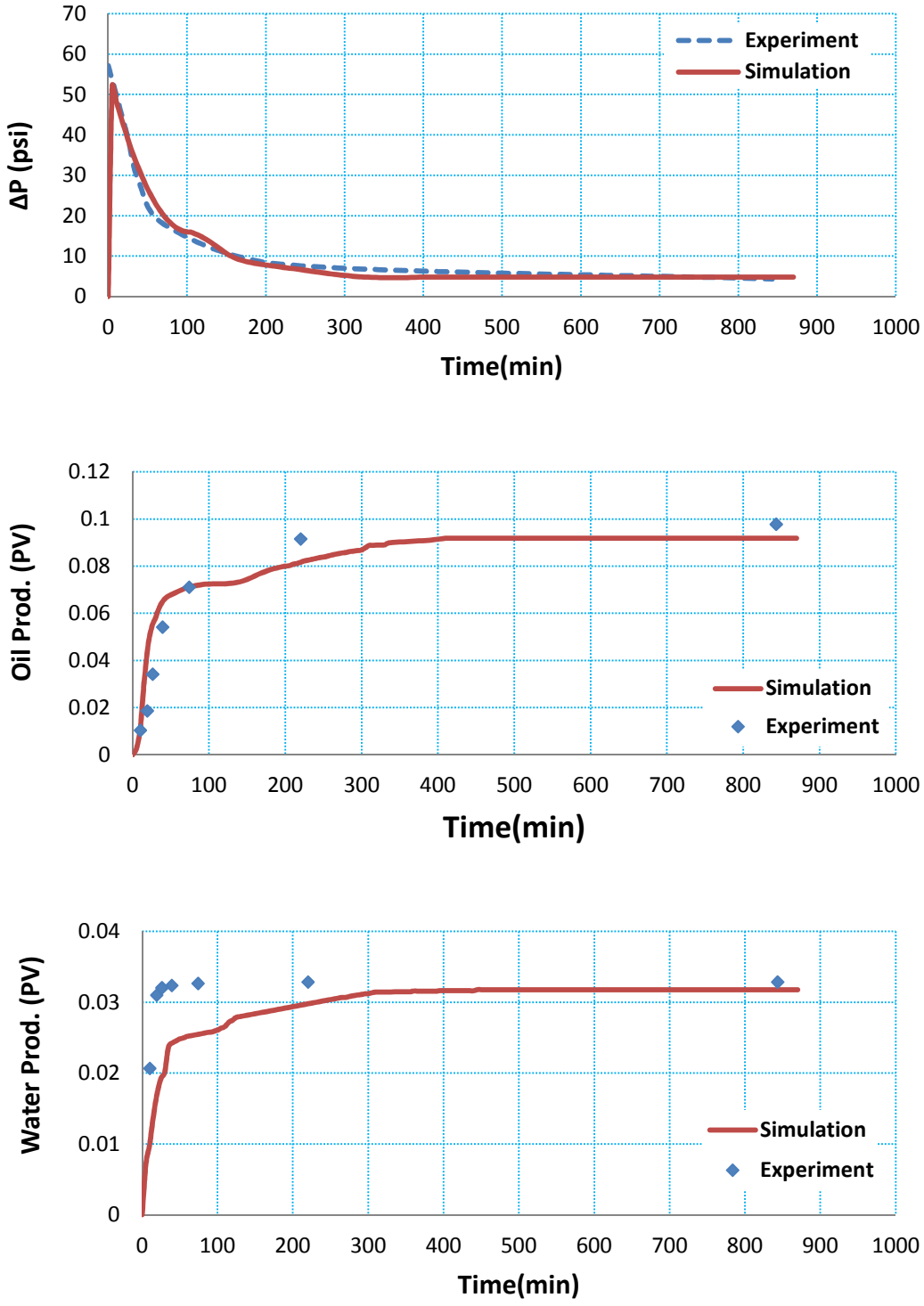

Figure 5.9: Results from matching test#1 for saturation path # 1, top (pressure drop), middle (oil production), and bottom (water production).

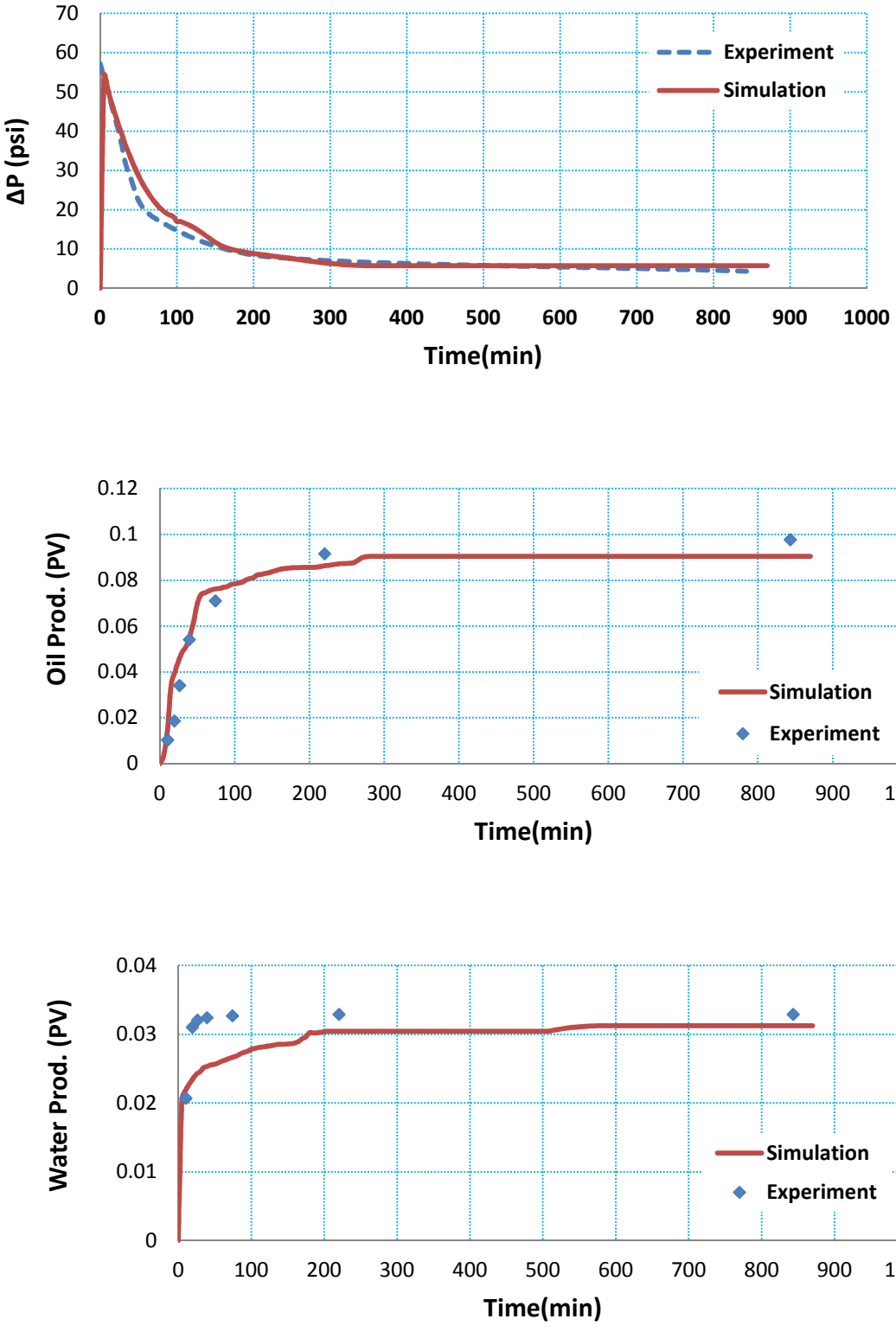

Figure 5.10: Results from matching test#1 for saturation path # 2, top (pressure drop), middle (oil production), and bottom (water production)

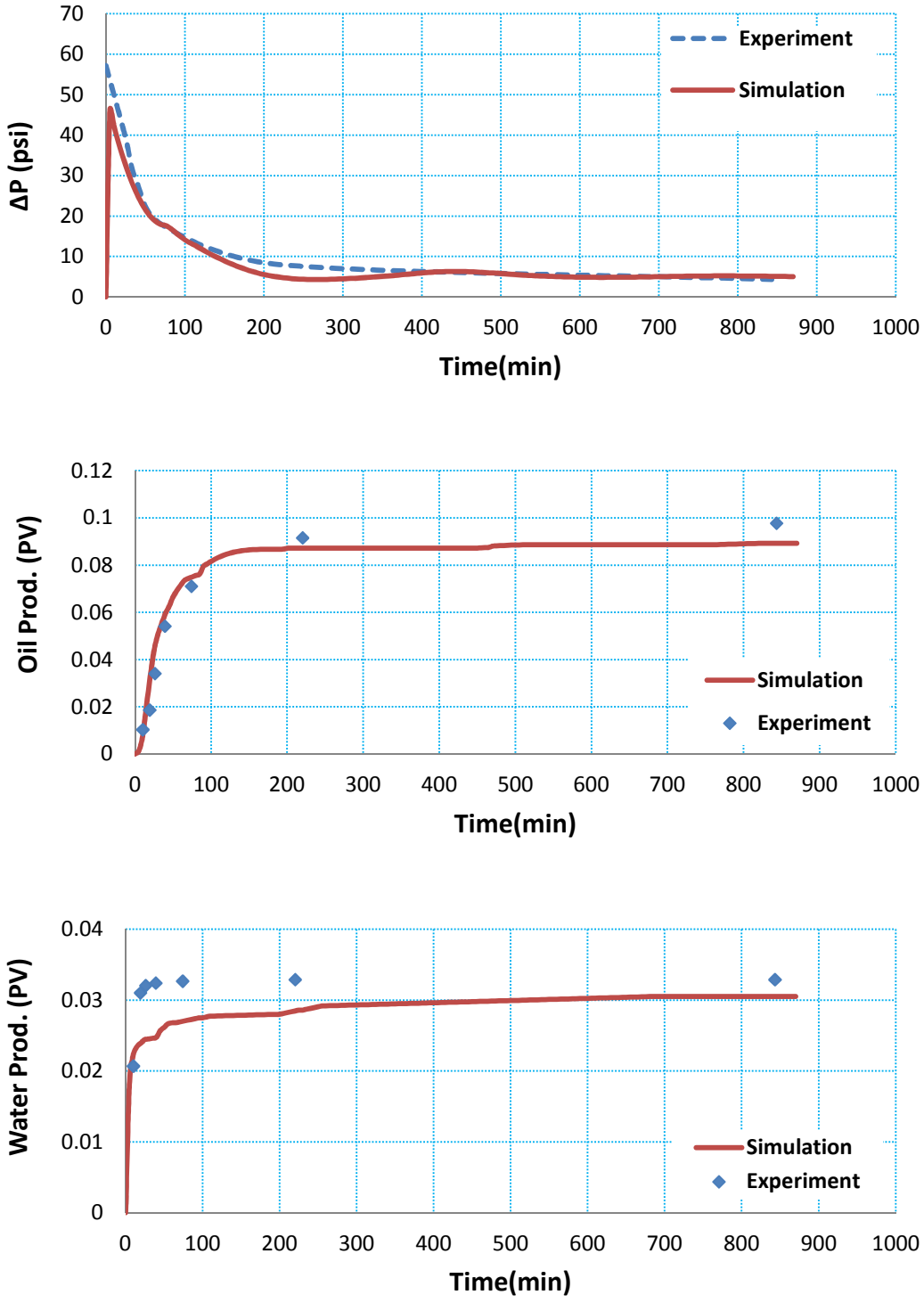

Figure 5.11: Results from matching test#1 for saturation path # 3, top (pressure drop), middle (oil production), and bottom (water production).

Final relative permeability isoperms of heavy oil / water / carbon dioxide are presented in Figures (5.12), (5.13), and (5.14) for oil, water, and carbon dioxide, respectively. User-friendly software was specially developed for this purpose (see Appendix E). For convenience, heavy oil, water, gas relative permeability isoperms are plotted in red, blue, and orange, respectively. Ternary diagrams including in this segment indicate that the three–phase flow zone is quite small for the heavy oil system due to high values of residual oil saturation (S_{or} = 40.85%). Although curvature is observed for all phases, the curvatures of the various phases are completely different. In the case of oil, the curvature is more complex than that of water or carbon dioxide. Oil relative permeability values are higher than those of water and carbon dioxide by an order of magnitude of three and five, respectively. This difference coincides with the difference between viscosity of the phases (heavy oil = 1174 cP, water = 0.84 cP, carbon dioxide = 0.015).

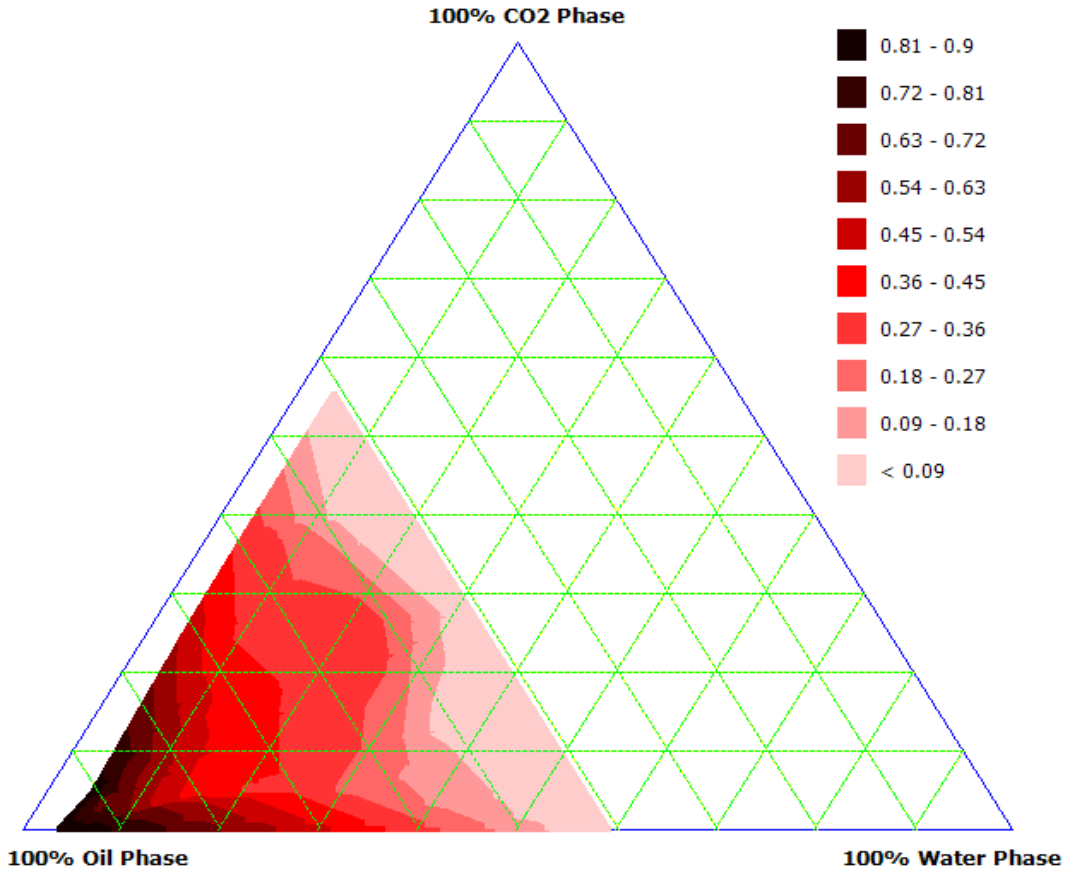

Figure 5.12: Oil relative permeability isoperms from test#1 (original in color).

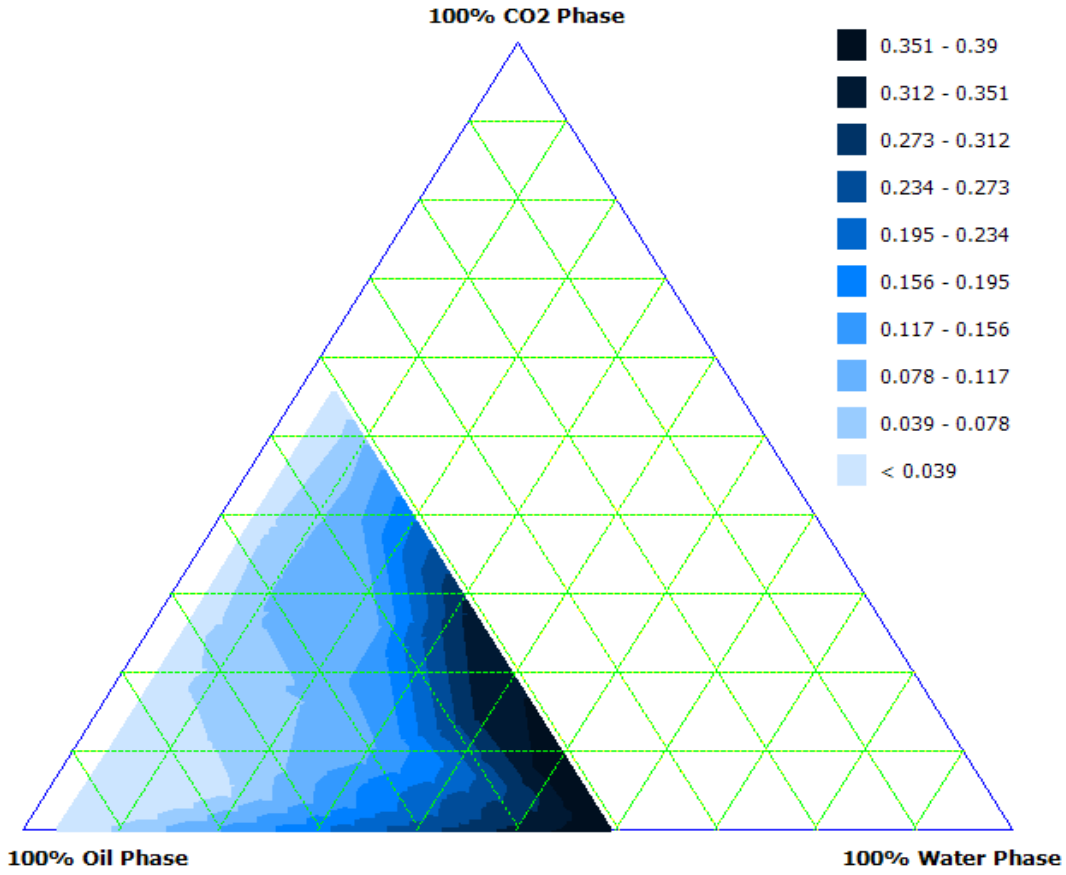

Figure 5.13: Water relative permeability isoperms from test#1 (×E+03) (original in color).

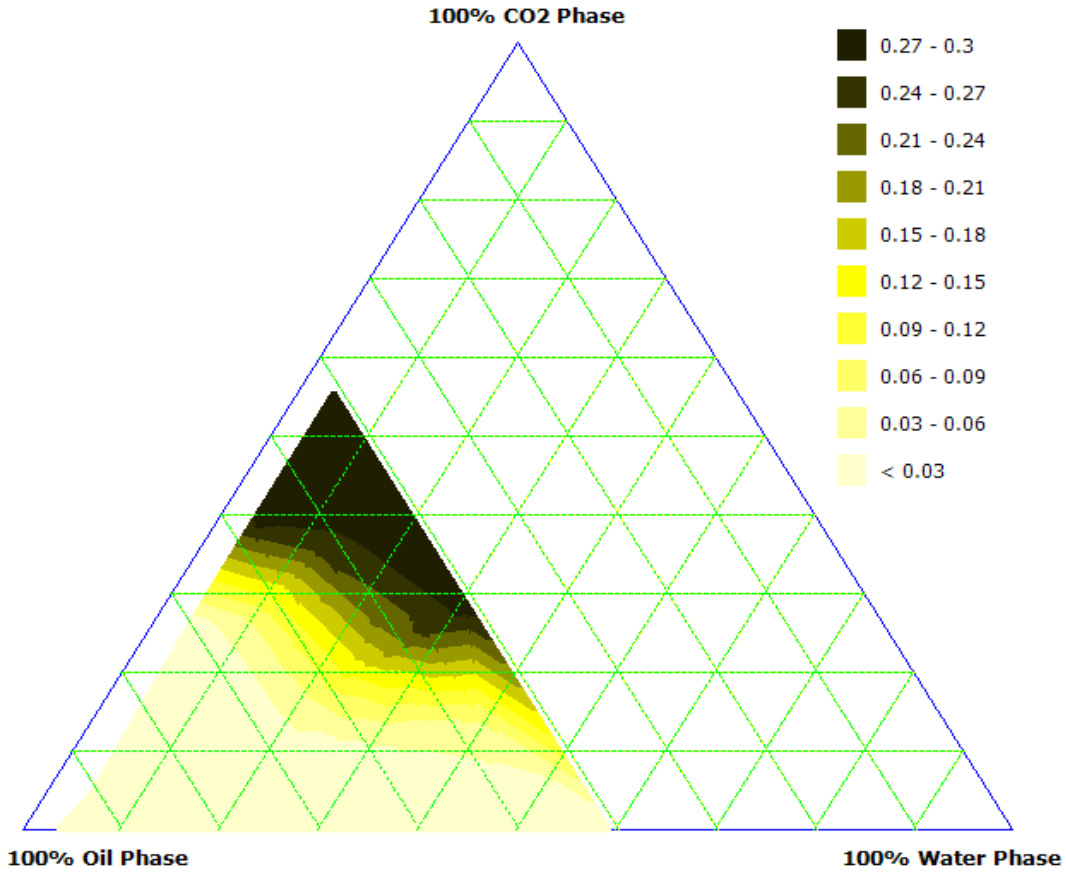

Figure 5.14: Carbon dioxide relative permeability isoperms from test#1 (×E+05) (original in color).

5.6.1 Validation of the results steady state experiments

In this section, the estimated relative permeabilities obtained previously are validated using a steady state experiment. The experimental setup shown in Figure (3.3) was used to simultaneously inject heavy oil, water and carbon dioxide into Berea core. Check valves were employed at the inlets to prevent back flow. After several failed attempts, an optimal procedure to reach and maintain simultaneous three-phase flow of heavy oil, water, and carbon dioxide was found. It is given as follows:

- Core was saturated 100% with water (brine).
- Heavy oil was injected at desired constant rate constant rate.
- After injection of heavy oil, with at least 1.5 pore volumes, water was also injected at constant rate, much higher than what was desired.
- After reaching an almost simultaneous flow of water and heavy oil, water flow rate was lowered to desired flow rate.
- Next, carbon dioxide was injected, again, at a flow rate higher than what was desired.
- After reaching simultaneous flow of heavy oil, water, and carbon dioxide, gas flow rate was lowered to desired flow rate
- Effluents were repeatedly taken, centrifuged, and read until no change in the flow rate out of the core (for each phase) is observed.
- Differential pressure and flow rates were then used to calculate relative permeability and saturations by the way of the following equations:

$$k_{ro} = -\frac{q_o \mu_o L}{kA\Delta P} \tag{5.1}$$

$$k_{rw} = -\frac{q_w \mu_w L}{kA\Delta P} \tag{5.2}$$

$$k_{rg} = -\frac{q_g \mu_g L}{kA\Delta P} \tag{5.3}$$

Note that capillary pressure was ignored as it implies that the differential pressure of all phases is the same. This, in turn, allows one to use Equations (5.1) to (5.3) to calculate relative permeability of each phase.

After establishing a steady state flow of heavy oil, water, and carbon dioxide in the core, saturation of the core was next calculated volumetrically using flow rates:

$$S_o = \frac{q_o}{q_o + q_w + q_g} \tag{5.4}$$

$$S_w = \frac{q_w}{q_o + q_w + q_g} \tag{5.5}$$

$$S_g = \frac{q_g}{q_o + q_w + q_g} \tag{5.6}$$

Table (5.4) presents the results of two successful steady state expedites conducted in order to verify the estimated relative permeabilities obtained by the base case. Figures (5.15), (5.16), and (5.17) show that the relative permeabilities obtained from the steady state tests are in good agreement with isoperms previously obtained in base case.

Table 5.4: Relative permeability from steady state experiments.

	Flow Rate (ml/min)			Saturation (Fraction)			Pressure Drop (psi)	Relative Permeability (Fraction)		
	Oil	Water	CO_2	Oil	Water	CO_2		Oil	Water	CO_2
Test # 1	0.15	0.01	0.1	0.58	0.04	0.38	477.5	0.34	1.62E-05	2.89E-06
Test # 2	0.2	0.09	0.1	0.51	0.23	0.26	681.2	0.32	0.000102	2.03E-06

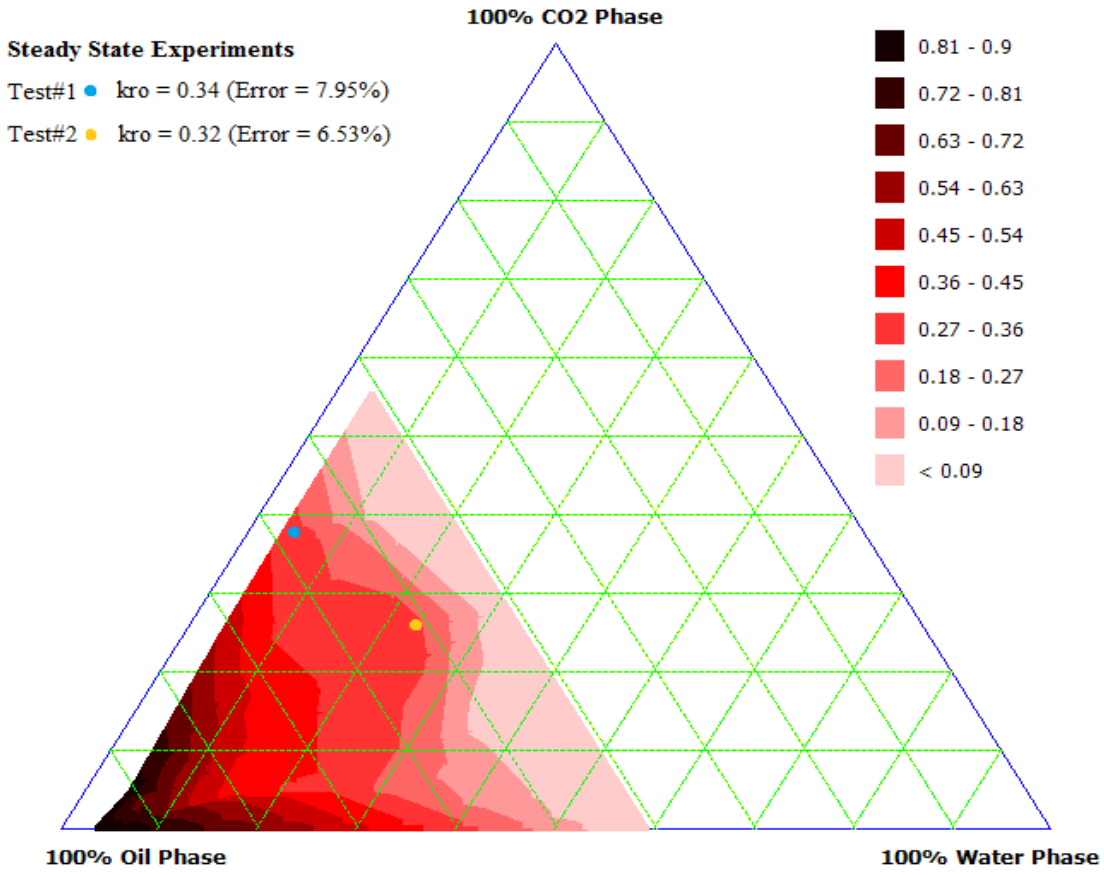

Figure 5.15: Validation of oil relative permeability isoperms with steady state tests (original in color).

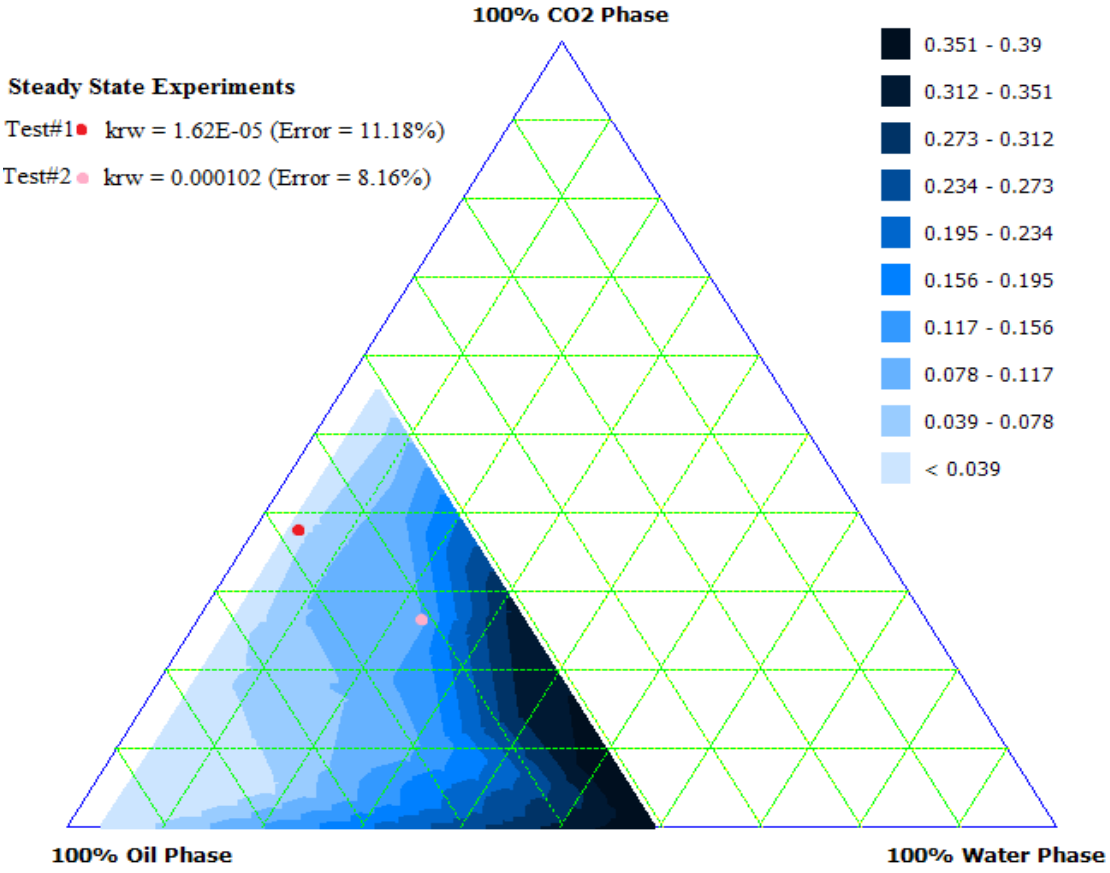

Figure 5.16: Validation of water relative permeability isoperms with steady state tests (×E+03) (original in color).

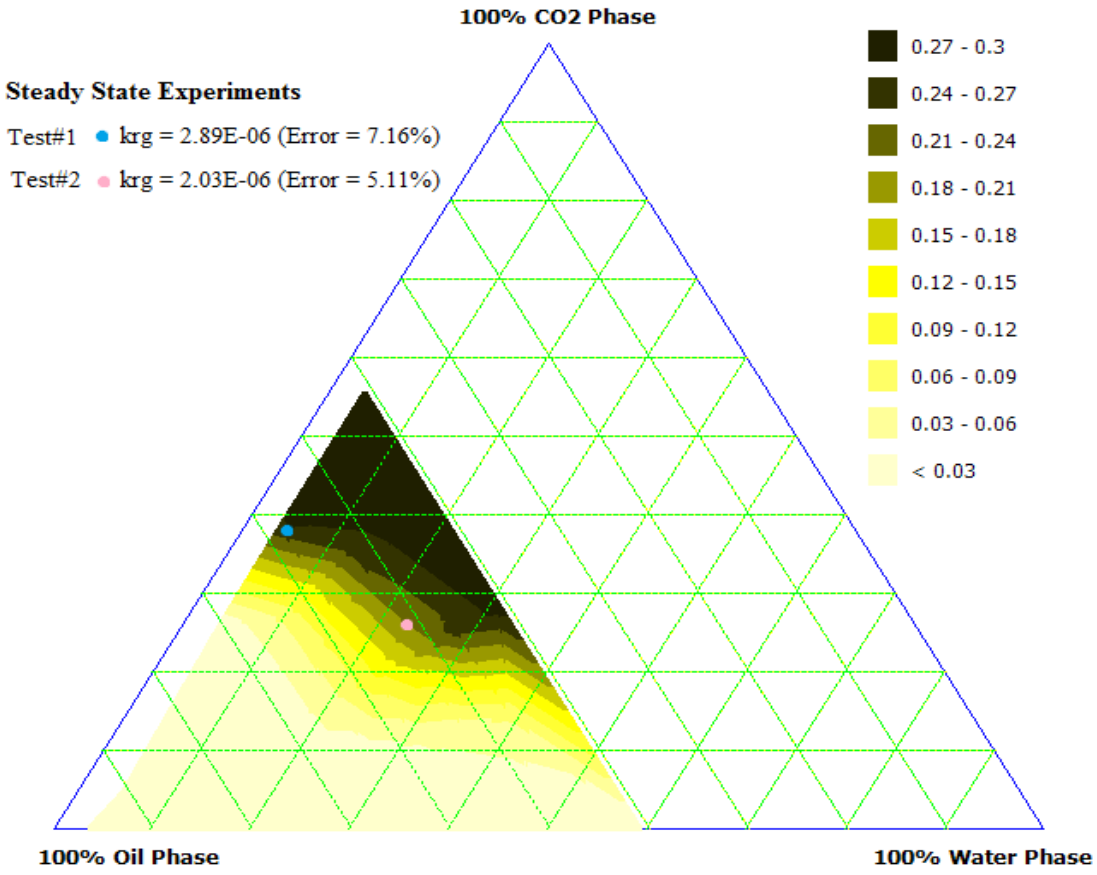

Figure 5.17: Validation of gas relative permeability isoperms with steady state tests (×E+05) (original in color).

5.6.2 Sensitivity analysis

A sensitivity analysis was also performed. It examines how manipulation of the estimated relative permeability data changes the results predicted by the numerical simulation. As one can see from Figures (5.18), (5.19), and (5.20), there is noticeable disagreement between the pressure drop simulated using the developed numerical simulator in comparison to the observation obtained from the three-phase displacement experiment. It is further inferred that the numerical simulation is more sensitive to gas relative permeability data in comparison to water and oil relative permeabilities, since more deviation occurs in simulation results, which used manipulated gas relative permeability data.

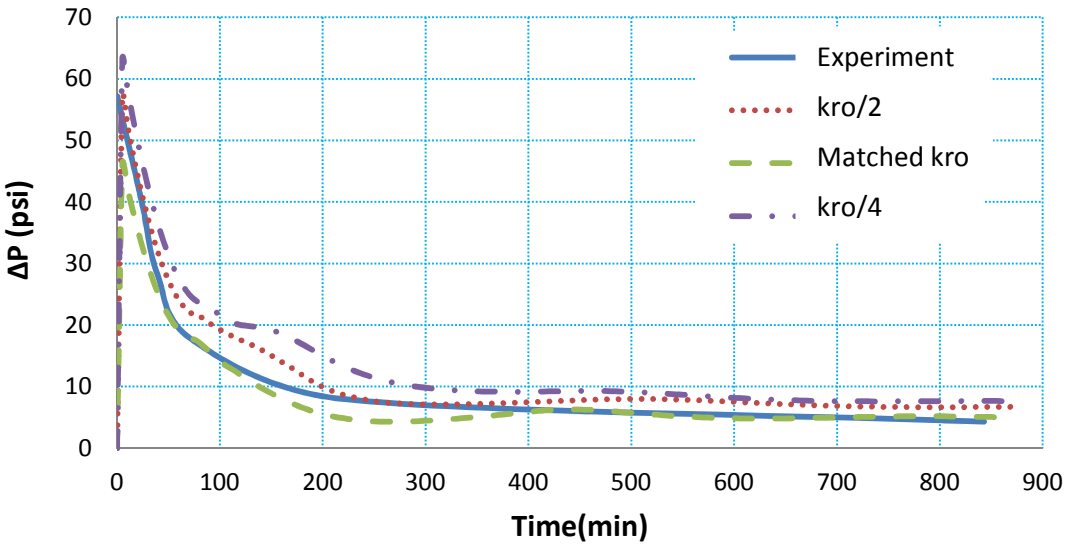

Figure 5.18: Effect of change in oil relative permeability data on the pressure drop predicted by the numerical simulator.

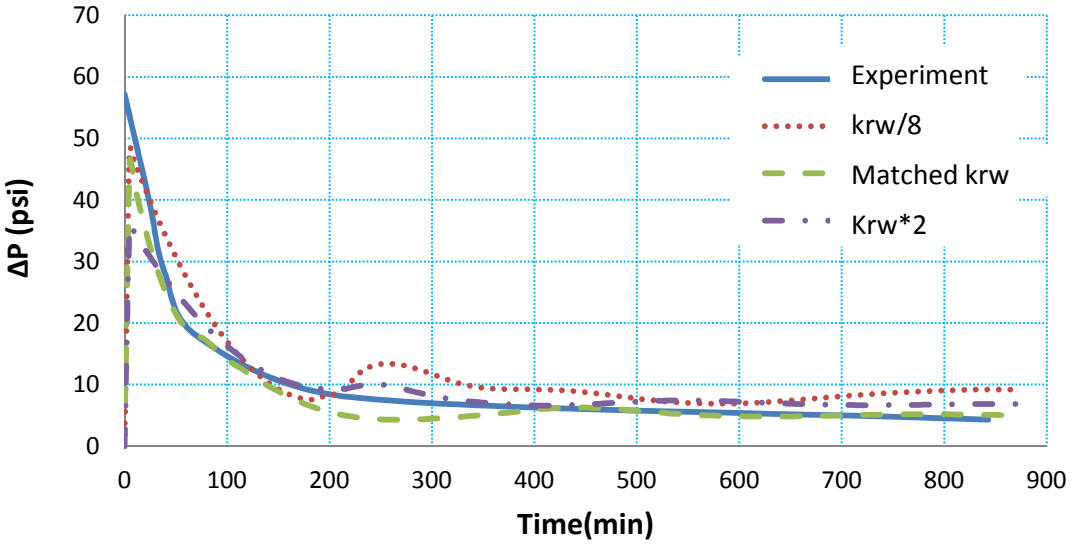

Figure 5.19: Effect of change in water relative permeability data on the pressure drop predicted by the numerical simulator.

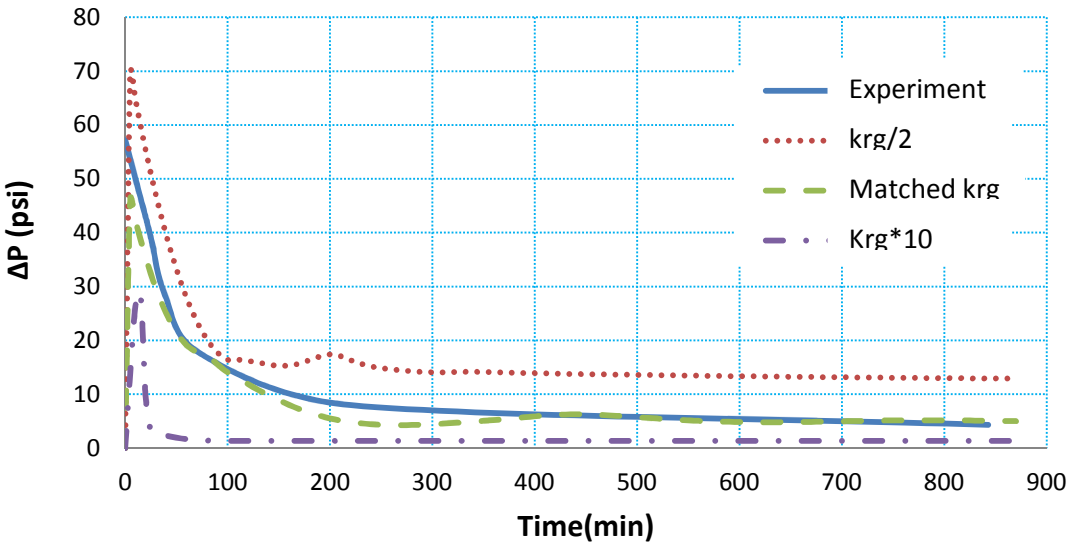

Figure 5.20: Effect of change in CO_2 relative permeability data on the pressure drop predicted by the numerical simulator.

5.7 Chapter Summary

The three-phase flow zone was determined in a ternary diagram using residual oil and irreducible water saturations obtained from two-phase heavy oil / water floods. A fully implicit three-phase simulator was developed to simulate a three-phase displacement experiment involving gas injection into a consolidated Berea core saturated with heavy oil and water. Three-phase relative permeability data corresponding to a saturation path, drawn across the three-phase flow zone in a ternary diagram, was tuned to match the simulated pressure drop, oil and water production with those observed in the displacement experiment. Results were then verified using three-phase steady state experiments and a sensitivity analysis. It has been established that, due to high values of residual oil saturation, a limited three-phase flow zone exists for heavy oil fluid systems. Different curvatures were observed for each of the phases. In the case of oil and water, these curvatures are more complex in comparison to those of carbon dioxide. It has been concluded that, due to significant viscosity contrast, oil relative permeability values are higher than those of water and carbon dioxide by an order of magnitude of three and five, respectively.

CHAPTER 6

EFFECT OF TEMPERATURE, OIL VISCOSITY, AND GAS PHASE ON RELATIVE PERMEABILITY ISOPERMS

6.1 Introduction

In the previous chapter, three-phase relative permeability isoperms were estimated as a base case for a heavy oil / water / carbon dioxide system at 28°C. Results were validated using both steady state experiments and a sensitivity analysis. In this chapter, results of a series of tests at different temperatures, oil viscosities, and gas phases are presented to:

- Investigate the effect of temperature on relative permeability isoperms
- Investigate the effect of oil viscosity on relative permeability isoperms
- Examine the relative permeability isoperms in the presence of carbon dioxide and methane

In this section, the final three-phase relative permeability isoperms (for different temperature conditions, etc.) obtained using the procedure described in the previous chapter are presented. The results of matching these three-phase displacement experiments using the developed simulator are detailed in Appendix F.

6.2 Effect of Temperature on Three-phase Relative Permeabilities

In Figures (6.1) and (6.2), relative permeabilities of three phases of a fluid system of heavy oil / water / gas taken at three temperature, specifically of 28°C, 40°C, and 52°C, are shown side by side. Comparing ternary diagrams, it can be seen that the

position of the three-phase flow zone shifts to the right as the temperature increases. This is due to the opposite effect of temperature on the water irreducible saturation and residual oil saturation (see Table 5.1). As the temperature rises from 28°C to 52°C, irreducible water saturation increases from 0.038 to 0.08. On the contrary, increasing the temperature reduces oil residual saturation from 0.41 to 0.31. This opposite effect causes the three-phase flow zone to move toward the water vertex, while the size of three-flow zone does not change significantly.

Relative permeability to oil seems to decline as temperature increases. This can be explained by rearranging Darcy's equation and solving for the relative permeability:

$$k_{ri} = -\frac{q_i \mu_i L}{kA\Delta P} \tag{6.1}$$

Although increases in temperature cause both oil viscosity and differential pressure (as it is a function of viscosity) to decrease, the effect of temperature on oil viscosity is more significant than differential pressure. In the case of relative permeability to water, a reversal trend is observed. Whereas water relative permeability increases from 28°C to 40°C, it drops as temperature further expands to 52°C. With the help of Darcy's equation, it can be said that the effect of temperature on water viscosity is more dominant over differential pressure at 28°C. As temperature increases, this trend reverses. In the case of gas (carbon dioxide and methane) relative permeability, it increases as temperature increases. This trend is expected seeing that temperature simultaneously increases gas viscosity and, consequently, decreases differential pressure. Detailed discussion on the effect of temperature on the three-phase relative permeability data can be found in the paper published out of this section (Akhlaghinia et al. 2013-c).

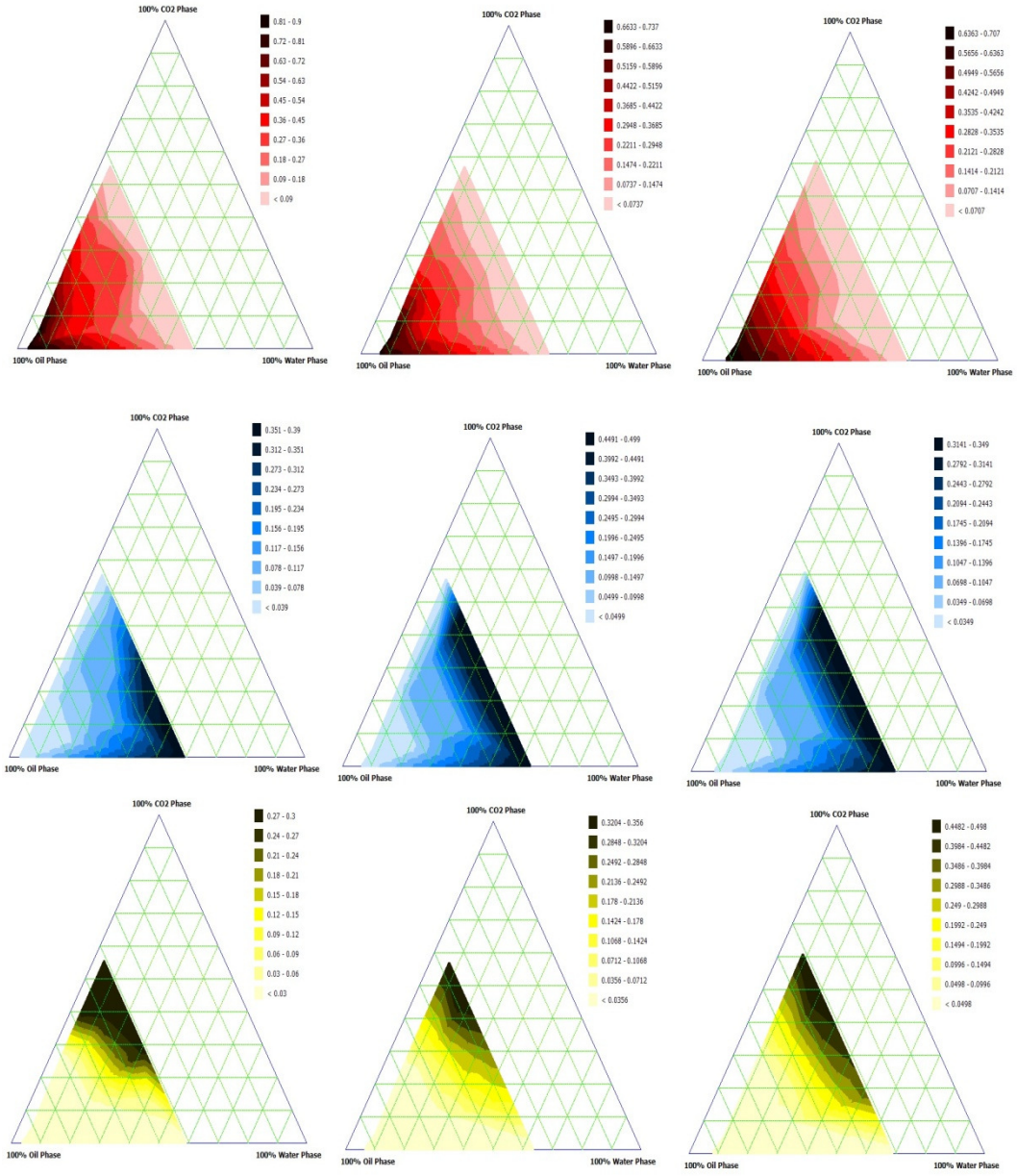

Figure 6.1: Relative permeability isoperms for heavy oil / water / CO_2 system of fluids from left to right: 28°C, 40°C, 52°C. Red (kro), Blue (krw×E+03), Yellow (krg×E+05) (original in color).

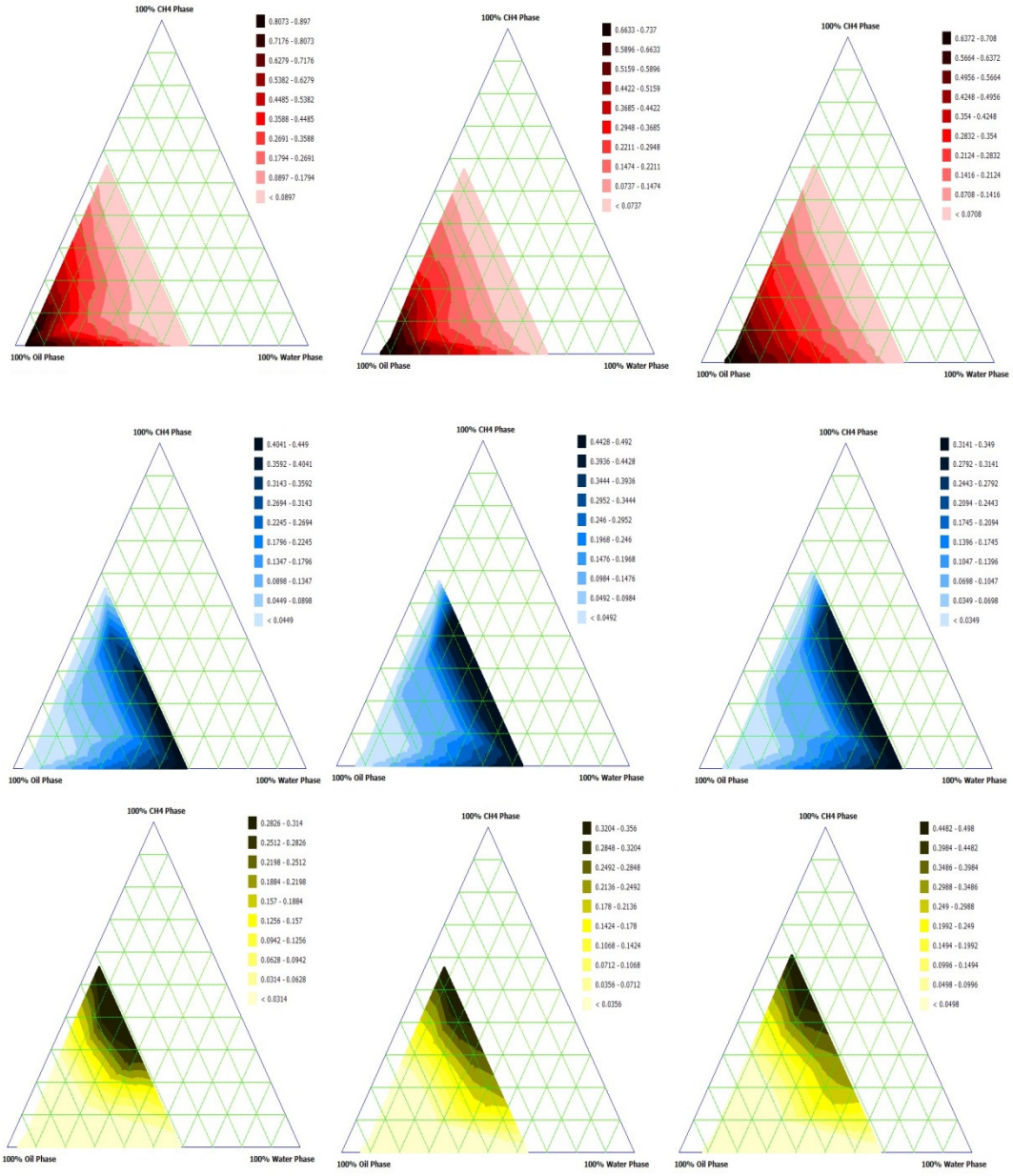

Figure 6.2: Relative permeability isoperms for heavy oil / water / CH_4 system of fluids from left to right: 28°C, 40°C, 52°C. Red (kro), Blue (krw×E+03), Yellow (krg×E+05) (original in color).

6.3 Effect of Oil Viscosity on Heavy oil / Water / CO_2 Systems

Both heavy oil / water / carbon dioxide and heavy oil / water / methane experiments were performed using two oil samples of different viscosities (1174 cP and 2658 cP at 28°C) to investigate the effect of oil viscosity on the three-phase relative permeabilities. Results, placed side by side in Figures (6.3) and (6.4) compare the two cases on carbon dioxide and methane. As oil viscosity tends to increase residual oil saturation and, in an opposite manner, decrease irreducible water saturation (see Table (5.1)), it is observed that, with increasingly viscous oil, the three-phase flow zone shifts to the left, while no significant change in the size of the three-phase flow zone occurs. In both cases, repeated experiments using more viscous oil results in a decrease in the relative permeability in all phases. Looking at Equation (6.1), in the case of oil, one sees that an increase in oil viscosity also leads to an increase differential pressure, though the effect of the increase in differential pressure is more pronounced. In the water and gas phases, however, only the differential pressure increases, leading to drops in relative permeabilities.

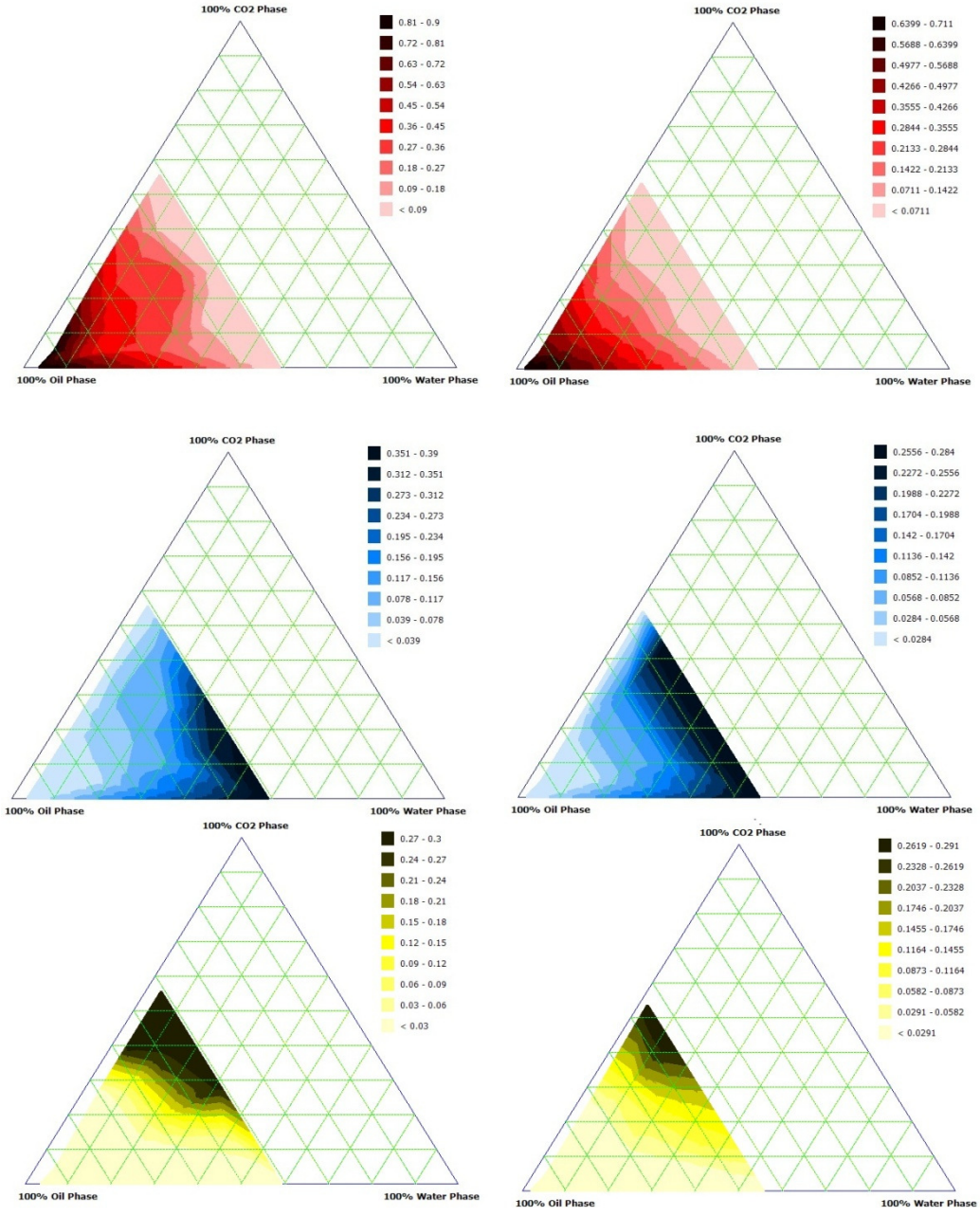

Figure 6.3: Relative permeability isoperms for heavy oil / water / CO_2 system of fluids. Left (Oil Viscosity = 1174 cP), Right (Oil Viscosity = 2658 cP). Red (kro), Blue (krw×E+03), Yellow (krg×E+05) (original in color).

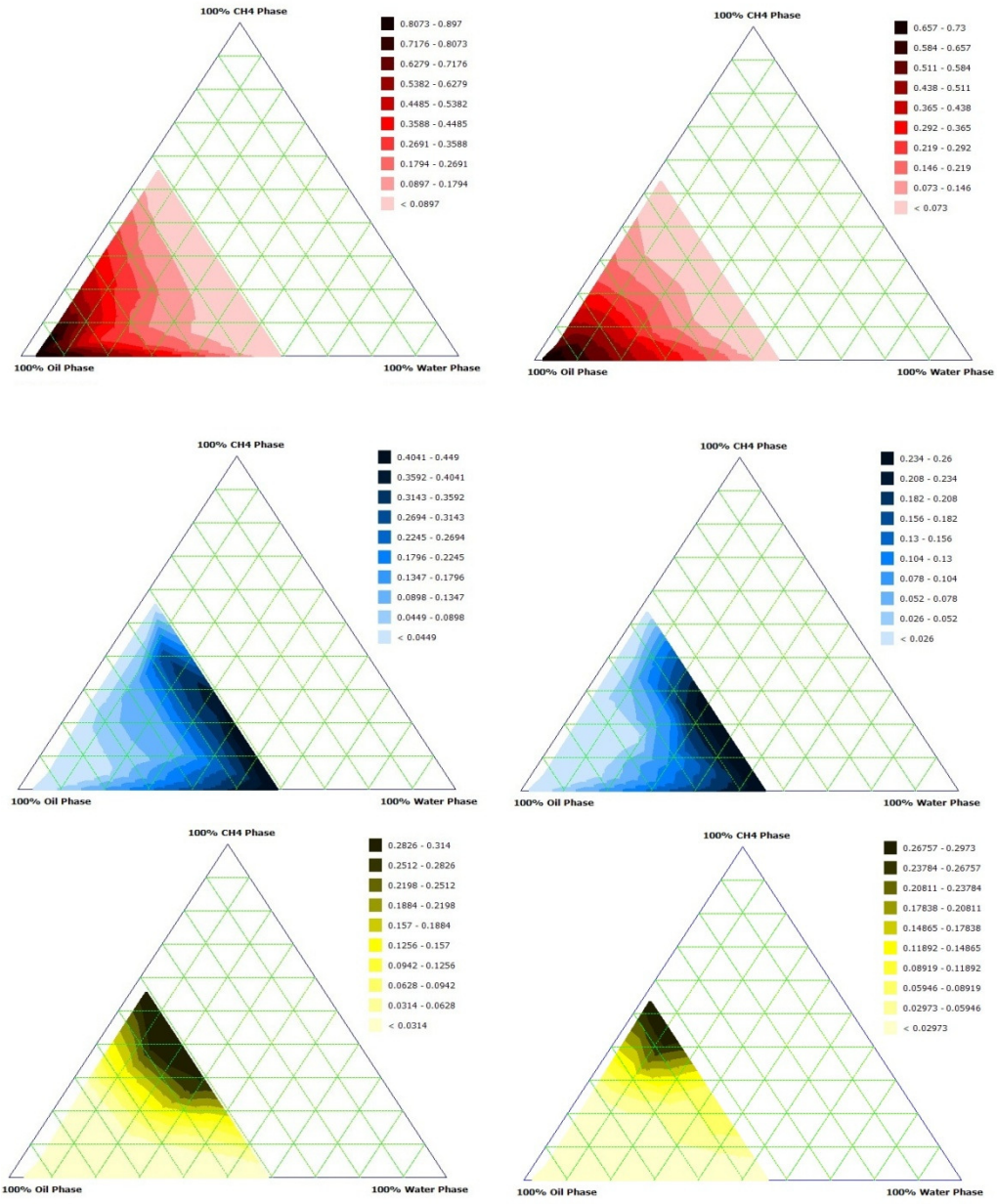

Figure 6.4: Relative permeability isoperms for heavy oil / water / CH_4 system of fluids. Left (Oil Viscosity = 1174 cP), Right (Oil Viscosity = 2658 cP). Red (kro), Blue (krw×E+03), Yellow (krg×E+05) (original in color).

6.4 Effect of Different Gas Phase on Heavy oil / Water / Gas Systems

Figure (6.5) compares relative permeabilities in the presence of carbon dioxide and methane. It is clear that oil relative permeability in the presence of carbon dioxide is higher as compared to methane. It is suspected that because carbon dioxide is more soluble in heavy oil than methane, this difference is the result of the absorption of carbon dioxide in the oil phase, which reduces oil relative permeability. In the case of the water phase, the shapes of isoperms are different when compared to the oil and gas isoperms. In contrast to the oil phase, water relative permeability in presence of methane is higher than those in presence of carbon dioxide. This difference may be due to the tendency of water to be absorbed by carbon dioxide which, in turn, reduces its mobility. Methane relative permeability values are higher when compared to carbon dioxide. This may be due to the difference in solubility values.

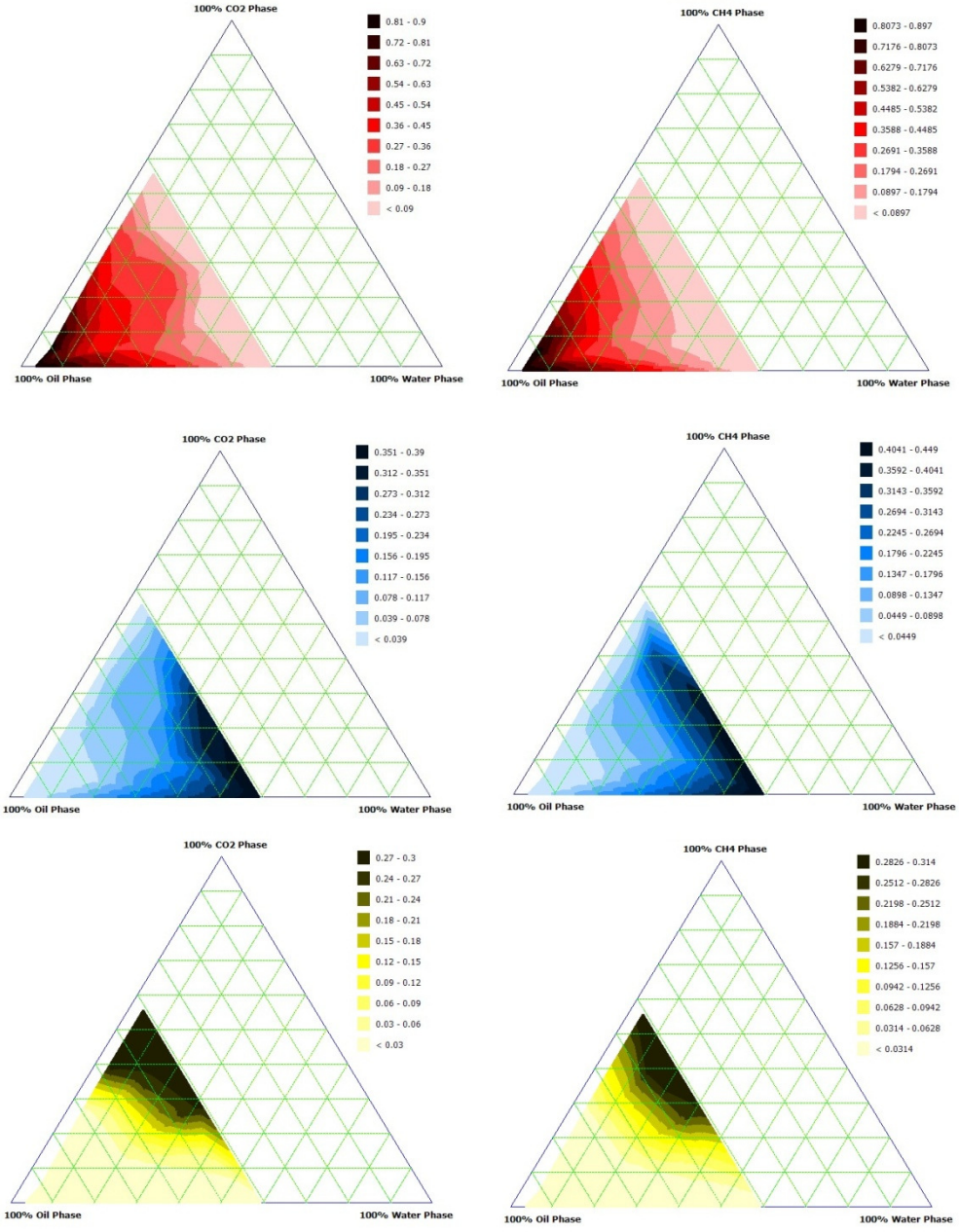

Figure 6.5: Relative permeability isoperms for heavy oil / water / gas system of fluids. Left (CO_2), Right (CH_4). Red (kro), Blue (krw×E+03), Yellow (krg×E+05) (original in color).

6.5 Chapter Summary

A procedure (validated in the previous chapter) was used to investigate the effect of temperature, oil viscosity, and different gas phase (carbon dioxide and methane) on three-phase relative permeability isoperms using a series of three-phase displacement experiments. As a convenience, a summary of the results obtained in this chapter are presented in tabular form in Table (6.1).

Table 6.1: Effect of different parameters on three-phase relative permeabilities..

		Relative Permeability to Oil	Relative Permeability to Water	Relative Permeability to Gas
Increasing Temperature	In Presence of CO_2	Decrease	Increase-Decrease	Increase
	In Presence of CH_4	Decrease	Increase-Decrease	Increase
Increasing Oil Viscosity	In Presence of CO_2	Decrease	Decrease	Decrease
	In Presence of CH_4	Decrease	Decrease	Decrease
Replacing CO_2 with CH_4		Decrease	Increase	Increase

CHAPTER 7

CONCLUSIONS AND RECOMMENDATIONS

7.1 Conclusions

Two- and three-phase relative permeabilities play a crucial role in the simulation of any multi-phase flow enhanced oil recovery process. A fast and convenient technique to provide reservoir simulators with reliable relative permeability data is necessary as it reduces simulation time (by eliminating time needed in history matching) and, in turn, total cost and uncertainty in any field-scale reservoir simulation. In addition, our understanding of relative permeability behavior at different temperatures, oil viscosities, and fluid systems should be revised, given the variety of enhanced heavy oil recovery techniques (e.g. thermal techniques, SAGD, CSS) that are now widely being used in the industry.

The following conclusions are the results of extensive experimental and numerical studies of two- and three-phase relative permeabilities at three temperatures, using two samples of oil, and in presence of carbon dioxide and methane:

- The JBN technique was applied in order to calculate two-phase relative permeabilities at different temperatures, oil viscosities, and fluid systems. It was discovered that two-phase relative permeability is not a single function of saturation, since temperature, oil viscosity, and even the presence of different gas phases have unique effects on the relative permeability data. Issues, such as short and bumpy curves, have been

observed with relative permeability data obtained with JBN technique in heavy oil systems.

- A three-phase displacement experiment coupled with a suitable lab-scale simulator seems to be a viable option for estimating three-phase relative permeabilities given that its results have been shown to be well correlated with the steady state experiments.
- The results of this study demonstrate that limited three-phase flow zone exists for heavy oil fluid systems due to high values of residual oil saturation. Different curvatures have been observed using the relative permeability isoperms of each of the phases. These curvatures are more complicated for oil and water than in the gas phase. It has been observed that, due to significant differences in the viscosities of heavy oil / water / gas system of fluid, oil relative permeability values are higher than those of water and carbon dioxide in order of magnitude of three and five, respectively.
- Temperature tends to change the position of the three-phase flow zone (towards the water vertex) as it changes water irreducible saturation and residual oil saturation. No significant change in the size of the three-phase flow zone was observed. In a heavy oil / water / gas fluid system, the effect of an increase in temperature on the relative permeability isoperms is very different in each phase. This process decreases the relative permeability of oil. In an opposite way, the relative permeability of the gas phase increases at elevated temperatures. When it comes to water, a

reversal trend was observed. Although water relative permeability increases from 28°C to 40°C, it decreases as temperature further rises to 52°C. It can be said that (with the help of Darcy's equation) the effect of temperature on water viscosity is more dominant in comparison to differential pressure (compared to water viscosity) at 28°C and, as temperature increases, this trend reverses.

- Three-phase displacement experiments involving two different samples of oil (1174 cP and 2658 cP at 28°C) indicate that oil viscosity tends to increase residual oil saturation and, conversely, decrease irreducible water saturation. As a consequence, the three-phase flow zone shifts to the left (towards the oil vertex), while no significant change in the size of the three-phase flow zone occurs. In both instances, additional experiments using more viscous oil results in a decrease in the relative permeability in each phase. In the case of oil, an increase in oil viscosity also leads to an increase in differential pressure. Note, however, that the effect of the increase in differential pressure is more substantial. In the water and gas phases, only the differential pressure increases, thereby, leading to a decrease in the relative permeabilities.
- Oil relative permeability in the presence of carbon dioxide is higher as compared to methane due to the higher solubility of carbon dioxide in heavy oil. In contrast to the oil phase, water relative permeability in the presence of methane is higher than those in the presence of carbon dioxide. This difference may be due to the tendency of water to be

absorbed by carbon dioxide which, in turn, reduces its mobility. Methane relative permeability values are higher in comparison to those of carbon dioxide, a fact which may be due to difference in solubility values.

7.2 Recommendations

The following is a list of recommendations that may be considered at some point in the future:

- A black oil, fully implicit, one-dimensional, three-phase simulator was used in this study to simulate three-phase displacement experiments. A more advanced compositional simulator is preferable since it can capture the interaction between phases, as it further reduces uncertainties in the results.
- Capillary pressure should be incorporated into any future work (especially in the case of light oil systems). It was not included in this study due to difficulties associated with measurements.
- The simulator developed for this study was written in MATLAB. As it was coupled with MS-Excel 2007, it required considerable time to import data, simulate a process, and export results. A faster and more user-friendly software/simulator (using a low level programming language such as C++ or FORTRAN) is needed in order to reduce the overall computational load. Techniques such as EnKF can also be incorporated into simulators to further reduce time needed to analyze experimental results.
- It is common for users of a commercial reservoir simulator to manipulate relative permeability data. Unfortunately, existing commercial simulators (e.g. CMG)

limit reservoir engineers to the Stone Models. What is needed, in effect, is more access to different options (e.g. relative permeabilities in the form of isoperms in all phases) in these software packages.

REFERNCES

Aleman, M. A., and Slattery, J. C.: Estimation of Three-Phase Relative Permeabilities. *Transport in Porous Media* 3(2), 111-131 (1988)

Akhlaghinia, M., Torabi, F., and Chan, C. W.: Experimental and Simulation Studies of Heavy Oil/Water Relative Permeability Curves: Effect of Temperature. *Special Topics & Reviews in Porous Media* 4(1), 99-109 (2013-a)

Akhlaghinia, M., Torabi, F., and Chan, C. W.: Effect of Temperature on Two Phase Relative Permeabilities of Heavy Oil, Water, Carbon Dioxide, and Methane Determined by Displacement Technique. *Energy and Fuels* 27(3), 1185-1193 (2013-b)

Akhlaghinia, M., Torabi, F., and Chan, C. W.: Experimental Investigation of Temperature Effect on Three-Phase Relative Permeability Isoperms in Heavy Oil Systems. Accepted to be published at Journal of Fuel. Manuscript ID JFUE-D-12-01944. (2013-c)

Ambastha, A. K., and Kumar, M.: New Insights into in-Situ Combustion Simulation for Heavy Oil Reservoirs. Paper SPE 56543 presented at the Annual Technical Conference and Exhibition, Houston, TX, US, 3-6 October (1999)

Amyx, W. J., Bass, D. M. Jr., and Whiting, R. L.: *Petroleum Reservoir Engineering*: Physical Properties. McGraw-Hill classic textbook reissue series. Printed in the United States of America. 64-65 (1988)

Archer, J.S., and S.W. Wong.: Use of a Reservoir Simulator to Interpret Laboratory Water Flood Data. *SPEJ* 13(6), 343-347 (1973)

Aziz, K., and Settari, A.: *Petroleum Reservoir Simulation*. Applied Science Publishers, London. (1979)

Balbinski, E. F., Fishlock, T. P., Goodyear, S. G., and Jones, P. J. R.: Key Characteristics of Three-Phase Oil Relative Permeability Formulations for Improve Oil Recovery Prediction. *Pet. Geosci*. 5(4), 339-346 (1999)

Batycky, J. P., McCaffery, F. G., Hodgins, P. K., and Fisher, D. B.: Interpreting Relative Permeability and Wettability from Unsteady-State Displacement Measurements. *SPEJ* 21(3), 296-308 (1981)

Blunt, M., Zhou, D., and Fenwick, D.: Three-Phase Flow and Gravity Drainage in Porous Media. *Transport in Porous Media* 20(1-2), 77-103 (1995)

Blunt, M., King, M. J., and Scher, H.: Simulation and Theory of Two-Phase in Porous Media. *Phys. Rev. A*. 46(12), 7680-7699 (1992)

Blunt, M.: An Empirical Model for Three-Phase Relative Permeability. *SPEJ* 5(4), 435-445 (2000)

Boukadi, F. H., Bemani, A. S., and Babadagli, T.: Investigating Uncertainties in Relative Permeability Measurements. *Energy Sources* 27(8), 719-728 (2005)

Briggs, P. J., Baron, R. P., Fulleylove, R. J., and Wright, m. S.: Development of Heavy-Oil Reservoirs. *JPT* 40(2), 206-214 (1988)

Brooks, R. H., and Corey, A. T.: Properties of Porous Media Affecting Fluid Flow. *J. of the Irrigation and Drainage Division*. Proceedings of the American Society of Civil Engineers. 92(2), 61-88 (1966)

Buckley, S. E., and Leverett, M. C.: Mechanism of Fluid Displacement in Sands. *SPEJ* 146(1), 107-116 (1942)

Burdine, N. T.: Relatively Permeability Calculations from Pore Size Distribution Data. *JPT* 5(3), 71-78 (1953)

Caldwell, R. H., and Heather, D. I.: Characterizing Uncertainty in Oil and Gas Evaluations. Paper SPE 68592 Hydrocarbon Economics and Evaluation Symposium, Dallas, TX, US, 2-3 April (2001)

Capen, E. C.: The Difficulty of Assessing Uncertainty. *SPEJ* 28(8), 843-850 (1976)

Caudle, B. H., Slobod, R. L., and Brownscombe, E. R.: Further Developments in the Laboratory Determination of Relative Permeability. *JPT* 3(5), 145-150 (1951)

Chalier, G., Giry, V., Madaoui, K., Sakthikumar, S., and Maquignon, P.: Three Phase Oil Relative Permeability Determination as a Key Point in the Evaluation of a Tertiary Gas Gravity Drainage Project. Paper SPE 30761 presented at the SPE Annual Technical Conference and Exhibition, Dallas, TX, US, 22-25 October (1996)

Chavent, G., Jaffre, J., and jegon, S. J.: Estimation of Relative Permeabilities in Three-Phase Flow in Porous Media. *French Institute of Petroleum*. (1999)

Christensen, J. R., Stenby, E. H., and Skauge, A.: Review of WAG Field Experience. International Petroleum Conference and Exhibition of Mexico, Villahermosa, Mexico, 3-5 March (1998)

Christiansen, R. L., and Kalbus, J. S., and Howarth, S. M.: *Evaluation of Methods for Measuring Relative Permeability of Anhydrite from the Salado Formation: Sensitivity Analysis and Data Reduction.* Sandia National Laboratories. SAND94-1346, Unlimited Release, May (1997)

Civan, F., and Donaldson, E. C.: Relative Permeability from Unsteady-State Displacements with Capillary Pressure Included. *SPEFE* 4(2), 189-193 (1989)

Coats, K. H.: *Reservoir Simulation, Petroleum Engineering Handbook*. Ed. H.B. Bradley. Richardson, TX: Society of Petroleum Engineers. (1987)

Corey, A. T., Rathjens, C. H., Henderson, J. H., and Wyllie, M. R. J.: Three-Phase Relative Permeability. *JPT* 8(11), 63-65 (1956)

Cromwell, V., Kortum, D. J., and Bradley, D. J.: The Use of a Medical Computer Tomography (CT) System to Observe Multiphase Flow in Porous Media. Paper SPE 13098 presented at the SPE Annual Technical Conference and Exhibition, Houston, TX, US, 16-19 September (1984)

Dandekar, A. T.: *Petroleum Reservoir Rock and Fluid Properties*. Taylor and Francis Group. (2006)

Delshad, M. and Pope, G. A.: Comparison of Three-Phase Oil Relative Permeability Models. *Transport in Porous Media* 4(1), 59-83 (1989)

Demond, A. H., Rathfelder, K., and Abriola, L. M.: Simulation of Organic Liquid Flow in Porous Media Using Estimated and Measured Transport Properties. *Journal of Contaminant Hydrology* 22(3-4), 123-240 (1996)

Dietrich, J. K.: Relative Permeability during Cyclic Steam Stimulation of Heavy-Oil Reservoirs. *JPT* 33(10), 1987-1989 (1981)

Dietrich, J. K. and Bondar, P. L.: Three Phase Oil Relative Permeability Models. Paper SPE 6044 presented at the Annual Fall Technical Conference and Exhibition, New Orleans, LA, US, 3-6 October (1976)

Donaldson, E. C., and Dean, G. W.: *Two and Three-Phase Relative Permeability Studies*. U.S. Dept. of the Interior, Bureau of Mines, RI 6826 (1966)

Dria, D. E., Pope, G. A., and Sepehrnoori, K.: Three-Phase Gas/Oil/Brine Relative Permeabilities Measured under CO_2 Flooding Conditions. *SPERE* 8(2), 143-150 (1993)

Dusseault, M. B.: Comparing Venezuelan and Canadian Heavy Oil and Tar Sands. Paper SPE 2001-006 presented at the Canadian International Petroleum Conference, Calgary, AB, Canada, 12-14 June (2001)

Element, D. J., Masters, J. H. K., Sargent, N. C., and Jayasekera, A. J.: Assessment of Three-Phase Relative Permeability Models Using Laboratory Hysteresis Data,

Paper SPE 84903 presented at the SPE International Improved Oil Recovery Conference, Kuala Lumpur, Malaysia, 20-21 October (2003)

Ertekin, T., Abou-Kassem, J. H., and King, G. R.: *Basic Applied Reservoir Simulation. Society of Petroleum textbook series* Vol. 7. (2001)

Esmail, M. N.: Problems in Numerical Simulation of Heavy Oil Reservoirs. *JCPT* 24(3), 80-82 (1985)

Etminan, S. R., Maini, B. B., Hassanzadeh, H., and Chen, Z.: Determination of Concentration Dependent Diffusivity Coefficient in Solvent Gas Heavy Oil System. Paper SPE 124832 presented at SPE Annual Technical Conference and Exhibition, New Orleans, LA, US, 4-7 October (2009)

Fassihi, M. R.: Estimation of Relative Permeability from Low Rate, Unsteady-State Tests - A Simulation Approach. *JCPT* 28(3), 29-38 (1989)

Foulser, R. W. S., Goodyear, S. G., and Sims, R. J.: Two- and Three-Phase Relative Permeability Studies at High-Capillary Numbers. Paper SPE/DOE 24152 presented at the SPE/DOE Eighth Symposium on Enhanced Oil Recovery, Tulsa, OK, US, 22-24 April (1992)

Ghannam, M. T., Shadi, W. H., Abu-Jdayil, B., and Esmail, N.: Rheological Properties of Heavy and Light Crude Oil Mixtures for Improving Flowability. *JPSE* 81, 122-128 (2012)

Gibson, B. J.: Methods of Classifying Heavy Crude Oils Using the UNIT AR Viscosity Based Definition. UNITAR Future of Heavy Crude and Tar Sands Conference, Caracas, Venezuela, 17-21 February (1982)

Grader, A. S. and O'Meara, D. J.: Dynamic Displacement Measurement of Three-Phase Relative Permeabilities Using Three Immiscible Liquids. Paper SPE/DOE 18293 presented at 63rd Annual Technical Conference and Exhibition. Houston, TX, US, 2-5 October (1988)

Hastings, J. J., Muggeridge, A. H., and Blunt, M.: A New Streamline Method for Evaluating Uncertainty in Small-Scale, Two-Phase Flow Properties. Paper SPE 66349 Reservoir Simulation Symposium, Houston, TX, US, 11-14 February (2001)

Heaviside, J., Black, C. J. J., and Berry, J. F.: Fundamentals of Relative Permeability: Experimental and Theoretical Considerations. Paper SPE 12173 presented at the Annual Technical Conference and Exhibition. San Francisco, CA, US, 5-8 October (1983)

Heinemann, Z. E.: *Fluid Flow in Porous Media*, Textbook Series Vol(1), Montanuniversität Leoben, Petroleum Engineering Department. (2005)

Hicks Jr., P. J. and Grader, A. S.: Simulation of Three-Phase Displacement Experiments. *Transport in Porous Media* 24(2), 221-245 (1996)

Honarpour, M., Koederitz, L., and Harvey, A. H.: *Relative Permeability of Petroleum Reservoirs*. CRC Press. (1986)

Honarpour, M. and Mahmood, S. M.: Relative-Permeability Measurements: An Overview. *JPT* 40(8), 963-966 (1988)

Hove, A. O., Ringen, J. K., and Read, P. A.: Visualization of Laboratory Corefloods with the Aid of Computerized Tomography of X-Rays. *SPERE* 2(2), 148-154 (1987)

Husted, O. S. and Hansen, A. G.: A Consistent Correlation for Three-Phase Relative Permeabilities and Phase Pressure Based on Three Sets of Two-Phase Data. Presented at the 8th European Symposium on Improved oil recovery, Vienna, Austria. May (1995)

Hyman, L. A., Brugler, M., Daneshjou, D., and Ohen, H.A.: *Improved Evaluation of Coal Reservoirs through Specialized Core Analysis.* Annual Report, GRI-91/0201. Carrollton, TX: Core Laboratories; Chicago, IL: Gas Research Institute. (1991)

Hyman, L. A., Ohen, H. A., Amaefule, J. O., and Daneshjou, D.: Simultaneous Determination of Capillary Pressure and Relative Permeability in Coalbed Methane Reservoirs. Coalbed Methane Symposium Proceedings. The University of Alabama/Tuscaloosa, 13-17 May (1991)

International Energy Agency (IEA), 2010. Oil Market Report. http://omrpublic.iea.org/.

Jennings, J. W., McGregor, D. S., and Morse, R. A.: Simultaneous Determination of Capillary Pressure and Relative Permeability by Automatic History Matching, *Formation Evaluation* 3(2), 322-328 (1988)

Johnson, E. F., Bossler, D. P., and Naumann, V. O.: Calculation of Relative Permeability from Displacement Experiments. *Pet. Trans. AIME* 216, 370-372 (1959)

Jones, S. C. and Roszelle, W. O.: Graphical Techniques for Determining Relative Permeability from Displacement Experiments. *JPT* 30(5), 807-817 (1978)

Juanes, R.: *Displacement Theory and Multiscale Numerical Modeling of Three-Phase Flow in Porous Media*. Ph.D. Dissertation, University of California at Berkeley, US (2003)

Kalaydjian, F. J. M., Moulu, J. C., Vizika, O., and Munkerud, P. K.: Three-Phase Flow in Water-Wet Porous Media: Gas/Oil Relative Permeabilities for Various Spreading Conditions. *JPSE* 17(3-4), 275-290 (1997)

Kerig, P. D. and Watson, A. T.: Relative-Permeability Estimation from Displacement Experiments: An Error Analysis. *SPERE* 1(2), 175-182 (1986)

Kerig, P. D. and Watson, A. T.: A New Algorithm for Estimating Relative Permeabilities from Displacement Experiments. *SPERE* 2(1), 103-112 (1987)

Koide, H., Tazaki, Y., Noguchi, Y., Nakayama, S., Iijima, M., Ito, K., and Shindo, Y.: Subterranean Containment and Long Term Storage of Carbon Dioxide in Unused Aquifers and in Depleted Natural Gas Reservoirs. *Energy Convers. Manag.* 33(5-8), 619-626 (1992)

Kokal, S., Maini, B. B.: An Improved Model for Estimating Three-Phase Oil-Gas-Water Relative Permeabilities from Two-phase Oil-Water and Oil-Gas phase. *JCPT* 29(2), 105-114 (1989)

Lai, W. and Brandt, h.: A Pressure-History-Matching Method for Determination of Relative Permeabilities. *SPERE* 3(2), 651-661 (1988)

Lake, L. W.: *Enhanced Oil Recovery*. Prentice Hall, Upper Saddle River, NJ, US (1989)

Land, C. S.: Calculation of Imbibition Relative Permeability for Two- and Three-Phase Flow from Rock Properties. *SPEJ* 8(2), 149-156 (1968)

Leverett, M. S. and Lewis, W. B.: Steady Flow of Gas-Oil Water Mixtures through Unconsolidated Sands. *Trans. AIME* 142(1), 107-116 (1941)

Lichiardopol, E. R.: *Estimation of Relative Permeability Parameters in Reservoir Engineering Applications*. M.Sc. Thesis, Delft University of Technology, Faculty of Electrical Engineering, Mathematics and Computer Science Delft Institute of Applied Mathematics. The Netherlands (1999)

Li, K. and Horne, R. N.: Numerical Simulation without Using Experimental Data of Relative Permeability. *JPSE* 61(2-4) 67-74 (2008)

Li, H.: Ensemble-based History Matching and Its Application in Estimating Reservoir Petrophysical Properties. Ph.D. Dissertation, The University of Regina, Canada, NR79962 (2011)

MacMillan, D. J.: Automatic History Matching of Laboratory Corefloods to Obtain Relative Permeability Curves. *SPERE* 2(1), 85-91 (1987)

Manjnath, A. and Honarpour, M.: An Investigation of Three-Phase Relative Permeability. Paper SPE 12915 presented at the 1984 Rocky Mountain Regional Meeting, Casper, WY, US, 21-23 May (1984)

Marin, A., Bornia, O., and Pinguet, B.: Case Study in Venezuela, Performance of Multiphase Meter in Extra Heavy oil. Paper SPE 117285 presented at the SPE International Thermal Operations and Heavy Oil Symposium, Calgary, AB, Canada, 20-23 October (2008)

Marle, C. M.: *Multiphase Flow in Porous Media*. Gulf Publishing, Houston. US (1981)

Marufuzzaman, M.: *Solubility and Diffusivity of Carbon Dioxide, Ethane and Propane in Heavy Oil and its SARA Fractions*. M.Sc. Thesis, The University of Regina, Canada, (2010)

Meyer, R. F. and Dietzman, W. D.: World Geography of Heavy Crude Oils. UNITAR Future of Heavy Crude and Tar Sands Conference, Edmonton, AB, Canada, 4-12 July (1979)

Moulu, J. C., Vizika, O., Egermann, P., and Kalaydjian, F.: A New Three-Phase Relative Permeability Model for Various Wettability Conditions. Paper SPE 56477 presented at the Annual Technical Conference and Exhibition, Houston, TX, US, 3-6 October (1999)

Muqeem, M. A., Bentsen, R. G., Maini, B. B.: An Improved Steady State Technique for Three-Phase Relative Permeability Measurements. CIM. Paper CIM 93-03 presented at the CIM Annual Technical Conference, Calgary, AB, Canada, 9-12 May (1993)

Naar, J. and Wygal, R. J.: Three-Phase Imbibition Relative Permeability. *SPEJ* 1(4), 254-258 (1961)

Nordtvedt, J. E., Ebeltft, E., Iversen, J. E., Stylte, A., Urkedal, H., Vatne, K. O., and Watson, A. T.: Determination of Three-Phase Relative Permeabilities from Displacement Experiments. *SPEFE* 12(4), 221-226 (1997)

Oak, M. J.: Three-Phase Relative Permeability of Water-Wet Berea. Paper SPE/DOE 20183 presented at the SPE/DOE 7th Symposium on Enhanced Oil Recovery, Tulsa, OK, US, 22-25 April (1990)

Oak, M. J. and Ehrlich, R.: A New X-Ray Absorption Method for Measurement of Three-Phase Relative Permeability. *SPERE* 3(1), 199-206 (1988)

Oak, M. J.: Three-Phase Relative Permeability of Intermediate-Wet Berea Sandstone. Paper SPE 22599 presented at the SPE Annual Technical Conference and Exhibition, Dallas, TX, US, 6-9 October (1991)

Oak, M. J., Baker, L. E., and Thomas, D. C.: Three-Phase Relative Permeability of Berea Sandstone. *JPT* 42(8), 1054-1061 (1990)

Ohen, H. A., Amaefule, J. O., Hyman, L. A., Daneshjou, D., and Schraufnagel, R. A.: A Systems Response Model for Simultaneous Determination of Capillary Pressure and Relative Permeability Characteristics of Coalbed Methane. Reservoir Engineering Proceedings, SPE Annual Technical Conference and Exhibition, Dallas, TX, US, 6-9 October (1991)

Oliveira, L. I. and Demond, A. H.: Estimation of Primary Drainage Three-Phase Relative Permeability for Organic Liquid Transport in the Vadose Zone. *J. of Contamination Hydrology* 66, 261-285 (2003)

Parker, M. A. and Williams, R.: Industry Steps Up Development of Heavy Oil Bitumen Reserves. *Oil and Gas J.* 46(12), 54-67 (1986)

Parmeswar, R. and Maerefat, N. L.: A Comparison of Methods for the Representation of Three-Phase Relative Permeability Data. Paper SPE 15061 presented at the 56th California Regional Meeting of the Society of Petroleum Engineers, Oakland, CA, US, 2-4 April (1986)

Pejic, D. and Maini, B. B.: Three-Phase Relative Permeability of Petroleum Reservoirs. Paper SPE 81021 presented at the SPE Latin America and Caribbean Petroleum Engineering Conference, Port of Spain, Trinidad, West Indies, April (2003)

Poulsen, S., Dyrhol, T. S., Stenby, S. O., and Skauge, A.: Including Capillary Pressure in Simulations of Steady State Relative Permeability Meaurements. SCA, (2000)

Qadeer, S., Dehghani, K., Ogbe, D. O., and Ostermann, R. D.: Correcting Oil/Water Relative Permeability Data for Capillary End Effect in Displacement

Experiments. Paper SPE 17423 presented at the California Regional Meeting of the Society of Petroleum Engineers, Long Beach, CA, US, 23-25 March (1988)

Reid, S.: *The Flow of Three Immiscible Fluids in Porous Media*. Ph.D. Dissertation, University of Birmingham, (1956)

Saraf, D. N. and Fatt, I.: Three-Phase Relative Permeability Measurement Using a Nuclear Magnetic Resonance Technique for Estimating Fluid Saturation. *SPEJ* 7(3), 235-242 (1967)

Sarem, A. M.: Three-Phase Relative Permeability Measurements by Unsteady-State Method. *SPEJ* 6(3), 199-205 (1966)

Schneider, F. N. and Owens, W. W.: Sandstone and Carbonate Two- and Three-Phase Relative Permeability Characteristics. *SPEJ* 10(1), 75-84 (1970)

Shojaei, H., Rastegar, R., and Jessen, K.: Mixing and Mass Transfer in Multicontact Miscible Misplacements. *Transport in Porous Media* 94(3), 837-857 (2012)

Siddiqui, S., Hicks, P. J., and Grader, A. S.: Verification of Buckley-Leverett Three-Phase Theory Using Computerized Tomography. *JPSE* 15(1), 1-21 (1995)

Sigmund, P. M. and McCaffery, F. G.: An Improved Unsteady-State Procedure for Determining the Relative-Permeability Characteristics of Heterogeneous Porous Media. *SPEJ* 19(1), 15-28 (1979)

Silpngarmlers, N., and Ertekin, T.: Artificial Neural Network Architectures for Predicting Two-Phase and Three-Phase Relative Permeability Characteristics. Paper SPE

Paper 77704 presented at the Annual Technical Conference and Exhibition, San Antonio, TX, US, 29 September-2 October (2002)

Shahverdi, H., Sohrabi, M., Fatemi, M., and Jamiolahmady, M.: Three-Phase Relative Permeability and Hysteresis Effect during WAG Process in Mixed Wet and Low IFT Systems. *JPSE* 78(1), 732-739 (2011)

Shahverdi, H, Sohrabi, M., and Jamiolahmady, M.: A New Algorithm for Estimating Three-Phase Relative Permeability from Unsteady-State Core Experiments. *Transport in Porous Media.* 90(3), 911-926 (2011)

Snell, R. W.: Measurement of Gas-Phase Saturation in a Porous Medium. *J. of the Institute of Pet.* 45, 428 (1959)

Snell, R. W.: Three-Phase Relative Permeability in an Unconsolidated Sand. *J. of the Institute of Pet.* 48, 459 (1962)

Snell, R. W.: The Saturation History Dependence of Three-Phase Oil Relative Permeability. *J. of the Institute of Pet.* 48, 459 (1963)

Spiteri, E. J. and Juanes, R.: Impact of Relative Permeability Hysteresis on the Numerical Simulation of WAG Injection. *JPSE,* 50(5), 115-139 (2006)

Stone, H. L.: Probability Model for Estimation of Three-Phase Relative Permeability. *JPT* 22(2), 214-218 (1970)

Stone, H. L.: Estimation of three-phase relative permeability and residual oil data. *JCPT* 12(4), 53-61 (1973)

Tharanivasan, A. K., Yang, C., and Gu, Y.: Measurements of Molecular Diffusion Coefficients of Carbon Dioxide, Methane and Propane in Heavy Oil under Reservoir Conditions. *Energy Fuels* 20(6), 2509-2517 (2006)

Udegbunam, E. O.: A FORTRAN Program for Interpretation of Relative Permeability from Unsteady-State Displacements with Capillary Pressure Included. *Computers and Geosciences* 17(10), 1351-1357 (1991)

Van Spronsen, E.: Three-Phase Relative Permeability Measurements Using the Centrifuge Method. Paper SPE/DOE 10688 presented at the SPE/DOE 3rd Symposium on EOR, Tulsa, OK, US, 4-7 April (1982)

Virnovsky, G. A., Mykkeltveit, J., and Nordtvedt, J. E.: Application of Steady State Three-Phase Simulator to Interpret Flow Experiments. SCA Conference paper 9635. (1996)

Watson, A. T., Richmond, P. C., Kerig, P. D., and Tao, T.M.: A Regression-Based Method for Estimating Relative Permeabilities from Displacement Experiments. *SPERE* 3(3), 953-958 (1988)

Welge, H. J.: A Simplified Method for Computing Oil Recovery by Gas or Water Drive. SPE paper 124 presented at the Petroleum Branch Fall Meeting, Oklahoma City, OK, US, 3-5 October (1952)

Wyllie, M. R. J. and Spanger, M. B.: *Application of Resistivity Measurements to Problem of Fluid Flow in Porous Media*, AAPG Bull., 36 359. (1952)

APPENDIX A: EXPERIMENTAL SETUPS

Images of experimental setups and major components.

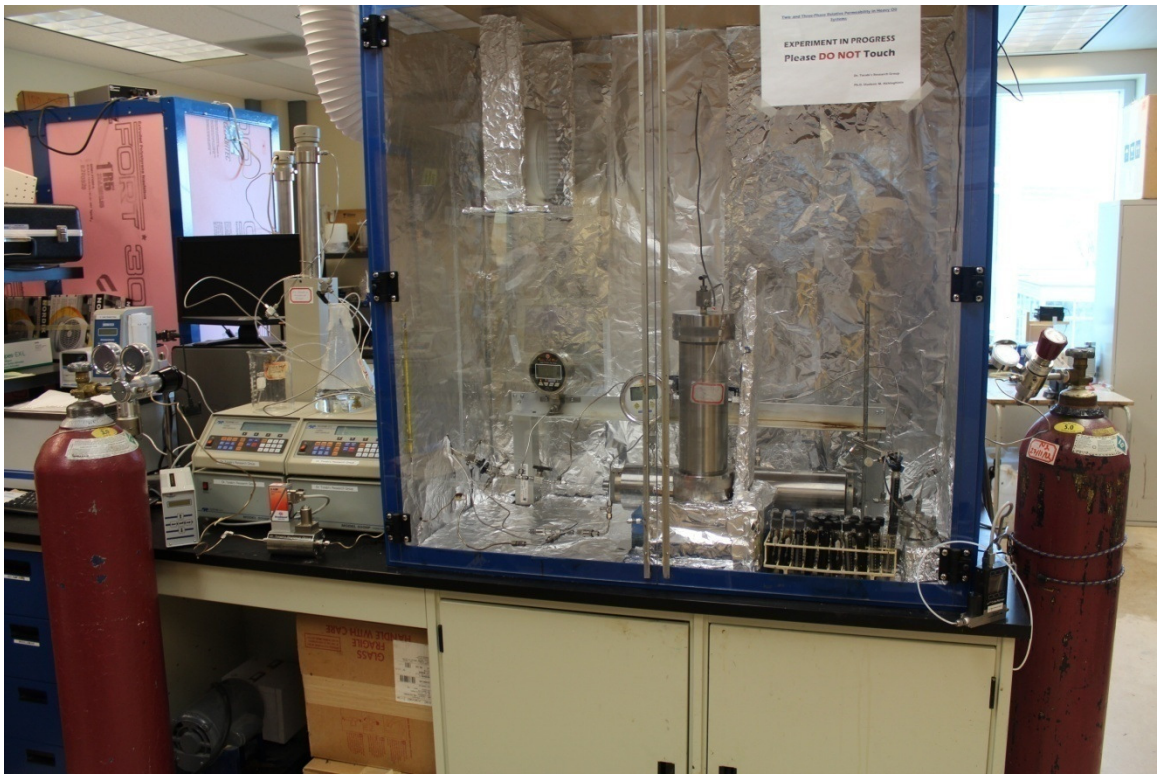

Figure A-1: Image of the experimental setup for three-phase steady state experiments.

Figure A-2: TEMCO core holder.

Figure A-3: ISCO 500D (D Series) syringe pump.

Figure A-4: MAKITA heating gun (Model HG1100).

Figure A-5: Precise HIGH-TECH BRONKHORST gas flow controller.

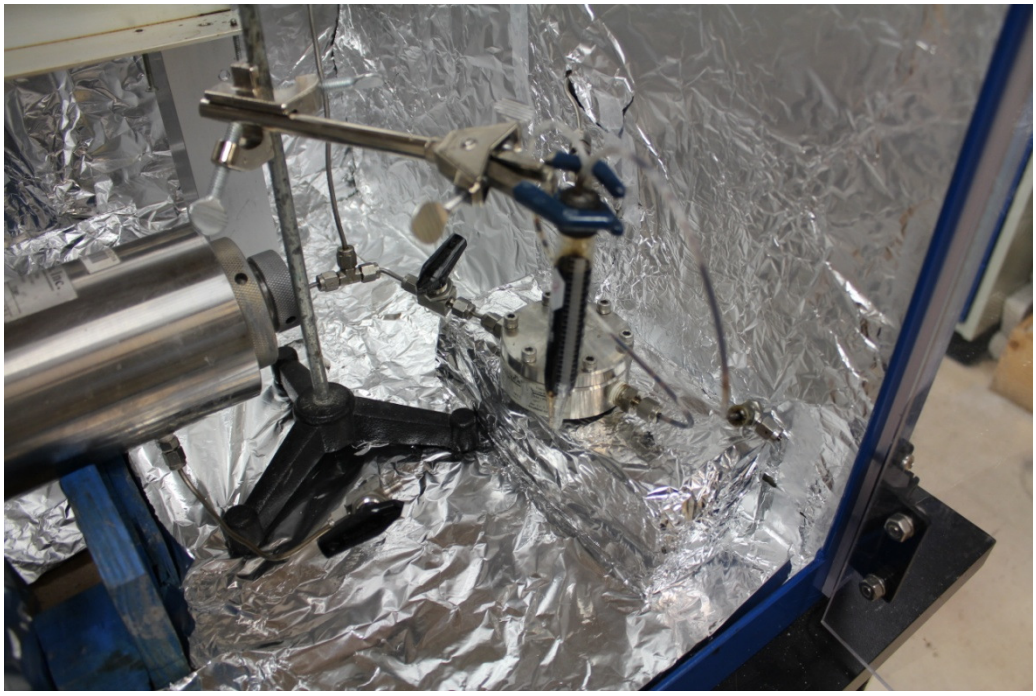

Figure A-6: Resin-sealed separator used for separating liquid effluent from the produced gas.

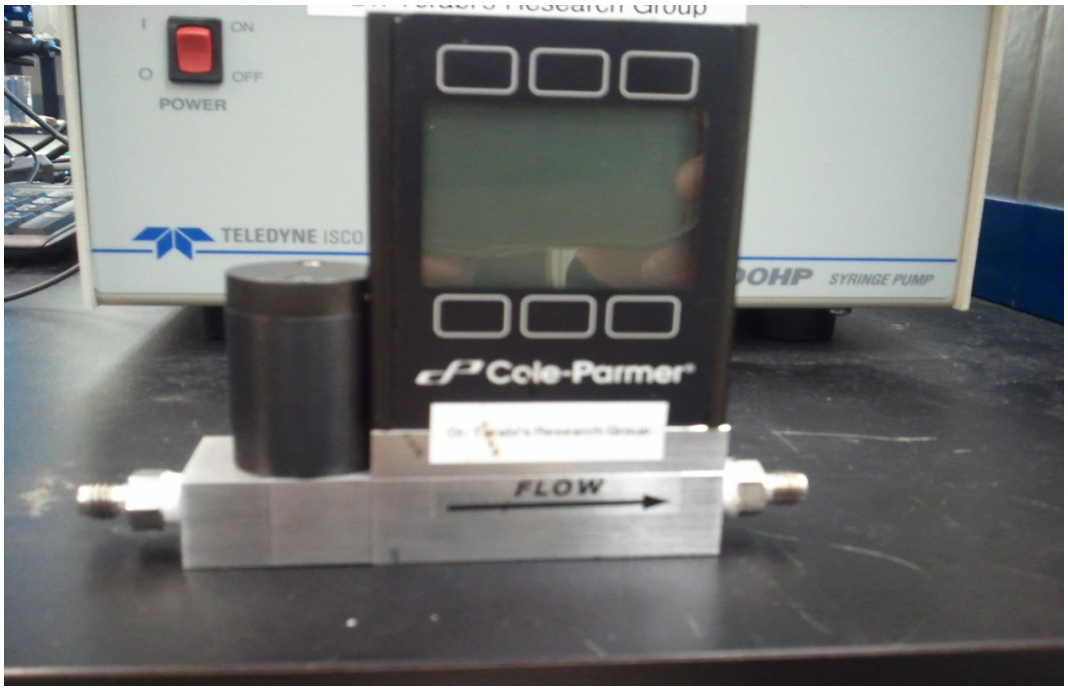

Figure A-7: COLE PARMER gas flow meter.

APPENDIX B: RESULTS OF THREE-PHASE DISPLACEMENT TESTS

Results from three-phase displacement experiments are presented below (see Section 5.4). Conditions for all tests are summarized in Table (5.2).

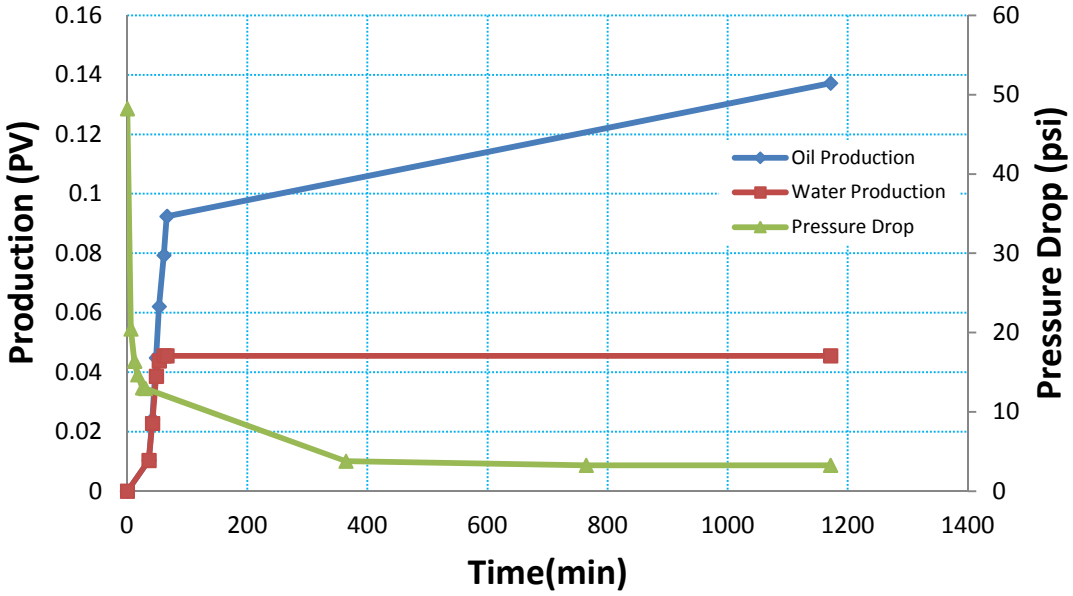

Figure B.1: Results from three-phase displacement experiment#2.

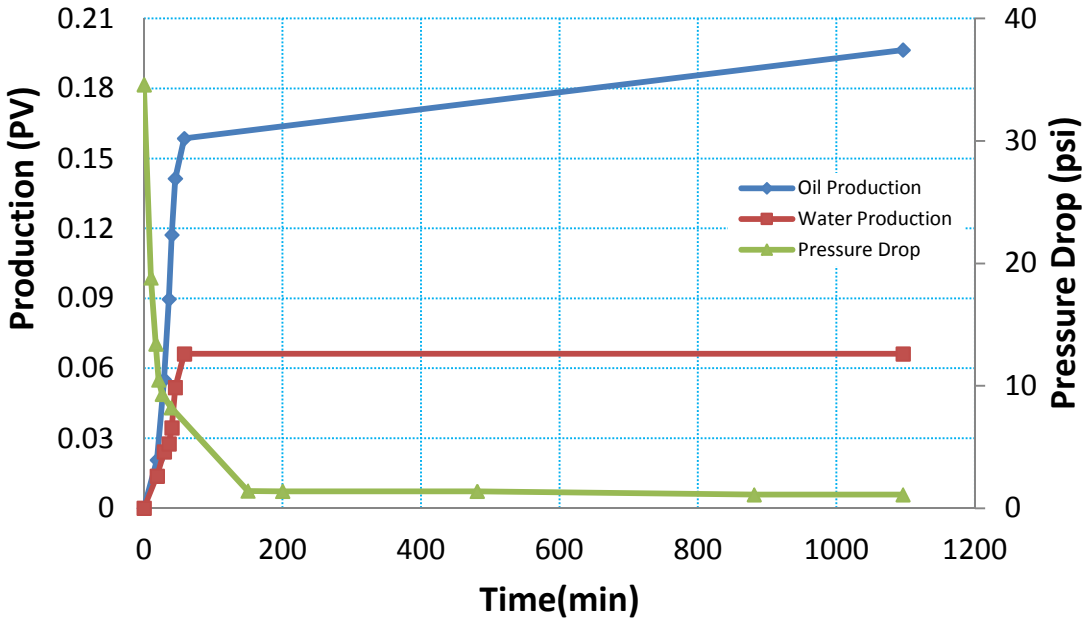

Figure B.2: Results from three-phase displacement experiment#3

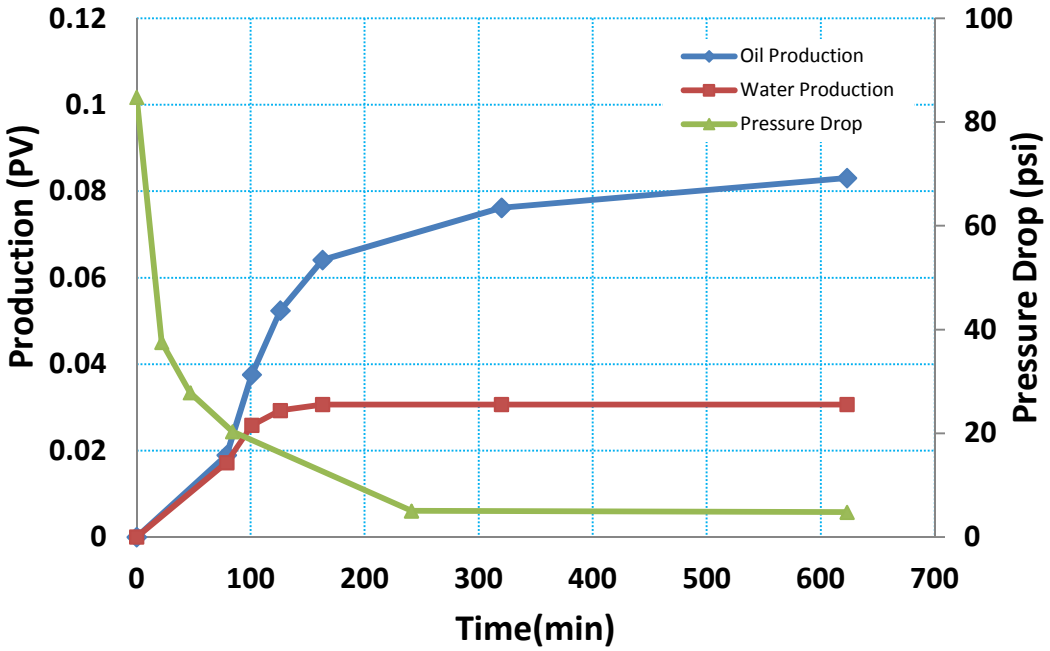

Figure B.3: Results from three-phase displacement experiment#4.

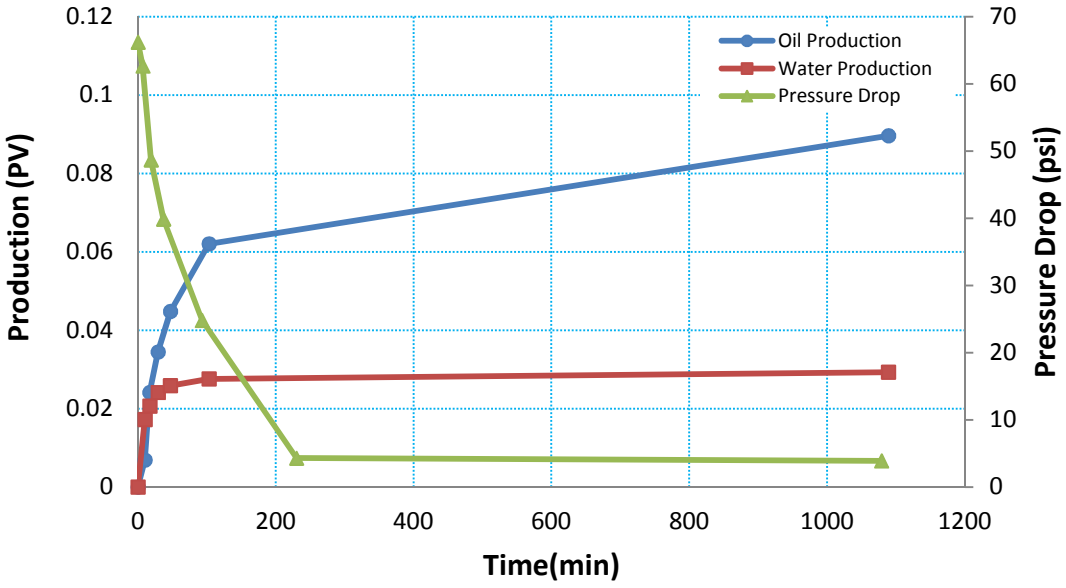

Figure B.4: Results from three-phase displacement experiment#5.

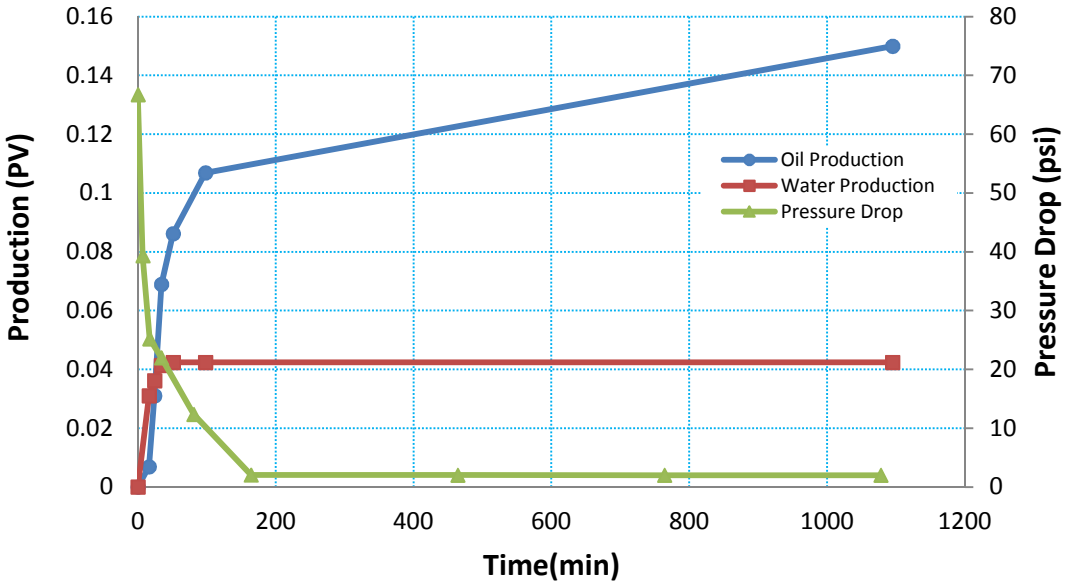

Figure B.5: Results from three-phase displacement experiment#6.

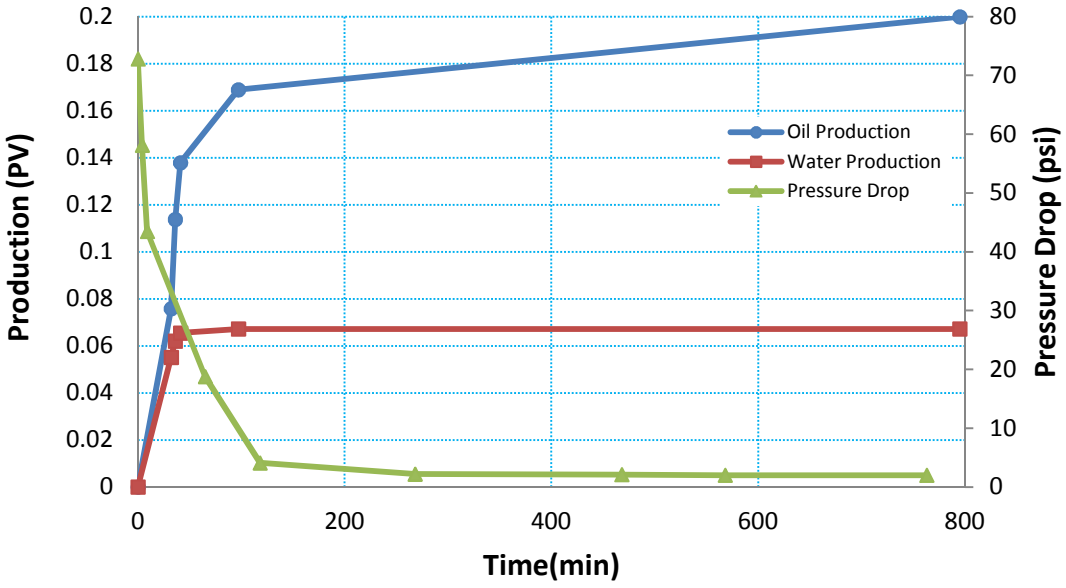

Figure B.6: Results from three-phase displacement experiment#7.

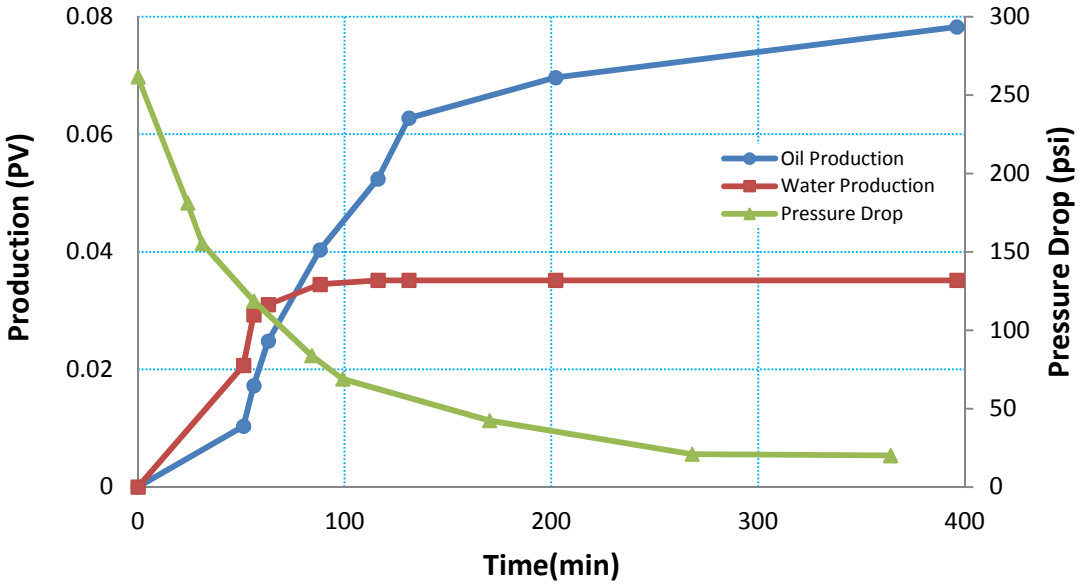

Figure B.7: Results from three-phase displacement experiment#8.

APPENDIX C: MATHEMATICAL MODEL OF DEVELOPED SIMULATOR

Procedure presented here was derived from Basic Applied Reservoir Simulation by Ertekin et al. (Ertekin et al., 2001). The simulation of hydrocarbon reservoir experiments involves the simultaneous flow of oil, water, and gas transporting multiphase fluid components. For a black oil three-phase displacement experiment described in the chapter 5, the three fluid components present are heavy oil, water, and gas. Ignoring mass transfer between phases, each fluid component is contained within its own phase, Figure (C.1). A combination of Darcy's law for multiphase flow with mass-conservation equations provides the following equations that govern three-phase flow of heavy oil, water, and gas in a one dimensional (x direction) horizontal core (Ertekin et al., 2001).

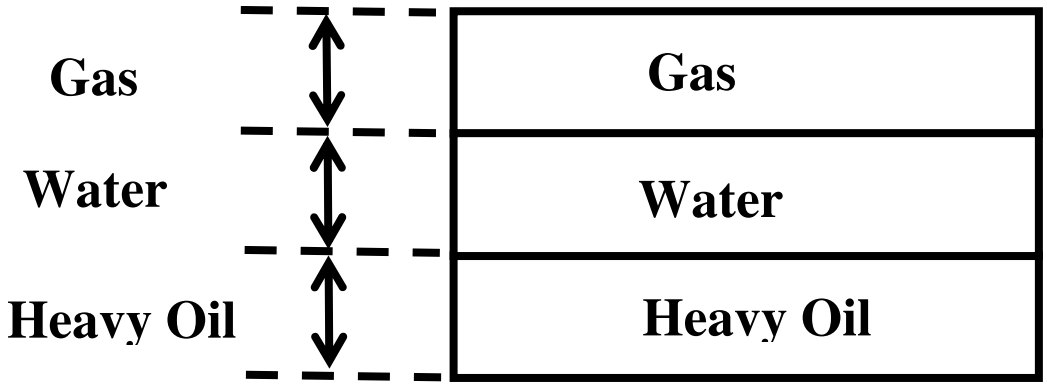

Figure C.1: Distribution of components among phases for a black oil system (Ertekin et al., 2001)

For oil phase:

$$\frac{\partial}{\partial x}\left[\beta_c kA\frac{k_{ro}}{\mu_o B_o}\left(\frac{\partial P}{\partial x}\right)\right]\Delta x = \frac{V_b}{\alpha_c}\frac{\partial}{\partial t}\left(\frac{\varphi S_o}{B_o}\right) - q_{osc} \quad \text{(C.1)}$$

Water phase:

$$\frac{\partial}{\partial x}\left[\beta_c kA\frac{k_{rw}}{\mu_w B_w}\left(\frac{\partial P}{\partial x}\right)\right]\Delta x = \frac{V_b}{\alpha_c}\frac{\partial}{\partial t}\left(\frac{\varphi S_w}{B_w}\right) - q_{wsc} \quad \text{(C.2)}$$

And gas phase:

$$\frac{\partial}{\partial x}\left[\beta_c kA\frac{k_{rg}}{\mu_g B_g}\left(\frac{\partial P}{\partial x}\right)\right]\Delta x = \frac{V_b}{\alpha_c}\frac{\partial}{\partial t}\left(\frac{\varphi S_g}{B_g}\right) - q_{gsc} \quad \text{(C.3)}$$

$$S_o + S_w + S_g = 1 \quad \text{(C.4)}$$

The terms q_{osc}, q_{wsc}, and q_{gsc} refer to production (injection) rates of the oil, water, and gas at standard condition. Subscripts o, w, and g refer to heavy oil, water, and gas. Assumptions for above equations are as follows:

- One dimensional flow in x-direction
- Horizontal flow
- Negligible capillary forces
- Absolutely dead oil (solution gas ratio is zero)
- Homogonous and isotropic condition for rock properties (porosity and absolute permeability)
- Isothermal condition
- No mass transfer between phases

Variables in Equations (5.1) to (5.4) are presented in Table (5.1) in field and metric units.

The flow equations can be reduced to three equations with three unknowns of P, S_w, and S_g if unknown S_o in the Equation (C.1) is replaced with 1-S_w-S_g from Equation (C.4). So the flow equations set of black oil model in this formulation become:

$$\frac{\partial}{\partial x}\left[\beta_c kA\frac{k_{ro}}{\mu_o B_o}\left(\frac{\partial P}{\partial x}\right)\right]\Delta x = \frac{V_b}{\alpha_c}\frac{\partial}{\partial t}\left(\frac{\varphi(1-S_w-S_g)}{B_o}\right) - q_{osc} \tag{C.5}$$

$$\frac{\partial}{\partial x}\left[\beta_c kA\frac{k_{rw}}{\mu_w B_w}\left(\frac{\partial P}{\partial x}\right)\right]\Delta x = \frac{V_b}{\alpha_c}\frac{\partial}{\partial t}\left(\frac{\varphi S_w}{B_w}\right) - q_{wsc} \tag{C.6}$$

$$\frac{\partial}{\partial x}\left[\beta_c kA\frac{k_{rg}}{\mu_g B_g}\left(\frac{\partial P}{\partial x}\right)\right]\Delta x = \frac{V_b}{\alpha_c}\frac{\partial}{\partial t}\left(\frac{\varphi S_g}{B_g}\right) - q_{gsc} \tag{C.7}$$

The analytical solution of these strongly non-linear partial difference equations is too complex. The finite difference approach, as a numerical solution, is used to solve the equation for P, S_w, S_g, and S_o. In this technique, the flow equations are discretized by use of algebraic approximations of the second order derivatives with respect to space and the first order derivatives with respect to time. Obtained equations are then solved by explicit or implicit solutions.

The finite difference approximation of the second order partial derivatives are:

$$\frac{\partial}{\partial x}\left[\beta_c kA\frac{k_{ro}}{\mu_o B_o}\left(\frac{\partial P}{\partial x}\right)\right]\Delta x \approx \Delta(T_o \Delta P) \tag{C.8}$$

Table C.1: Variables used in flow equations (Ertekin et al., 2001).

Quantity	Symbol	Customary Unit	Metric Unit	Conversion Factor
Length	x	ft	m	0.3048
Area	A	ft^2	m^2	0.0929
Permeability	k	darcy	μm^2	0.9869
Viscosity	μ	cP	Pa.s	0.001
Gas FVF*	B_g	bbl/scf	m^3/std m^3	5.5519
Liquid FVF	B_o, B_w	bbl/STB	m^3/std m^3	1
Pressure	P	psia	kPa	6.8947
Gas flow rate	q_{gsc}	scf/D	std m^3/D	0.0286
Liquid flow rate	q_{osc}, q_{wsc}	STB/D	std m^3/D	0.1589
Absolute temperature	T	ºR	K	0.5555
Relative permeability	k_r	fraction	fraction	1
Porosity	φ	fraction	fraction	1
Saturation	S	fraction	fraction	1
Compressibility factor	Z	dimensionless	dimensionless	1
Time	t	day	day	1
Transmissibility conversion factor	β_c	1.127	86.4×10^{-6}	---
Volume conversion factor	α_c	5.614583	1	---

* FVF or Formation Volume Factor

$$\frac{\partial}{\partial x}\left[\beta_c kA\frac{k_{rw}}{\mu_w B_w}\left(\frac{\partial P}{\partial x}\right)\right]\Delta x \approx \Delta(T_w \Delta P) \tag{C.9}$$

$$\frac{\partial}{\partial x}\left[\beta_c kA\frac{k_{rg}}{\mu_g B_g}\left(\frac{\partial P}{\partial x}\right)\right]\Delta x \approx \Delta(T_g \Delta P) \tag{C.10}$$

Where transmissibilities are defined as:

$$T_o = \beta_c \frac{kA}{\Delta x}\frac{k_{ro}}{\mu_o B_o} \tag{C.11}$$

$$T_w = \beta_c \frac{kA}{\Delta x}\frac{k_{rw}}{\mu_w B_w} \tag{C.12}$$

$$T_g = \beta_c \frac{kA}{\Delta x}\frac{k_{rg}}{\mu_g B_g} \tag{C.13}$$

Equations (C.5) to (C.7) now can be written in compact forms:

$$\Delta[T_o \Delta P] = \frac{V_b}{\alpha_c}\frac{\partial}{\partial t}\left[\frac{\varphi(1-S_w-S_g)}{B_o}\right] - q_{osc} \tag{C.14}$$

$$\Delta[T_w \Delta P] = \frac{V_b}{\alpha_c}\frac{\partial}{\partial t}\left[\frac{\varphi S_w}{B_w}\right] - q_{wsc} \tag{C.15}$$

$$\Delta\left[T_g \Delta P\right] = \frac{V_b}{\alpha_c}\frac{\partial}{\partial t}\left[\frac{\varphi S_g}{B_g}\right] - q_{gsc} \tag{C.16}$$

Discretization in space means applying a finite difference approximation to the second order derivative terms. In Figure (C.2), the core is divided into three gridblocks with length Δx_i. The distance between grid point (i) and (i-1) is $\Delta x_{i-1/2}$, and is $\Delta x_{i+1/2}$ between (i) and (i+1). The following relationship hold for both block centered and point distributed girds.

$$\Delta x_i = x_i - x_{i-1/2} \tag{C.17}$$

$$\Delta x_{i-1/2} = x_i - x_{i-1} \tag{C.18}$$

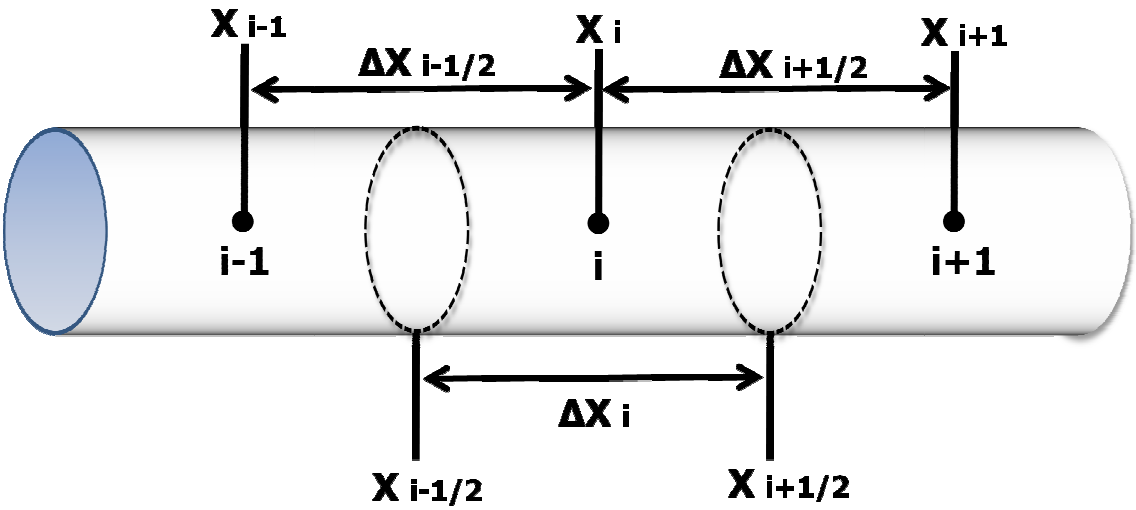

Figure C.2: Discretization in space.

$$\Delta x_{i+1/2} = x_{i+1} - x_i \tag{C.19}$$

The first derivative of an arbitrary variable f by the central difference approximation with f evaluated at gridblock boundaries (i+1/2) and (i-1/2) in x direction is:

$$\frac{\partial f}{\partial x} \approx \frac{f_{i+1/2} - f_{i-1/2}}{\Delta x_i} \tag{C.20}$$

Using Equation (C.20) twice for the left hand side of Equation (C.8) to (C.10) gives:

$$\Delta[T_o \Delta P] = To_{i+1/2}(P_{i+1} - P_i) - To_{i-\frac{1}{2}}(P_i - P_{i-1}) \tag{C.21}$$

$$\Delta[T_w \Delta P] = Tw_{i+1/2}(P_{i+1} - P_i) - Tw_{i-\frac{1}{2}}(P_i - P_{i-1}) \tag{C.22}$$

$$\Delta\left[T_g \Delta P\right] = Tg_{i+1/2}(P_{i+1} - P_i) - Tg_{i-\frac{1}{2}}(P_i - P_{i-1}) \tag{C.23}$$

For an arbitrary variable f, the partial derivative with respect to time becomes an ordinary derivative at i if the space domain is fixed at grid point i.

$$(\frac{\partial f}{\partial t})_i = \frac{d}{dt}(f_i) \approx \frac{1}{\Delta t}\Delta_t(f_i) = \frac{1}{\Delta t}({f_i}^{n+1} - {f_i}^n) \tag{C.24}$$

where n+1 means one time step after time level n.

With this approach, the partial derivative term of the right hand side of Equations (C.14) to (C.16) can be written as follows:

$$\frac{\partial}{\partial t}\left[\frac{\varphi(1-S_w-S_g)}{B_o}\right] = \frac{1}{\Delta t}\left[\left(\frac{\varphi(1-S_w-S_g)}{B_o}\right)^{n+1} - \left(\frac{\varphi(1-S_w-S_g)}{B_o}\right)^{n}\right] \tag{C.25}$$

$$\frac{\partial}{\partial t}\left[\frac{\varphi S_w}{B_w}\right] = \frac{1}{\Delta t}\left[\left(\frac{\varphi S_w}{B_w}\right)^{n+1} - \left(\frac{\varphi S_w}{B_w}\right)^{n}\right] \tag{C.26}$$

$$\frac{\partial}{\partial t}\left[\frac{\varphi S_g}{B_g}\right] = \frac{1}{\Delta t}\left[\left(\frac{\varphi S_g}{B_g}\right)^{n+1} - \left(\frac{\varphi S_g}{B_g}\right)^{n}\right] \tag{C.27}$$

Now implicit finite difference equations for all phases in the black oil model can be written in the following compact form if the right hand sides of the equations are also written at time level n+1:

$$To_{i+\frac{1}{2}}{}^{n+1}\left(P_{i+1}{}^{n+1}-P_i{}^{n+1}\right)-To_{i-\frac{1}{2}}{}^{n+1}\left(P_i{}^{n+1}-P_{i-1}{}^{n+1}\right)=\frac{V_b}{\alpha_c\Delta t}\left[\left(\frac{\varphi(1-S_w-S_g)}{B_o}\right)^{n+1}-\left(\frac{\varphi(1-S_w-S_g)}{B_o}\right)^{n}\right]-q_{osc}{}^{n+1} \quad \text{(C.28)}$$

$$Tw_{i+\frac{1}{2}}{}^{n+1}\left(P_{i+1}{}^{n+1}-P_i{}^{n+1}\right)-Tw_{i-\frac{1}{2}}{}^{n+1}\left(P_i{}^{n+1}-P_{i-1}{}^{n+1}\right)=\frac{V_b}{\alpha_c\Delta t}\left[\left(\frac{\varphi S_w}{B_w}\right)^{n+1}-\left(\frac{\varphi S_w}{B_w}\right)^{n}\right]-q_{wsc}{}^{n+1} \quad \text{(C.29)}$$

$$Tg_{i+\frac{1}{2}}{}^{n+1}\left(P_{i+1}{}^{n+1}-P_i{}^{n+1}\right)-Tg_{i-\frac{1}{2}}{}^{n+1}\left(P_i{}^{n+1}-P_{i-1}{}^{n+1}\right)=\frac{V_b}{\alpha_c\Delta t}\left[\left(\frac{\varphi S_g}{B_g}\right)^{n+1}-\left(\frac{\varphi S_g}{B_g}\right)^{n}\right]-q_{gsc}{}^{n+1} \quad \text{(C.30)}$$

To preserve mass conservation, the time difference operator acting on a function should be expressed in terms of the difference of the unknowns. For an arbitrary variable, such as f, an expansion scheme is described as conservative if the following identity is satisfied:

$$\Delta_t f = f^{n+1}-f^n \quad \text{(C.31)}$$

The general conservative expansion formula is:

$$\Delta_t(UVY)=(VY)^n\Delta_t U+U^{n+1}(Y)^n\Delta_t V+(UV)^{n+1}\Delta_t Y \quad \text{(C.32)}$$

For conservation expansion of a term $\Delta_t((\varphi S_w)/B_w)$, assume that $U=\varphi$, $V=1/B_w$, and $Y=S_w$. To preserve the conservative property of the expansion given by $\Delta_t(\varphi)$, $\Delta_t(S_i)$, and $\Delta_t(1/B_i)$, it should be expressed as product of the chord slope between successive time levels (n and n+1) and the time difference of the unknowns. That is,

$$\Delta_t(\varphi)=\varphi'\Delta_t P \quad \text{(C.33)}$$

$$\Delta_t(1/B_w) = (1/B_w)'\Delta_t P \tag{C.34}$$

$$\Delta_t(S_w) = \Delta_t S_w \tag{C.35}$$

Where

$$\varphi' = \frac{\varphi^{n+1}-\varphi^n}{P^{n+1}-p^n} \tag{C.36}$$

$$(1/B_w)' = \frac{(1/B_w)^{n+1}-(1/B_w)^n}{P^{n+1}-p^n} \tag{C.37}$$

Substituting in Equation (C.32) gives:

$$\Delta_t(\frac{\varphi S_w}{B_w})=(\frac{S_w}{B_w})^n\varphi'\Delta_t P + \varphi^{n+1}{S_w}^n(\frac{1}{B_w})'\Delta_t P + (\frac{\varphi}{B_w})^{n+1}\Delta_t S_w \tag{C.38}$$

Applying this approach for oil and gas phases gives the final form of the finite difference equation for the black oil system.

$$To_{i+\frac{1}{2}}{}^{n+1}\left({P_{i+1}}^{n+1} - {P_i}^{n+1}\right) - To_{i-\frac{1}{2}}{}^{n+1}\left({P_i}^{n+1} - {P_{i-1}}^{n+1}\right) = C_{ow}\left({Sw_i}^{n+1} - {Sw_i}^n\right) + C_{og}\left({Sg_i}^{n+1} - {Sg_i}^n\right) - {q_{osc}}^{n+1} \tag{C.39}$$

$$Tw_{i+\frac{1}{2}}{}^{n+1}\left({P_{i+1}}^{n+1} - {P_i}^{n+1}\right) - Tw_{i-\frac{1}{2}}{}^{n+1}\left({P_i}^{n+1} - {P_{i-1}}^{n+1}\right) = C_{ww}\left({Sw_i}^{n+1} - {Sw_i}^n\right) - {q_{wsc}}^{n+1} \tag{C.40}$$

$$Tg_{i+\frac{1}{2}}{}^{n+1}\left({P_{i+1}}^{n+1} - {P_i}^{n+1}\right) - Tg_{i-\frac{1}{2}}{}^{n+1}\left({P_i}^{n+1} - {P_{i-1}}^{n+1}\right) = C_{gp}\left({P_i}^{n+1} - {P_i}^n\right) + C_{gg}\left({Sg_i}^{n+1} - {Sg_i}^n\right) - {q_{gsc}}^{n+1} \tag{C.41}$$

Where

$$C_{ow} = -\frac{V_b}{\alpha_c \Delta t}(\frac{\varphi}{B_o})^{n+1} \tag{C.42}$$

$$C_{og} = -\frac{V_b}{\alpha_c \Delta t}(\frac{\varphi}{B_o})^{n+1} \tag{C.43}$$

$$C_{ww} = -\frac{V_b}{\alpha_c \Delta t}(\frac{\varphi}{B_w})^{n+1} \tag{C.44}$$

$$C_{gp} = \frac{V_b}{\alpha_c \Delta t}\varphi^{n+1}(\frac{1}{B_g})'Sg^n \tag{C.45}$$

$$C_{gg} = \frac{V_b}{\alpha_c \Delta t}(\frac{\varphi}{B_g})^{n+1} \tag{C.46}$$

In Equations (C.39) to (C.41), transmissibility terms of oil, water, and gas phases for a homogenous core are in the form of:

$$T_{i\pm1/2} = \beta_c \frac{kA}{\Delta x} \left(\frac{k_r}{\mu B}\right)_{i\pm1/2} \tag{C.47}$$

Where the plus and minus signs in the subscripts are used to identify gridblock boundaries in the positive and negative directions of the Cartesian coordinates. Single point upstream weighting has been used to determine $\left(\frac{k_r}{\mu B}\right)_{i+1/2}$ at interblocks. It means that at the boundary *i*+1/2 between gridblocks *i* and *i*+1

$$\left(\frac{k_r}{\mu B}\right)_{i+1/2} = \left(\frac{k_r}{\mu B}\right)_i \tag{C.48}$$

If flow is from gridblock i to gridblock *i*+1, and

$$\left(\frac{k_r}{\mu B}\right)_{i+1/2} = \left(\frac{k_r}{\mu B}\right)_{i+1} \tag{C.49}$$

If flow is from gridblock *i*+1 to gridblock *i*.

In the three-phase displacement experiment described in the previous chapter, is injected at a constant flow rate from one end of the core and the three-phase production of oil, water, and gas occur at a constant pressure imposed by the back pressure regulator. In Figure (C.2), it is assumed that gas is injected at grid *i*-1. For treatment of gas injection at this grid, since flow always occur from gridblock *i*-1 to gridblock *i*, a no-flow boundary is used at the left hand side of the gird *i*-1 by setting the left hand side transmissibility equal to zero at all time steps. In the case of production under constant pressure from the last grid *i*+1, an imaginary grid is assumed at the right hand side of the grid *i*+1, with pressure equal to pressure set on the back pressure regulator for all time steps.

In Equations (C.39) to (C.41), P, S_w, and S_g are the primary variables, and unknowns to be solved for. All the coefficients in the equations, transmissibilities, as well as storage coefficients, are functions of these unknowns. Thus, these equations cannot be solved before the coefficients are calculated, and the coefficients cannot be calculated before the unknown pressures and saturations have been solved. Obviously, a solution method is needed that either iterates on the solution and updates coefficients and capillary pressures until convergence is reached. A fully implicit technique has been used to solve multiphase difference equations. Although this technique is an iterative method, there is no concern about the stability of the solution at higher time levels. As the name implies, all the equations for multiphase flow are solved simultaneously. The flowchart of the implicit technique is presented in Figure (C.3). This scheme has been implemented in a MATLAB software environment to simulate three-phase displacement experiments.

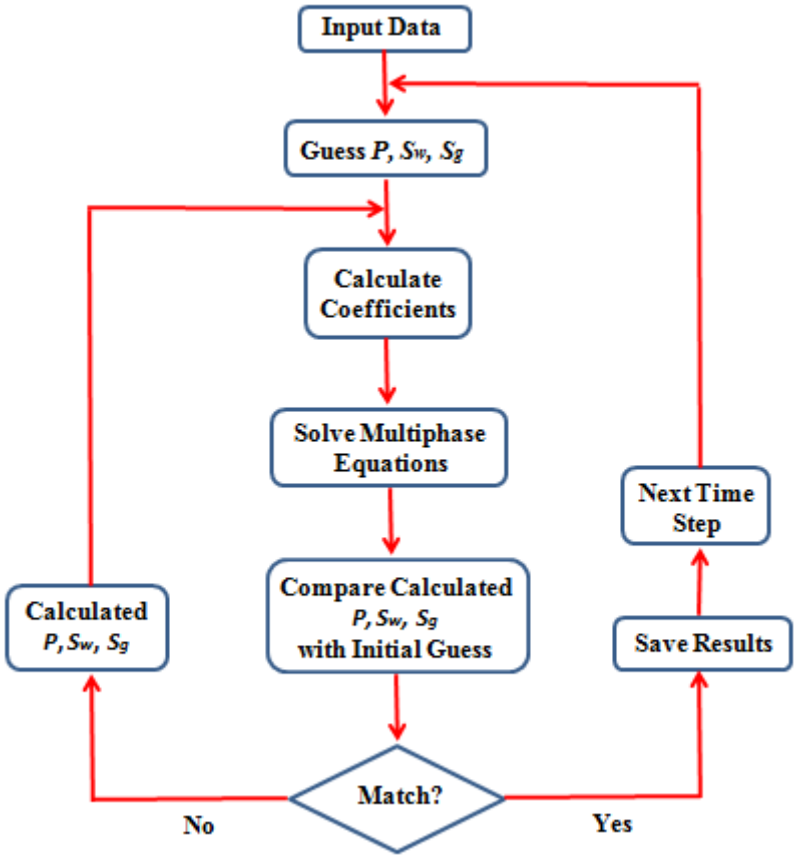

Figure C.3: Flowchart of solving flow equations with implicit technique.

APPENDIX D: MATLAB CODE FOR DEVELOPED SIMULATOR

Following program has been developed in the MATLAB software environment to simulate three-phase displacement experiments. It couples with EXCEL software to compare simulation results to observed data from experiments. Transmissibility functions are presented after the main program. All input data to the simulator such as rock/fluid properties are those presented in details in chapter 3. Initial condition (e.g. initial saturation), injection rate, pressure constraint etc were also presented in chapter 5. Calculations were performed with one minute as time step over ten grids in the x direction. Time

```
clear all
close all
clc
Length=input('Enter Length of the Core = ');
Area=input('Enter Cross Sectional Area of The Core = ');
Alpha=input('Enter Volume conversion factor = ');
Beta=input('Enter Transmissibility conversion factor = ');
Grids=input('Enter Number of Grids = ');
Phi=input('Enter Porosity = ');
Temp=input('Enter Temperature = ');
K=input('Enter Absolute Permeability = ');
Bw=input('Enter Formation Volume Factor for Water = ');
Bo=input('Enter Formation Volume Factor for Oil = ');
Visc_w=input('Enter Water Viscosity = ');
Visc_o=input('Enter Oil Viscosity = ');
x=1:Grids;
Delta_x=Length/Grids;
Phi=Phi.*ones(1,length(x));
K=K.*ones(1,length(x));
Bw=Bw.*ones(1,length(x));
Bo=Bo.*ones(1,length(x));
Visc_w=Visc_w.*ones(1,length(x));
Visc_o=Visc_o.*ones(1,length(x));
Vb=Area*Delta_x;
Swi=input('Enter Irreducible Water Saturation = ');
Sor=input('Enter Residual Oil Saturation = ');
Delta_t=input('Enter Time Step = ');
Delta_t=5*Delta_t;
Time=input('Enter Final Time = ');
t=0:Delta_t:Time;
P_Initial=input('Enter Initial Core Pressure = ');
Back_Pressure=input('Enter Pressure Set at BAck Pressure Regulator = ');
Sw_Initial=input('Enter Initial Water Saturation = ');
So_Initial=input('Enter Initial Oil Saturation = ');
Q_Gas=input('Enter CO2 Injection Rate = ');
Q_Gas=Q_Gas*0.00138;
steps=length(t);
P=ones(length(x),steps);
So=ones(length(x),steps);
Sw=ones(length(x),steps);
Sg=ones(length(x),steps);
P(:,1)=P_Initial;
So(:,1)=So_Initial;
Sw(:,1)=Sw_Initial;
Sg(:,1)=Sg_Initial;
Bg=ones(length(x),steps);
Z_g=ones(length(x),steps);
a=1;
aa=a.*(Grids:-1:1);
P(:,2)=P(:,1)+aa';
Error=1;
for m=1:(steps-1)
    m=m;
    for i=1:length(x)
        if Sw(i,m)<=Swi
            Sw(i,m)=Swi;
        end
```

```
        if Sg(i,m)<=0.01
            Sg(i,m)=0.01;
        end
    end
    for i=1:length(x)
        if Sw(i,m)>=(1-Sor-0.01)
            Sw(i,m)=1-Sor-0.01;
        end
        if Sg(i,m)>=(1-Sor-Swi)
            Sg(i,m)=1-Sor-Swi;
        end
    end
    Sw(:,m+1)=Sw(:,m);
    Sg(:,m+1)=Sg(:,m);
    So(:,m+1)=1-Sw(:,m+1)-Sg(:,m+1);
    kk=1
    Error=1;
    while Error>0.01
        Visc_g=%Recall CO2 Viscosity at P and T%
        Z_g(:,m)=%Recall CO2 Compressibility Factor at P and T%
        Bg(:,m)=0.005035.*((Temp.*Z_g(:,m))./(P(:,m)));
        Z_g(:,m+1)=Z_g_Cal(P(:,m+1));
        Bg(:,m+1)=0.005035.*((Temp.*Z_g(:,m+1))./(P(:,m+1)));
        Kro=%Recall Relative Permeability to Oil%
        Krw=%Recall Relative Permeability to Water%
        Krg=%Recall Relative Permeability to CO2%
        To=ones(length(x),2);
        for i=1:length(x)
            for o=1:2

To(i,o)=To_Cal(i,o,Beta,K,Area,Delta_x,Visc_o,Bo,Kro,P(:,m+1));
            end
        end
        Tw=ones(length(x),2);
        for i=1:length(x)
            for o=1:2

Tw(i,o)=Tw_Cal(i,o,Beta,K,Area,Delta_x,Visc_w,Bw,Krw,P(:,m+1));
            end
        end
        Tg=ones(length(x),2);
        for i=1:length(x)
            for o=1:2

Tg(i,o)=Tg_Cal(i,o,Beta,K,Area,Delta_x,Visc_g,Bg(:,m+1),Krg,P(:,m+1));
            end
        end
        Oil_P=zeros(length(x));
        Oil_Sw=zeros(length(x));
        Oil_Sg=zeros(length(x));
        Water_P=zeros(length(x));
        Water_Sw=zeros(length(x));
        Water_Sg=zeros(length(x));
        Gas_P=zeros(length(x));
        Gas_Sw=zeros(length(x));
        Gas_Sg=zeros(length(x));
        Cow=ones(length(x),1);
```

```
        Cog=ones(length(x),1);
        Cww=ones(length(x),1);
        Cgg=ones(length(x),1);
        Cgp=ones(length(x),1);
        for i=1:length(x)
            Cow(i)=-(Vb/(Delta_t*Alpha))*(Phi(i)/Bo(i));
            Cog(i)=-(Vb/(Delta_t*Alpha))*(Phi(i)/Bo(i));
            Cww(i)=(Vb/(Delta_t*Alpha))*(Phi(i)/Bw(i));
            Cgg(i)=(Vb/(Delta_t*Alpha))*(Phi(i)/Bg(i,m+1));
            if P(i,m+1)==P(i,m)
                Cgp(i)=0;
            else
                A=((1/Bg(i,m+1))-(1/Bg(i,m)))/(P(i,m+1)-P(i,m));
                Cgp(i)=(Vb/(Delta_t*Alpha))*Phi(i)*A*Sg(i,m);
            end
        end
       for i=1:length(x)
           if i==length(x)
               Oil_P(i,i)=-
(To(i,1)+2*(Beta*((K(i)*Area)/Delta_x)*(1/(Visc_o(i)*Bo(i)))*Kro(i)));
               Water_P(i,i)=-
(Tw(i,1)+2*(Beta*((K(i)*Area)/Delta_x)*(1/(Visc_w(i)*Bw(i)))*Krw(i)));
               Gas_P(i,i)=-
(Tg(i,1)+Cgp(i)+2*(Beta*((K(i)*Area)/Delta_x)*(1/(Visc_g(i)*Bg(i,m+1)))*
Krg(i)));
           else
              Oil_P(i,i)=-(To(i,1)+To(i,2));
              Water_P(i,i)=-(Tw(i,1)+Tw(i,2));
              Gas_P(i,i)=-(Tg(i,1)+Tg(i,2)+Cgp(i));
           end
       end
        for i=1:length(x)
            Oil_Sw(i,i)=-Cow(i);
            Oil_Sg(i,i)=-Cog(i);
            Water_Sw(i,i)=-Cww(i);
            Water_Sg(i,i)=0;
            Gas_Sw(i,i)=0;
            Gas_Sg(i,i)=-Cgg(i);
        end
        for i=2:length(x)
            Oil_P(i-1,i)=To(i-1,2);
            Water_P(i-1,i)=Tw(i-1,2);
            Gas_P(i-1,i)=Tg(i-1,2);
        end
         for i=2:length(x)
             Oil_P(i,i-1)=To(i,1);
             Water_P(i,i-1)=Tw(i,1);
             Gas_P(i,i-1)=To(i,1);
         end
         Known_Oil=ones(length(x),1);
         Known_Water=ones(length(x),1);
         Known_Gas=ones(length(x),1);
         for i=1:length(x)
             if i==1
                 Known_Oil(i)=-Cow(i)*Sw(i,m)-Cog(i)*Sg(i,m);
                 Known_Water(i)=-Cww(i)*Sw(i,m);
                 Known_Gas(i)=-Cgp(i)*P(i,m)-Cgg(i)*Sg(i,m)-Q_Gas;
```

```
            elseif 1==length(x)
                Known_Oil(i)=-
2*(Beta*((K(i)*Area)/Delta_x)*(1/(Visc_o(i)*Bo(i)))*Kro(i))*Back_Pressur
e-Cow(i)*Sw(i,m)-Cog(i)*Sg(i,m);
                Known_Water(i)=-
2*(Beta*((K(i)*Area)/Delta_x)*(1/(Visc_w(i)*Bw(i)))*Krw(i))*Back_Pressur
e-Cww(i)*Sw(i,m);
                Known_Gas(i)=-
2*(Beta*((K(i)*Area)/Delta_x)*(1/(Visc_g(i)*Bg(i,m+1)))*Krg(i))*Back_Pre
ssure-Cgp(i)*P(i,m)-Cgg(i)*Sg(i,m);
            else
                Known_Oil(i)=-Cow(i)*Sw(i,m)-Cog(i)*Sg(i,m);
                Known_Water(i)=-Cww(i)*Sw(i,m);
                Known_Gas(i)=-Cgp(i)*P(i,m)-Cgg(i)*Sg(i,m);
            end
        end
         Coefficient=[Oil_P Oil_Sw Oil_Sg;Water_P Water_Sw
Water_Sg;Gas_P Gas_Sw Gas_Sg];
         Known=[Known_Oil;Known_Water;Known_Gas];
         Javab=(Coefficient^(-1))*Known;
         feshar=Javab(1:length(x));
         ab=(Javab(length(x)+1:2*length(x)));
         gaz=(Javab(2*length(x)+1:3*length(x)));
         naft=1-ab-gaz;
         if min(abs(feshar-P(:,m+1)))<1
             P(:,m+1)=feshar;
             Sw(:,m+1)=ab;
             Sg(:,m+1)=gaz;
             So(:,m+1)=1-Sg(:,m+1)-Sw(:,m+1);
             Error=0.001;
         else
            P(:,m+1)=feshar;
         end
         kk=kk+1;
    end
end
T_Lab1=%Read Time Data For Experiment%
P_Lab=%Read Observed Pressure Data from Experiment%
figure (1)
plot(T_Lab1,P_Lab,'k-')
ylim([0 200])
title(['Pressure vs. Time']);
xlabel('Time (min)');
ylabel('Pressure (Psi)');
T_Sim=[0:m-1];
T_Sim=24.*60.*Delta_t.*T_Sim;
P_Sim=ones(1,m);
for i=1:m
    P_Sim(i)=P(1,i)-P(length(x),i);
end
hold on
plot(T_Sim,P_Sim,'r-')
IOIP=Grids*Vb*Phi(1)*So_Initial*28317;
Oil_Rec_Sim=ones(1,m);
for i=1:m
    Oil_Rec_Sim(i)=(IOIP-sum(28317.*Vb.*Phi(1).*So(:,i)))/32.6118;
end
```

```
T_Lab2=%Read Time Data For Experiment%
Oil_Lab=%Read Observed Oil Production Data from Experiment%
figure (2)
plot(T_Lab2,Oil_Lab,'k-')
ylim([0 0.5])
title(['Oil Recovery']);
xlabel('Time (min)');
ylabel('Oil Recovery (Psi)');
hold on
plot(T_Sim,Oil_Rec_Sim,'r-')
IWIP=Grids*Vb*Phi(1)*Sw_Initial*28317;
Water_Rec_Sim=ones(1,m);
for i=1:m
    Water_Rec_Sim(i)=(IWIP-sum(28317.*Vb.*Phi(1).*Sw(:,i)))/32.6118;
end
Water_Lab=%Read Observed Water Production Data from Experiment%
figure (3)
plot(T_Lab2,Water_Lab,'k-')
ylim([-0.05 0.22])
title(['Water Recovery']);
xlabel('Time (min)');
ylabel('Water Recovery (Psi)');
hold on
plot(T_Sim,Water_Rec_Sim,'r-')
%Save Time Data from Simulation%
%Save Pressure Data from Simulation%
%Save Oil Production Data from Simulation%
%Save Water Production Data from Simulation%
close all
clear all
clc
Swi=input('Enter Irreducible Water Saturation = ');
Sor=input('Enter Residual Oil Saturation = ');
x=0:0.1:100/(3^(0.5));
y=(3^(0.5)).*x;
plot(x,y,'k-')
clear x
clear y
hold on
x=100/(3^(0.5)):0.1:200/(3^(0.5));
y=-(3^(0.5)).*(x-(200/(3^(0.5))));
plot(x,y,'k-')
clear x
clear y
x=0:0.1:200/(3^(0.5));
for i=1:length(x)
    y(i)=0;
end
plot(x,y,'k-')
clear x
clear y
hold on
for i=10:10:90
    x(i/10,:)=(1/(3^(0.5)))*i:0.1:-(1/(3^(0.5)))*i+200/(3^(0.5));
    for j=1:length(x(i/10,:))
        y(i/10,j)=i;
    end
```

```
    plot(x(i/10,:),y(i/10,:),'b-.')
    clear x
    clear y
end
for i=10:10:90
    x(i/10,:)=(2/(3^(0.5)))*i:0.1:((3^(0.5))/6)*(200+2*i);
    for j=1:length(x(i/10,:))
        y(i/10,j)=(3^(0.5))*(x(i/10,j)-(2/(3^(0.5)))*i);
    end
    plot(x(i/10,:),y(i/10,:),'b-.')
    clear x
    clear y
end
for i=10:10:90
    x(i/10,:)=(1/(3^(0.5)))*i:0.1:(2/(3^(0.5)))*i;
    for j=1:length(x(i/10,:))
        y(i/10,j)=-(3^(0.5))*(x(i/10,j)-(2/(3^(0.5)))*i);
    end
    plot(x(i/10,:),y(i/10,:),'b-.')
    clear x
    clear y
end
i=Swi;
x=(2/(3^(0.5)))*i:0.1:((3^(0.5))/6)*(200+2*i);
for j=1:length(x)
    y(j)=(3^(0.5))*(x(j)-(2/(3^(0.5)))*i);
end
P1=plot(x,y,'g-');
clear x
clear y
clear i
i=100-Sor;
x=(1/(3^(0.5)))*i:0.1:(2/(3^(0.5)))*i;
for j=1:length(x)
    y(j)=-(3^(0.5))*(x(j)-(2/(3^(0.5)))*i);
end
P2=plot(x,y,'m-');
clear x
clear y
clear i
Oil1=%Read Oil Saturation Data, Path 1%
Water1=%Read Water Saturation Data, Path 1%
Oil1=100.*Oil1;
Water1=100.*Water1;
Gas1=100-Oil1-Water1;
y1=Gas1;
x1=-(2.*Oil1+y1-200)./(3^(0.5));
Krg1=%Read Gas Relative Permeability Data Correspond to  Path 1%
plot(x1,y1,'K.')
Oil2=%Read Oil Saturation Data, Path 2%
Water2=%Read Oil Saturation Data, Path 2%
Oil2=100.*Oil2;
Water2=100.*Water2;
Gas2=100-Oil2-Water2;
y2=Gas2;
x2=-(2.*Oil2+y2-200)./(3^(0.5));
Krg2=%Read Gas Relative Permeability Data Correspond to  Path 2%
```

```
plot(x2,y2,'K.')
Oil3=%Read Oil Saturation Data, Path 3%
Water3=%Read Oil Saturation Data, Path 3%
Oil3=100.*Oil3;
Water3=100.*Water3;
Gas3=100-Oil3-Water3;
y3=Gas3;
x3=-(2.*Oil3+y3-200)./(3^(0.5));
Krg3=%Read Gas Relative Permeability Data Correspond to  Path 3%
plot(x3,y3,'K.')
min1=min(Krg1);
min2=min(Krg2);
min3=min(Krg3);
max1=max(Krg1);
max2=max(Krg2);
max3=max(Krg3);
Krg_min=max([min1 min2 min3]);
Krg_max=min([max1 max2 max3]);
Curves=Krg_min:(Krg_max-Krg_min)/7:Krg_max;
U=ones(3,2,(length(Curves)-2));
for i=2:(length(Curves)-1)
    U(1,1,i-1)=interp1(Krg1,x1,Curves(i));
    U(1,2,i-1)=((3^(0.5))/3).*(U(1,1,i-1)-(2/(3^(0.5)))*(Swi));
    U(2,1,i-1)=interp1(Krg2,x2,Curves(i));
    U(2,2,i-1)=((3^(0.5))/6).*(U(2,1,i-1)-(2/(3^(0.5)))*(Swi));
    U(3,1,i-1)=interp1(Krg3,x3,Curves(i));
    U(3,2,i-1)=((3^(0.5))/(3/2)).*(U(3,1,i-1)-(2/(3^(0.5)))*(Swi));
end
P3=plot(U(:,1,1),U(:,2,1),'ro');
P4=plot(U(:,1,2),U(:,2,2),'r+');
P5=plot(U(:,1,3),U(:,2,3),'r*');
P6=plot(U(:,1,4),U(:,2,4),'rs');
P7=plot(U(:,1,5),U(:,2,5),'rh');
P8=plot(U(:,1,6),U(:,2,6),'rv');
legend([P1 P2 P3 P4 P5 P6 P7
P8],'Swi','Sor',num2str(Curves(2)),num2str(Curves(3)),num2str(Curves(4))
,num2str(Curves(5)),num2str(Curves(6)),num2str(Curves(7)))
close all
clear all
clc
Swi=input('Enter Irreducible Water Saturation = ');
Sor=input('Enter Residual Oil Saturation = ');
x=0:0.1:100/(3^(0.5));
y=(3^(0.5)).*x;
plot(x,y,'k-')
clear x
clear y
hold on
x=100/(3^(0.5)):0.1:200/(3^(0.5));
y=-(3^(0.5)).*(x-(200/(3^(0.5))));
plot(x,y,'k-')
clear x
clear y
x=0:0.1:200/(3^(0.5));
for i=1:length(x)
    y(i)=0;
end
```

```
plot(x,y,'k-')
clear x
clear y
hold on
for i=10:10:90
    x(i/10,:)=(1/(3^(0.5)))*i:0.1:-(1/(3^(0.5)))*i+200/(3^(0.5));
    for j=1:length(x(i/10,:))
        y(i/10,j)=i;
    end
    plot(x(i/10,:),y(i/10,:),'b-.')
    clear x
    clear y
end
for i=10:10:90
    x(i/10,:)=(2/(3^(0.5)))*i:0.1:((3^(0.5))/6)*(200+2*i);
    for j=1:length(x(i/10,:))
        y(i/10,j)=(3^(0.5))*(x(i/10,j)-(2/(3^(0.5)))*i);
    end
    plot(x(i/10,:),y(i/10,:),'b-.')
    clear x
    clear y
end
for i=10:10:90
    x(i/10,:)=(1/(3^(0.5)))*i:0.1:(2/(3^(0.5)))*i;
    for j=1:length(x(i/10,:))
        y(i/10,j)=-(3^(0.5))*(x(i/10,j)-(2/(3^(0.5)))*i);
    end
    plot(x(i/10,:),y(i/10,:),'b-.')
    clear x
    clear y
end
i=Swi;
x=(2/(3^(0.5)))*i:0.1:((3^(0.5))/6)*(200+2*i);
for j=1:length(x)
    y(j)=(3^(0.5))*(x(j)-(2/(3^(0.5)))*i);
end
P1=plot(x,y,'g-');
clear x
clear y
clear i

i=100-Sor;
x=(1/(3^(0.5)))*i:0.1:(2/(3^(0.5)))*i;
for j=1:length(x)
    y(j)=-(3^(0.5))*(x(j)-(2/(3^(0.5)))*i);
end
P2=plot(x,y,'m-');
clear x
clear y
clear i
Oil1=%Read Oil Saturation Data, Path 1%
Water1=%Read Water Saturation Data, Path 1%
Oil1=100.*Oil1;
Water1=100.*Water1;
Gas1=100-Oil1-Water1;
y1=Gas1;
x1=-(2.*Oil1+y1-200)./(3^(0.5));
```

```
Kro1=%Read Oil Relative Permeability Data Correspond to  Path 1%
plot(x1,y1,'K.')
Oil2=%Read Oil Saturation Data, Path 2%
Water2=%Read Water Saturation Data, Path 2%
Oil2=100.*Oil2;
Water2=100.*Water2;
Gas2=100-Oil2-Water2;
y2=Gas2;
x2=-(2.*Oil2+y2-200)./(3^(0.5));
Kro2=%Read Oil Relative Permeability Data Correspond to  Path 2%
plot(x2,y2,'K.')
Oil3=%Read Oil Saturation Data, Path 3%
Water3=%Read Water Saturation Data, Path 3%
Oil3=100.*Oil3;
Water3=100.*Water3;
Gas3=100-Oil3-Water3;
y3=Gas3;
x3=-(2.*Oil3+y3-200)./(3^(0.5));
Kro3=%Read Oil Relative Permeability Data Correspond to  Path 3%
plot(x3,y3,'K.')
min1=min(Kro1);
min2=min(Kro2);
min3=min(Kro3);
max1=max(Kro1);
max2=max(Kro2);
max3=max(Kro3);
Kro_min=max([min1 min2 min3]);
Kro_max=min([max1 max2 max3]);
Curves=Kro_min:(Kro_max-Kro_min)/7:Kro_max;
U=ones(3,2,(length(Curves)-2));
for i=2:(length(Curves)-1)
    U(1,1,i-1)=interp1(Kro1,x1,Curves(i));
    U(1,2,i-1)=((3^(0.5))/3).*(U(1,1,i-1)-(2/(3^(0.5)))*(Swi));
    U(2,1,i-1)=interp1(Kro2,x2,Curves(i));
    U(2,2,i-1)=((3^(0.5))/6).*(U(2,1,i-1)-(2/(3^(0.5)))*(Swi));
    U(3,1,i-1)=interp1(Kro3,x3,Curves(i));
    U(3,2,i-1)=((3^(0.5))/(3/2)).*(U(3,1,i-1)-(2/(3^(0.5)))*(Swi));
end
P3=plot(U(:,1,1),U(:,2,1),'ro');
P4=plot(U(:,1,2),U(:,2,2),'r+');
P5=plot(U(:,1,3),U(:,2,3),'r*');
P6=plot(U(:,1,4),U(:,2,4),'rs');
P7=plot(U(:,1,5),U(:,2,5),'rh');
P8=plot(U(:,1,6),U(:,2,6),'rv');
legend([P1 P2 P3 P4 P5 P6 P7
P8],'Swi','Sor',num2str(Curves(2)),num2str(Curves(3)),num2str(Curves(4))
,num2str(Curves(5)),num2str(Curves(6)),num2str(Curves(7)))
close all
clear all
clc
Swi=input('Enter Irreducible Water Saturation = ');
Sor=input('Enter Residual Oil Saturation = ');
x=0:0.1:100/(3^(0.5));
y=(3^(0.5)).*x;
plot(x,y,'k-')
clear x
clear y
```

```
hold on
x=100/(3^(0.5)):0.1:200/(3^(0.5));
y=-(3^(0.5)).*(x-(200/(3^(0.5))));
plot(x,y,'k-')
clear x
clear y
x=0:0.1:200/(3^(0.5));
for i=1:length(x)
    y(i)=0;
end
plot(x,y,'k-')
clear x
clear y
hold on
for i=10:10:90
    x(i/10,:)=(1/(3^(0.5)))*i:0.1:-(1/(3^(0.5)))*i+200/(3^(0.5));
    for j=1:length(x(i/10,:))
        y(i/10,j)=i;
    end
    plot(x(i/10,:),y(i/10,:),'b-.')
    clear x
    clear y
end
for i=10:10:90
    x(i/10,:)=(2/(3^(0.5)))*i:0.1:((3^(0.5))/6)*(200+2*i);
    for j=1:length(x(i/10,:))
        y(i/10,j)=(3^(0.5))*(x(i/10,j)-(2/(3^(0.5)))*i);
    end
    plot(x(i/10,:),y(i/10,:),'b-.')
    clear x
    clear y
end
for i=10:10:90
    x(i/10,:)=(1/(3^(0.5)))*i:0.1:(2/(3^(0.5)))*i;
    for j=1:length(x(i/10,:))
        y(i/10,j)=-(3^(0.5))*(x(i/10,j)-(2/(3^(0.5)))*i);
    end
    plot(x(i/10,:),y(i/10,:),'b-.')
    clear x
    clear y
end
i=Swi;
x=(2/(3^(0.5)))*i:0.1:((3^(0.5))/6)*(200+2*i);
for j=1:length(x)
    y(j)=(3^(0.5))*(x(j)-(2/(3^(0.5)))*i);
end
P1=plot(x,y,'g-');
clear x
clear y
clear i
i=100-Sor;
x=(1/(3^(0.5)))*i:0.1:(2/(3^(0.5)))*i;
for j=1:length(x)
    y(j)=-(3^(0.5))*(x(j)-(2/(3^(0.5)))*i);
end
P2=plot(x,y,'m-');
clear x
```

```
clear y
clear i
Oil1=%Read Oil Saturation Data, Path 1%
Water1=%Read Water Saturation Data, Path 1%
Oil1=100.*Oil1;
Water1=100.*Water1;
Gas1=100-Oil1-Water1;
y1=Gas1;
x1=-(2.*Oil1+y1-200)./(3^(0.5));
Krw1=%Read Water Relative Permeability Data Correspond to  Path 1%
plot(x1,y1,'K.')
Oil2=%Read Oil Saturation Data, Path 2%
Water2=%Read Water Saturation Data, Path 2%
Oil2=100.*Oil2;
Water2=100.*Water2;
Gas2=100-Oil2-Water2;
y2=Gas2;
x2=-(2.*Oil2+y2-200)./(3^(0.5));
Krw2=%Read Water Relative Permeability Data Correspond to  Path 2%
plot(x2,y2,'K.')
Oil3=%Read Oil Saturation Data, Path 3%
Water3=%Read Water Saturation Data, Path 3%
Oil3=100.*Oil3;
Water3=100.*Water3;
Gas3=100-Oil3-Water3;
y3=Gas3;
x3=-(2.*Oil3+y3-200)./(3^(0.5));
Krw3=%Read Water Relative Permeability Data Correspond to  Path 3%
plot(x3,y3,'K.')
min1=min(Krw1);
min2=min(Krw2);
min3=min(Krw3);
max1=max(Krw1);
max2=max(Krw2);
max3=max(Krw3);
Krw_min=max([min1 min2 min3]);
Krw_max=min([max1 max2 max3]);
Curves=Krw_min:(Krw_max-Krw_min)/7:Krw_max;
U=ones(3,2,(length(Curves)-2));
for i=2:(length(Curves)-1)
    U(1,1,i-1)=interp1(Krw1,x1,Curves(i));
    U(1,2,i-1)=((3^(0.5))/3).*(U(1,1,i-1)-(2/(3^(0.5)))*(Swi));
    U(2,1,i-1)=interp1(Krw2,x2,Curves(i));
    U(2,2,i-1)=((3^(0.5))/6).*(U(2,1,i-1)-(2/(3^(0.5)))*(Swi));
    U(3,1,i-1)=interp1(Krw3,x3,Curves(i));
    U(3,2,i-1)=((3^(0.5))/(3/2)).*(U(3,1,i-1)-(2/(3^(0.5)))*(Swi));
end
P3=plot(U(:,1,1),U(:,2,1),'ro');
P4=plot(U(:,1,2),U(:,2,2),'r+');
P5=plot(U(:,1,3),U(:,2,3),'r*');
P6=plot(U(:,1,4),U(:,2,4),'rs');
P7=plot(U(:,1,5),U(:,2,5),'rh');
P8=plot(U(:,1,6),U(:,2,6),'rv');
legend([P1 P2 P3 P4 P5 P6 P7
P8],'Swi','Sor',num2str(Curves(2)),num2str(Curves(3)),num2str(Curves(4))
,num2str(Curves(5)),num2str(Curves(6)),num2str(Curves(7)))
```

```
function T = Tg_Cal(i,dir,Beta,K,Area,Delta_x,Visc_g,Bg,Krg,P);
%   Tg_Cal function calculate transmiscibility for each cell:
%   Detailed explanation goes here:

switch dir
    case 1
        if i==1
            T=0;
        else
            if P(i)>=P(i-1)
            T=Beta*((K(i)*Area)/Delta_x)*(1/(Visc_g(i)*Bg(i)))*Krg(i);
            else
            T=Beta*((K(i-1)*Area)/Delta_x)*(1/(Visc_g(i-1)*Bg(i-
1)))*Krg(i-1);
            end
        end
    case 2
        if i==length(P)
            T=0;
        else
            if P(i)>=P(i+1)
            T=Beta*((K(i)*Area)/Delta_x)*(1/(Visc_g(i)*Bg(i)))*Krg(i);
            else

T=Beta*((K(i+1)*Area)/Delta_x)*(1/(Visc_g(i+1)*Bg(i+1)))*Krg(i+1);
            end
        end
end

end
```

```
function T = To_Cal(i,dir,Beta,K,Area,Delta_x,Visc_o,Bo,Kro,P);
%   To_Cal function calculate transmiscibility for each cell:
%   Detailed explanation goes here:

switch dir
    case 1
        if i==1
            T=0;
        else
            if P(i)>=P(i-1)
            T=Beta*((K(i)*Area)/Delta_x)*(1/(Visc_o(i)*Bo(i)))*Kro(i);
            else
            T=Beta*((K(i-1)*Area)/Delta_x)*(1/(Visc_o(i-1)*Bo(i-
1)))*Kro(i-1);
            end
        end
    case 2
        if i==length(P)
            T=0;
        else
            if P(i)>=P(i+1)
            T=Beta*((K(i)*Area)/Delta_x)*(1/(Visc_o(i)*Bo(i)))*Kro(i);
            else

T=Beta*((K(i+1)*Area)/Delta_x)*(1/(Visc_o(i+1)*Bo(i+1)))*Kro(i+1);
            end
        end
end

end
```

```
function T = Tw_Cal(i,dir,Beta,K,Area,Delta_x,Visc_w,Bw,Krw,P);
%   Tw_Cal function calculate transmiscibility for each cell:
%   Detailed explanation goes here:

switch dir
    case 1
        if i==1
            T=0;
        else
            if P(i)>=P(i-1)
            T=Beta*((K(i)*Area)/Delta_x)*(1/(Visc_w(i)*Bw(i)))*Krw(i);
            else
            T=Beta*((K(i-1)*Area)/Delta_x)*(1/(Visc_w(i-1)*Bw(i-
1)))*Krw(i-1);
            end
        end
    case 2
        if i==length(P)
            T=0;
        else
            if P(i)>=P(i+1)
            T=Beta*((K(i)*Area)/Delta_x)*(1/(Visc_w(i)*Bw(i)))*Krw(i);
            else

T=Beta*((K(i+1)*Area)/Delta_x)*(1/(Visc_w(i+1)*Bw(i+1)))*Krw(i+1);
            end
        end
end

end
```

APPENDIX E: 3RELPERM PLOT

E.1 Applications

3RelPerm Plot, Figure (E.1) is an easy-to-use software specially designed to represent three-phase relative permeability data in ternary diagrams. However, it can be used in other engineering and science disciplines such as:

- Petroleum Engineering (PVT)
- Chemical Engineering / Physical Chemistry
- Geology / Mineralogy / Petrophysics / Petrology / Soil Science
- Metallurgy
- Other Physical Sciences

E.2 System Requirement

3RelPerm Plot is a portable, executable (.exe) file developed in Microsoft Visual Studio 2010. A .net Framework is required to run the application.

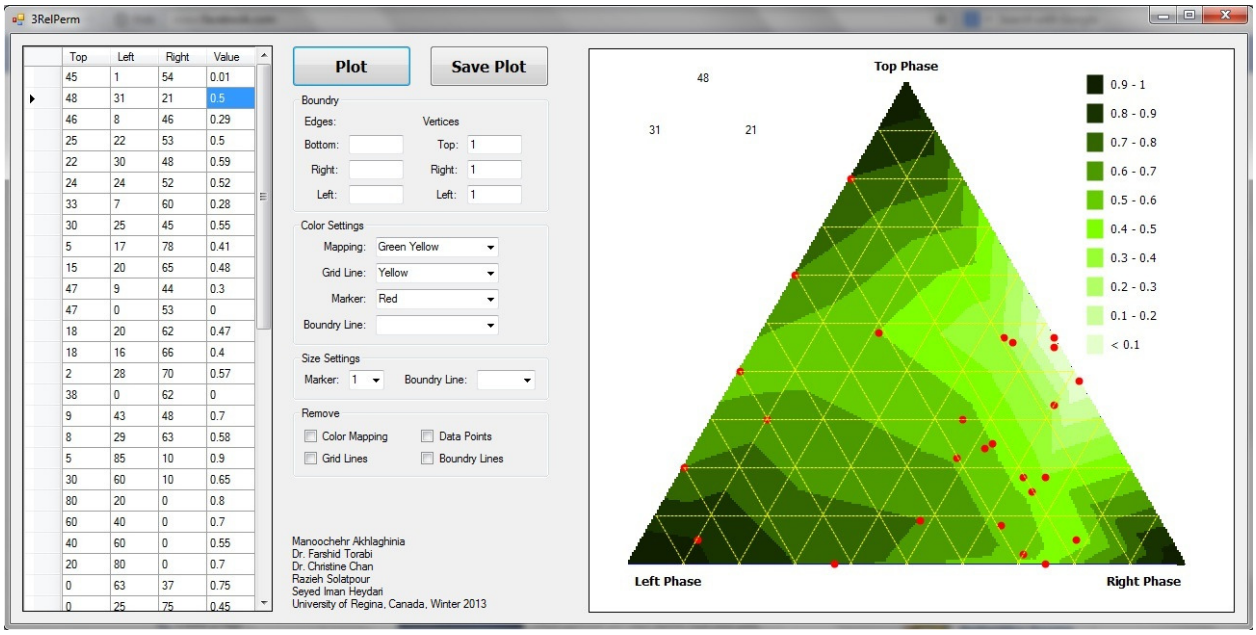

Figure E.1: *3RelPerm Plot* Interface (original in color).

E.3 Features

E.3.1 Three-Phase Flow Zone

The Boundary settings allow the user to confine data in an arbitrary triangle inside the main triangle. This ability is very useful to present three-phase relative permeability data since the concept of three-phase flow zone is encountered. As an example, Figure E.2 shows how relative permeabilities to gas phase are plotted in a confined three-phase flow zone. The bottom edge value (entered zero) represents zero irreducible gas saturation; the right edge value (entered 40) represents 40% residual oil saturation; and the left edge value (entered 3) represents 3% irreducible water saturation. Values at the vertices of the confined triangle should be known (yellow circles). In the example shown in Figure E.2, relative permeability at the top vertex (S_o = 40%, S_w = 3%, S_g = 57%) is entered as 0.33, the right vertex (S_o = 40%, S_w = 60%, S_g = 0%) and the left vertex (S_o = 97%, S_w = 3%, S_g = 0%) are entered as zero.

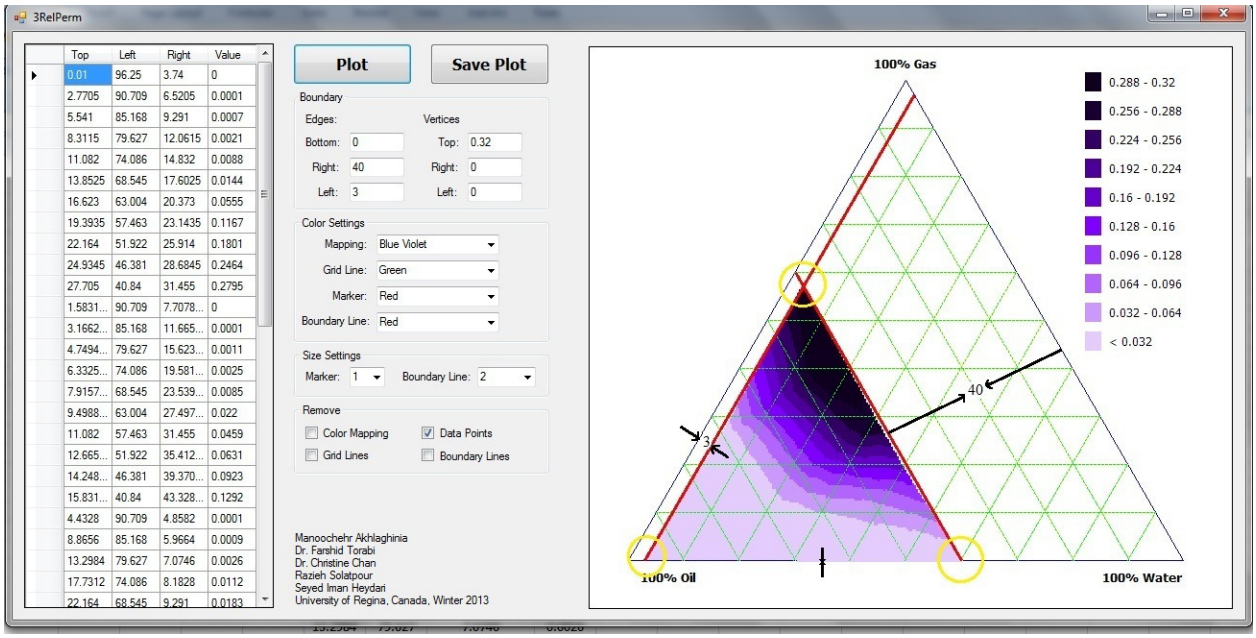

Figure E.2: Plotting a three-phase flow zone with *3RelPerm Plot* (original in color).

E.3.2 User-Friendly Setting

3RelPerm Plot provides a variety of colours for colour mapping, gridlines, marker, and boundary lines (Figure E.3). In addition, marker size and thickness of boundary lines can be changed in the setting. Also user is able to add/remove colour mapping, gridlines, data points, and boundary lines.

Figure E.3: Colour options in *3RelPerm Plot*. (from www.rapidtables.com) (original in color).

E.3.3 Interpolation

3RelPerm Plot exceptionally allows user to analyze and interpolate within the ternary diagram. Once the mouse curser is hovered within the main triangle, all information appears in the top left corner of the plotting panel (Figure E.4). As an example, following information can be read based on the location of the curser within the ternary diagram:

Top Phase: 54%

Left Phase: 23%

Right Phase: 23%

Corresponding property: 0.508515136469834

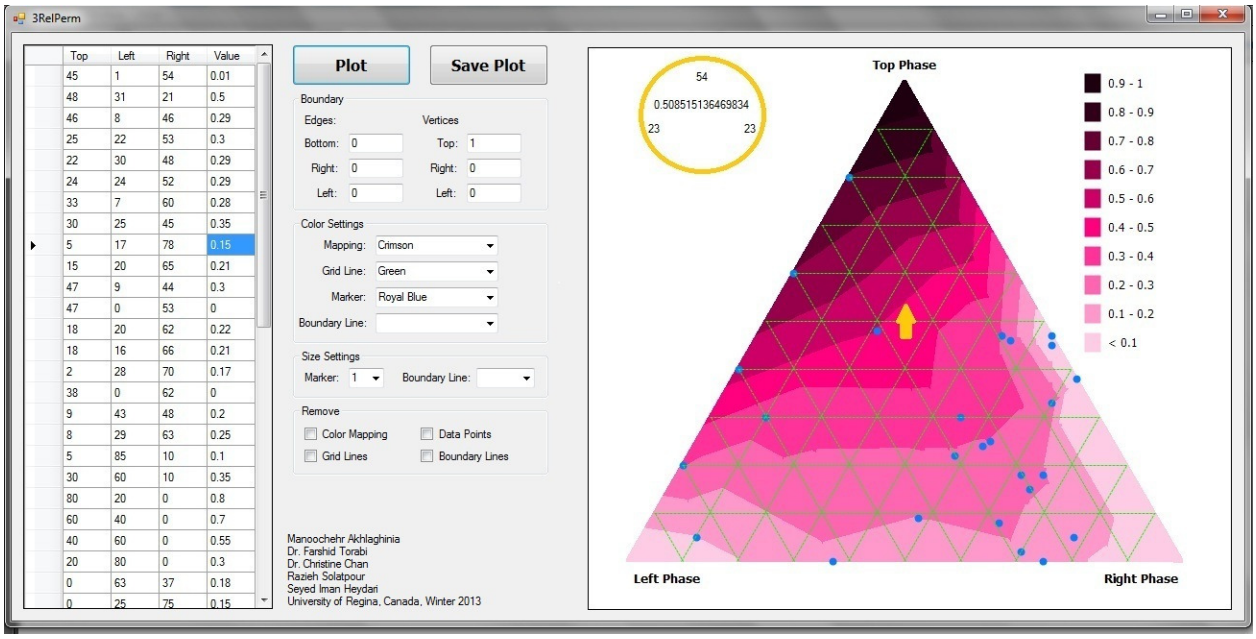

Figure E.4: Interpolation between point in *3RelPerm Plot* (original in color).

E.4 Meshing/Graphics Algorithm:

Delaunay Triangulation with incremental technique has been used to build meshes and then color-mapping. The procedure is as following:

1. The first triangle constructed is called a supertriangle. It is an equilateral triangle that entirely contains the convex hull of the points to be triangulated. The vertices of this construction will be removed in the last step, leaving the triangulated network.

2. Points to be triangulated are added one by one. The list of points is ordered by their y co-ordinate.

3. Circumcircles pass through the three vertices of each triangle in the network. As each additional point is added to the structure, triangles who's circumcircle contains the new point are identified and their associated triangles removed.

5. New triangles are formed between the most recently inserted point and the segments of the void left after removing the triangles.

6. After the final point is added, the vertices of the supertriangle and any triangles that share these vertices are removed.

Corresponding algorithm has been developed independently and successfully examined several times with MATLAB software, Figure E.5.

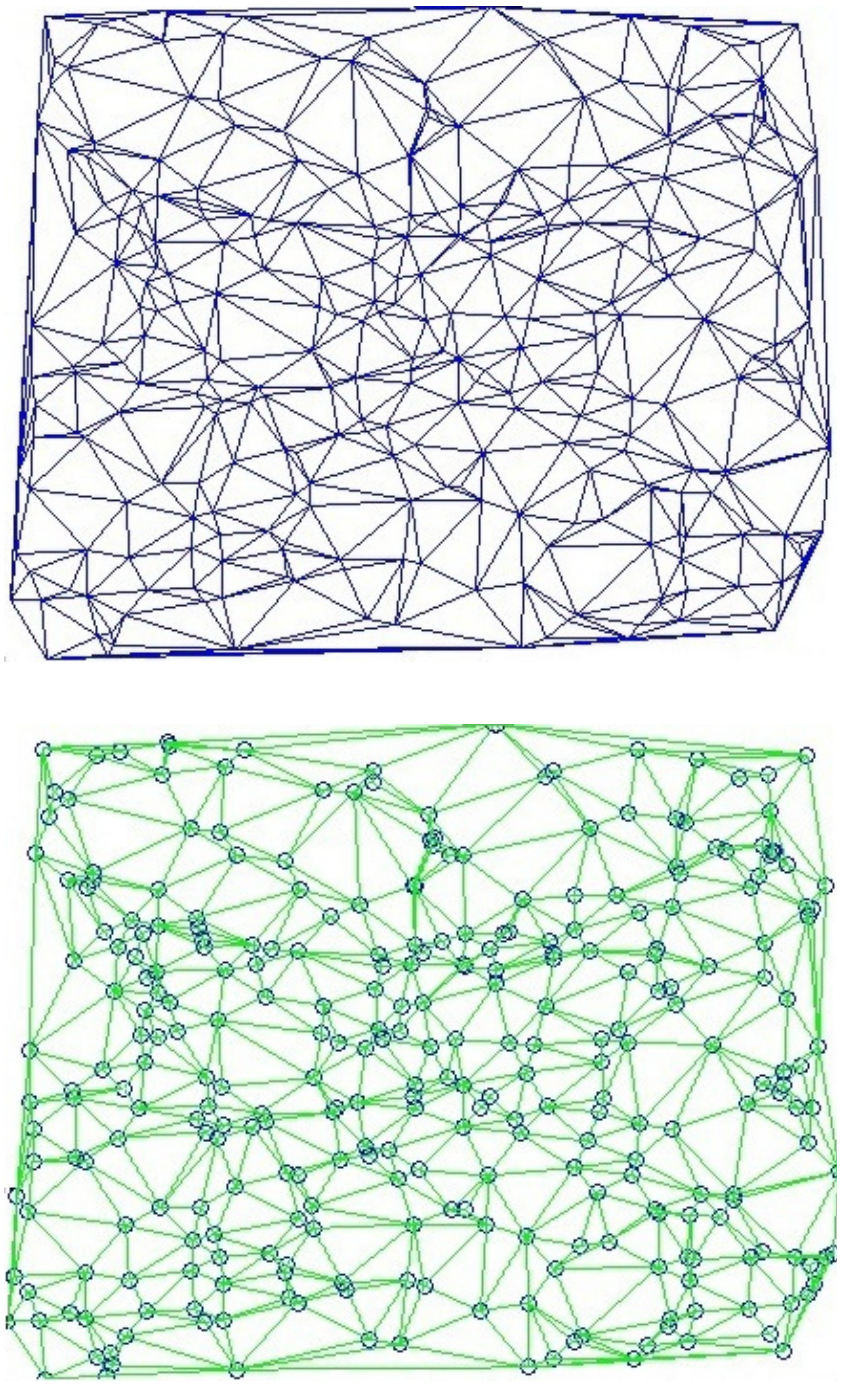

Figure E.5: The Delaunay Triangulation of a random set of 300 points in a plane by MATLAB algorithm (TOP) and self-developed algorithm (BOTTOM) (original in color).

APPENDIX F: FINAL MATCHING RESULTS

Results presented here are the final results of matching observed data from the three-phase displacement experiments (pressure drop, oil production, and water production) with those obtained from the developed numerical simulator. Corresponding relative permeability isoperms have been presented in Chapter 6.

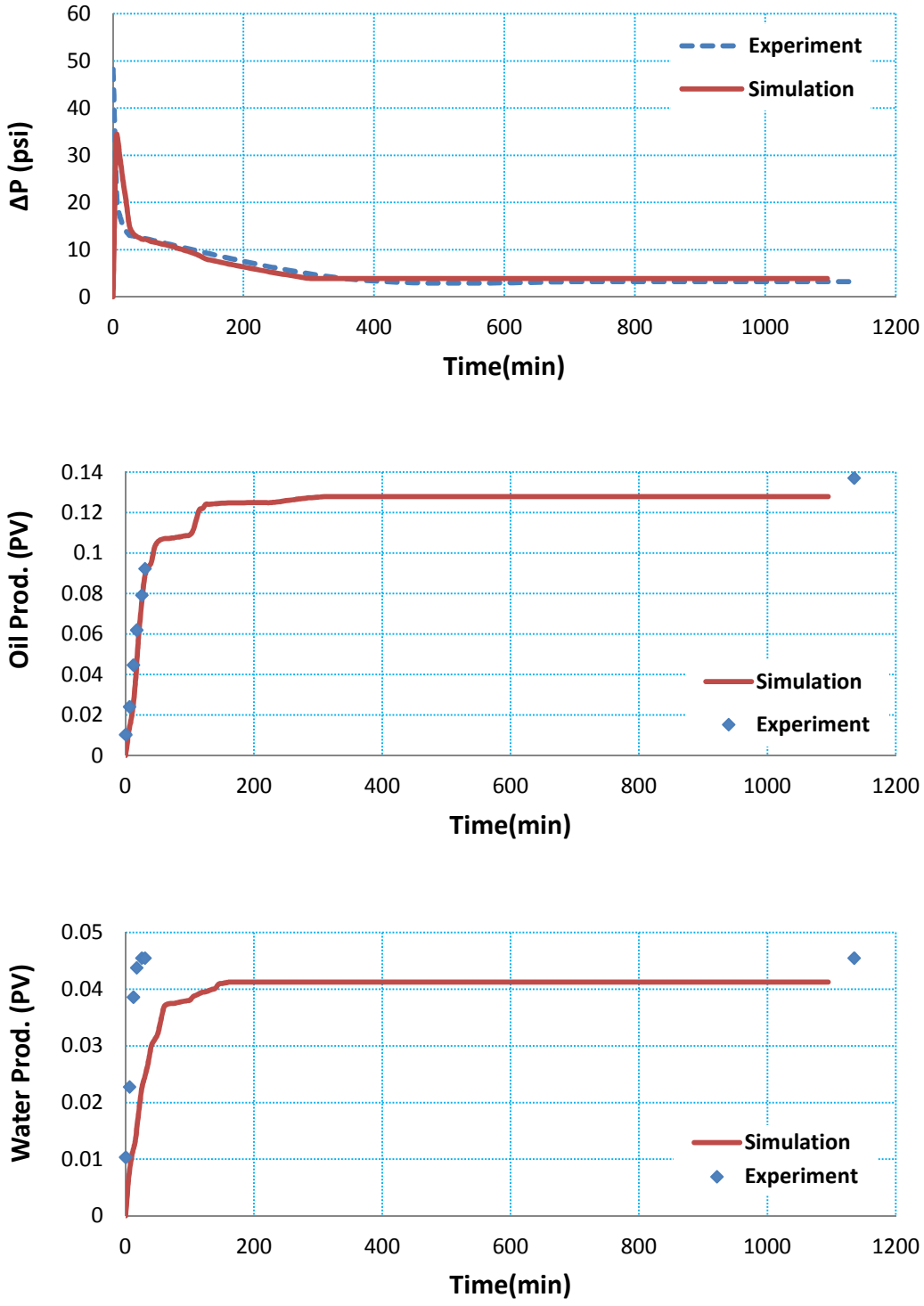

Figure F.1: Results from matching test#2 for saturation path # 1, top (pressure drop), middle (oil production), and bottom (water production).

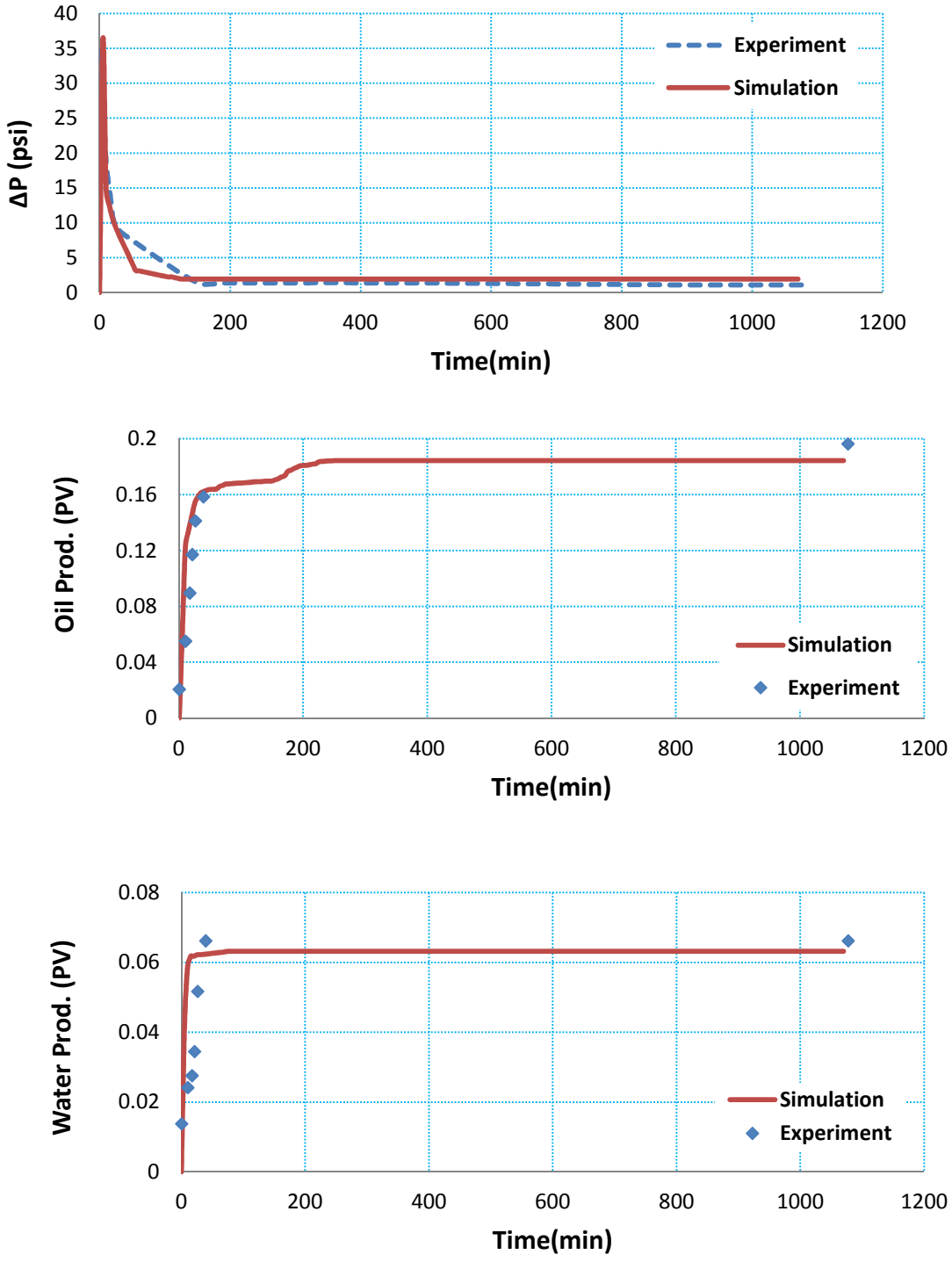

Figure F.2: Results from matching test#3 for saturation path # 1, top (pressure drop), middle (oil production), and bottom (water production).

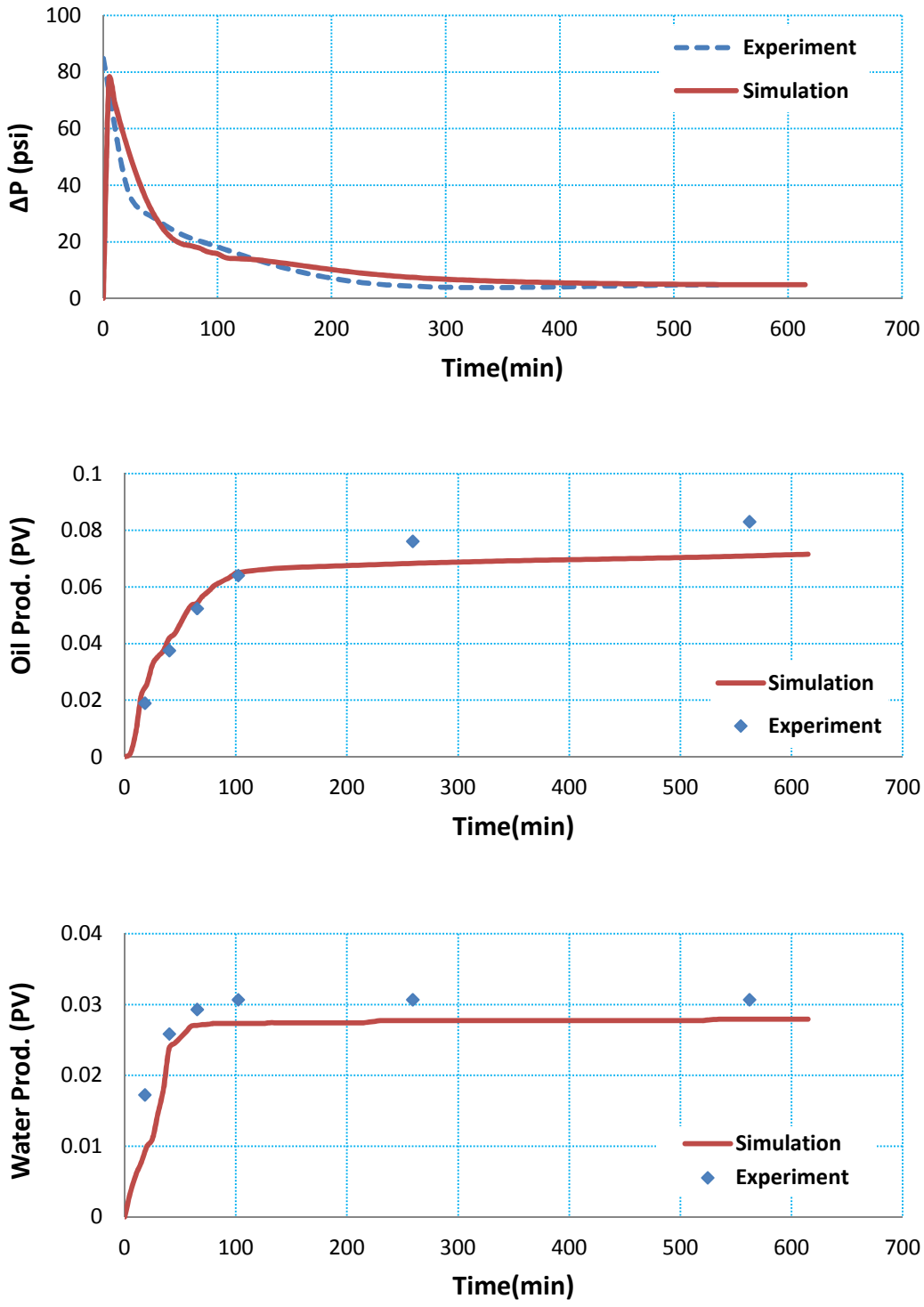

Figure F.3: Results from matching test#4 for saturation path # 1, top (pressure drop), middle (oil production), and bottom (water production).

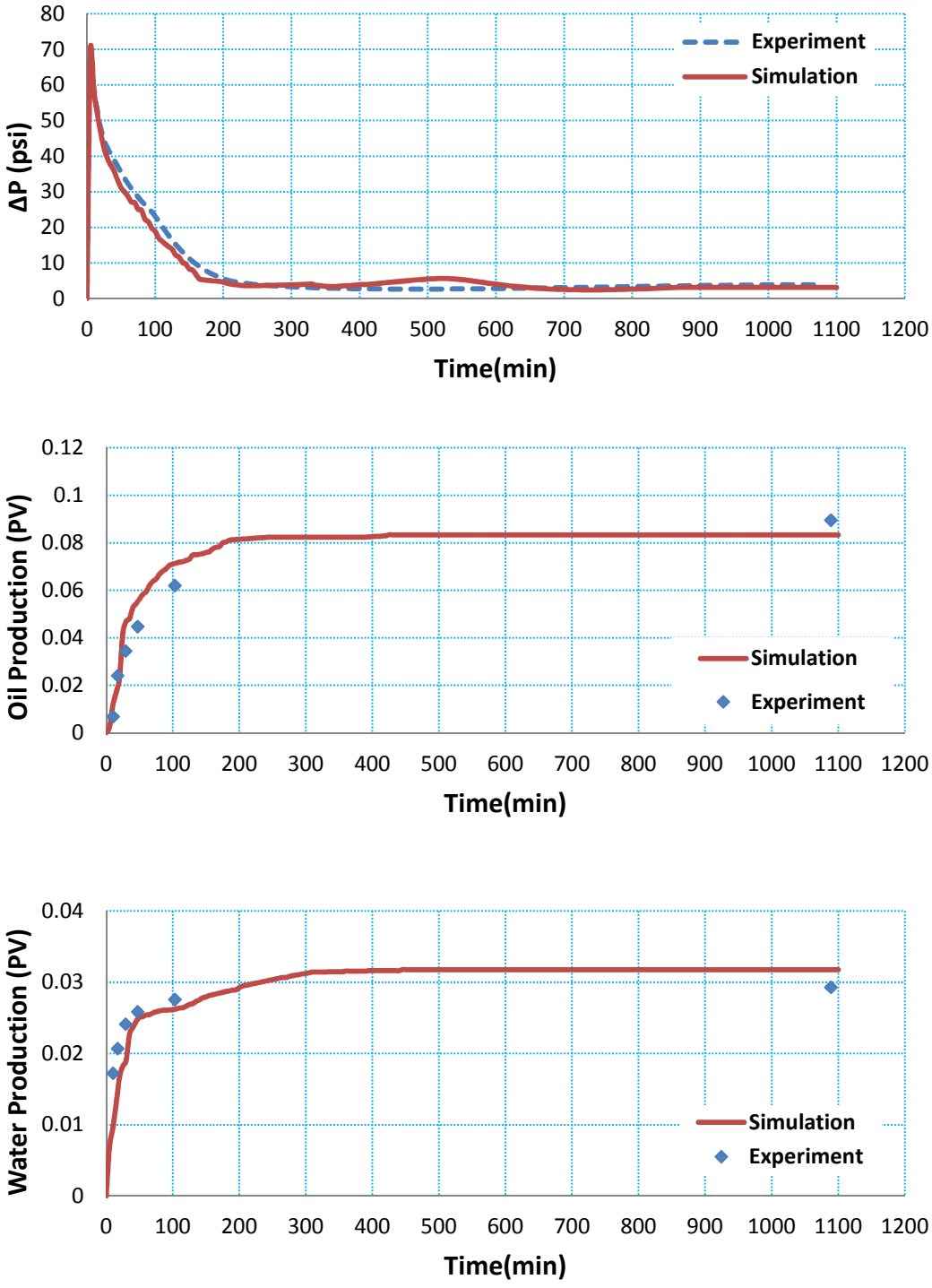

Figure F.4: Results from matching test#5 for saturation path # 1, top (pressure drop), middle (oil production), and bottom (water production).

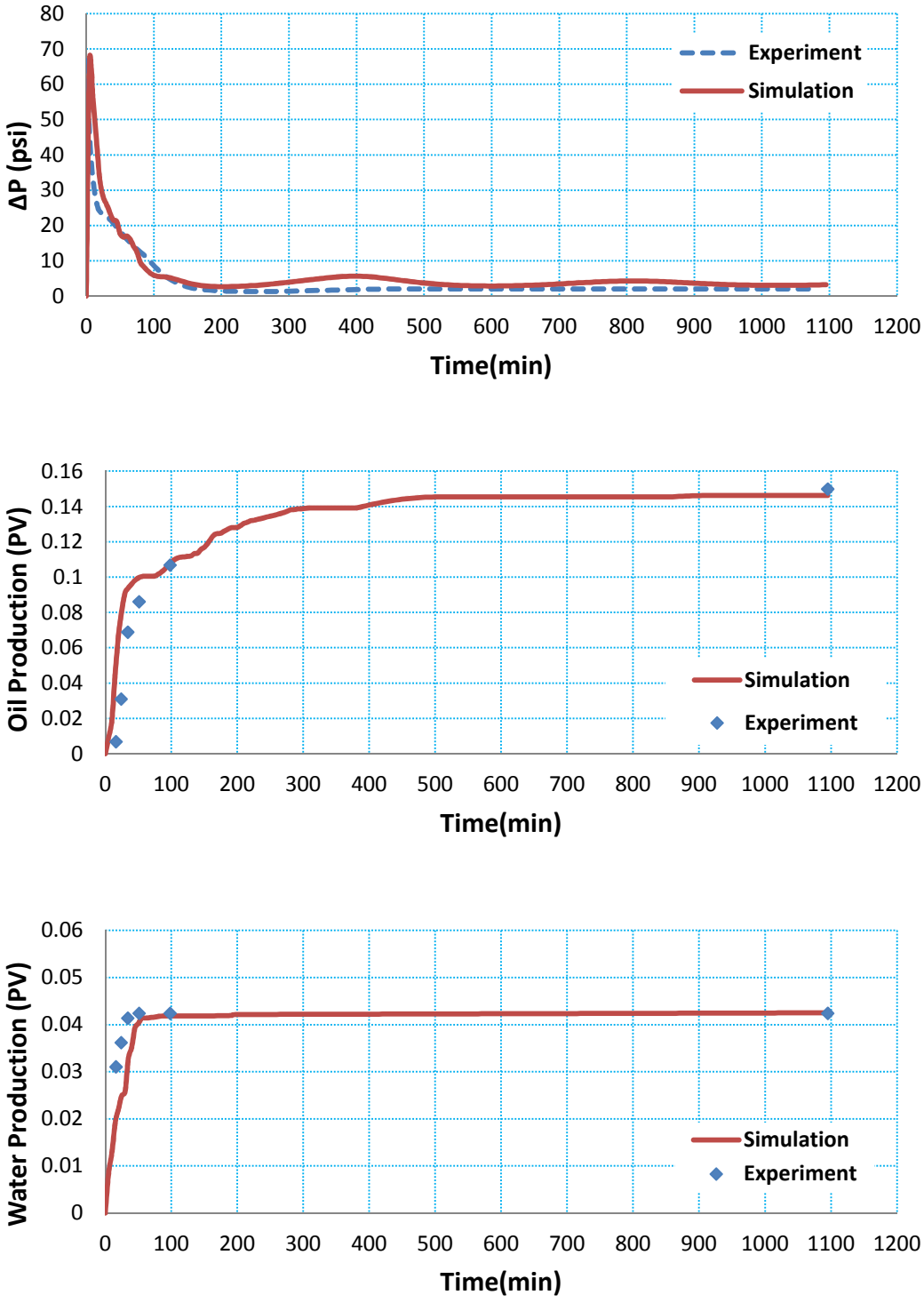

Figure F.5: Results from matching test#5 for saturation path # 1, top (pressure drop), middle (oil production), and bottom (water production).

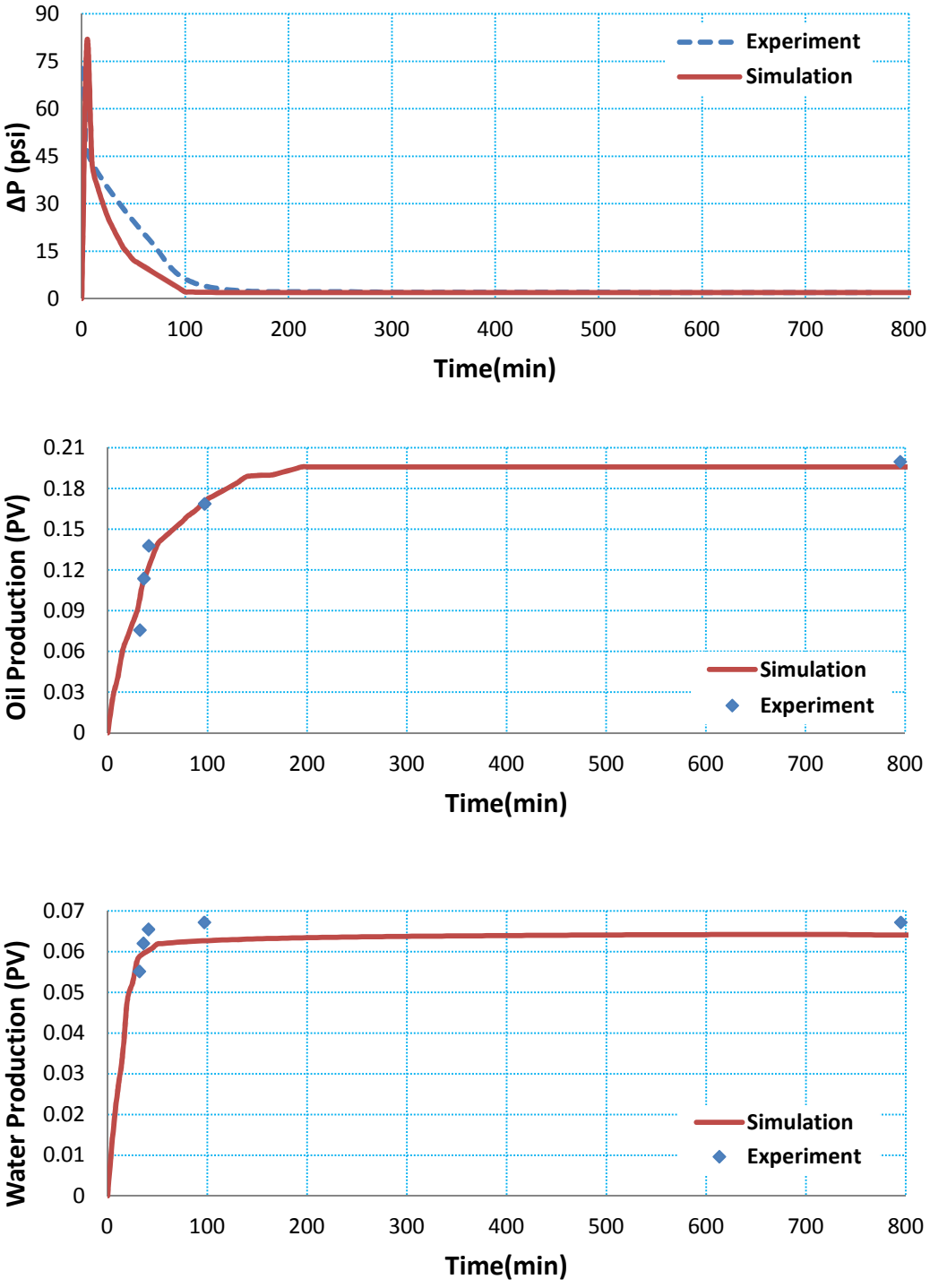

Figure F.6: Results from matching test#7 for saturation path # 1, top (pressure drop), middle (oil production), and bottom (water production).

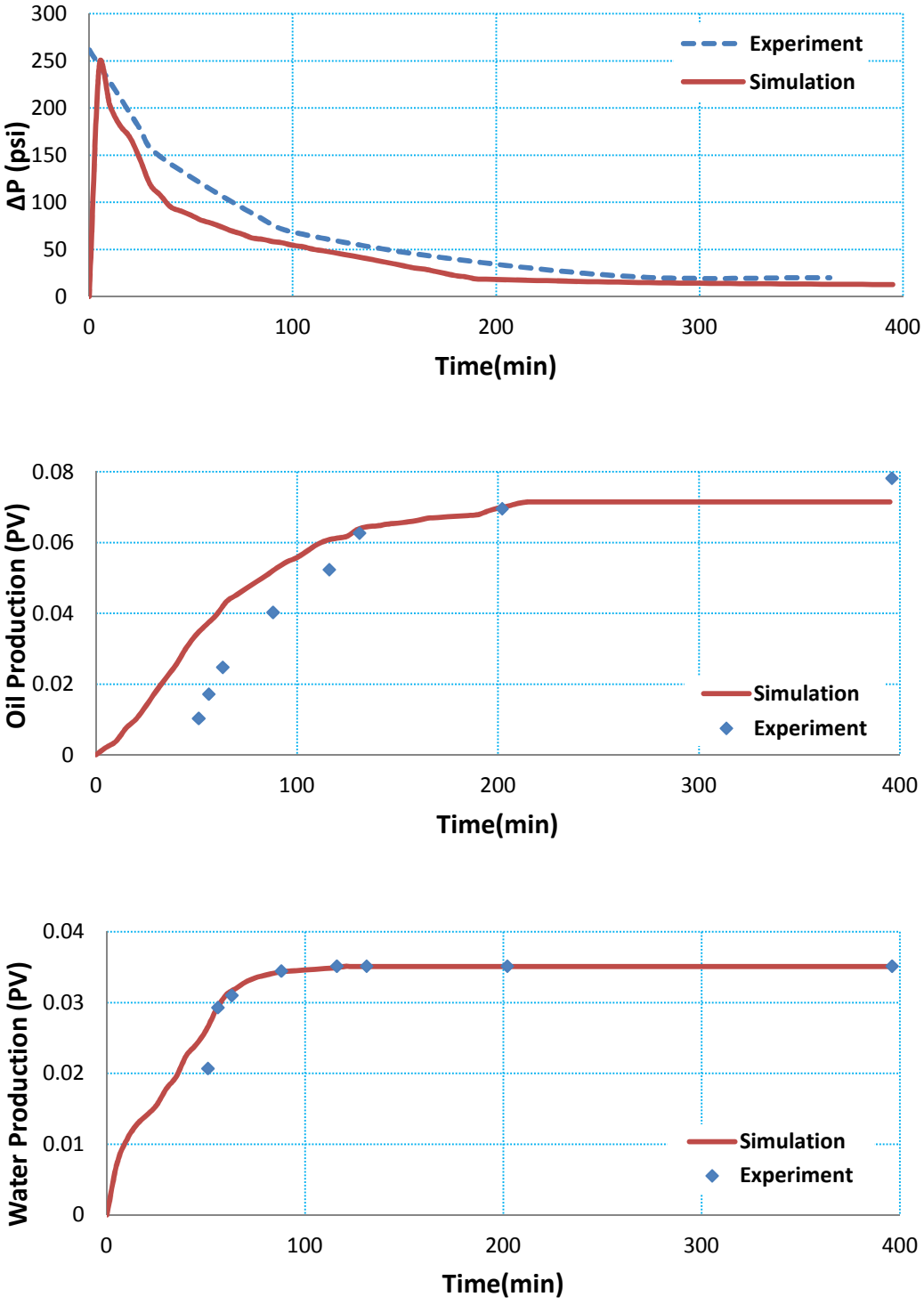

Figure F.7: Results from matching test#8 for saturation path # 1, top (pressure drop), middle (oil production), and bottom (water production).